UNIVERSITY OF LINCOLN

UNIVERSITY OF
LINCOLN

Advanced Robust Control Design For High Speed Tilting Trains

by

Fazilah Hassan

A thesis submitted in partial fulfillment for the
degree of Doctor of Philosophy

in the
College of Science
School of Engineering

May 2018

Declaration of Authorship

I, FAZILAH HASSAN, declare that this thesis titled, 'Advanced Robust Control Design For High Speed Tilting Trains' and the work presented in it are my own. I confirm that:

- This work was done wholly or mainly while in candidature for a research degree at this University.
- Where any part of this thesis has previously been submitted for a degree or any other qualification at this University or any other institution, this has been clearly stated.
- Where I have consulted the published work of others, this is always clearly attributed.
- Where I have quoted from the work of others, the source is always given. With the exception of such quotations, this thesis is entirely my own work.
- I have acknowledged all main sources of help.
- Where the thesis is based on work done by myself jointly with others, I have made clear exactly what was done by others and what I have contributed myself.

Signed: _____

Date: _____

Abstract

Tilting is a worldwide accepted technology concept in railway transportation. The particular benefit from tilting trains use is reduction in journey times due to speed increase on track corners (while maintaining acceptable passenger comfort), a point that facilitates improved customer service. An additional benefit is cost effectiveness due to the train running on existing rail tracks. Many countries opted to using tilting trains as means of fast public transportation (UK, USA, Canada, Sweden, Norway, Switzerland, Germany, Japan).

The industrial norm of tilting high speed trains is that of precedence tilt whereby preview tilt enabling signals are used to provide the required information to the vehicles (it can also use a combination of track database information or GPS but the concept is the same). Precedence tilt tends to be complex (mainly due to the signal interconnections between vehicles and the advanced signal processing required for monitoring). Research studies of earlier than precedence schemes,i.e. the so-called nulling-type schemes whereby local-per-vehicle signals are used to provide tilt (a disturbance rejection-scheme although tends to suffer from inherent delays in the control feedback), are still an important research aim due to the simple nature and most importantly due to the more straightforward fault detection compared to precedence. Use of nulling-type tilt has been supported by recent studies in this context.

The research presented in this thesis highly contributes to simplified single-input-single-output robust tilt control using the simplest rail vehicle tilt structure, i.e. an Active Anti-Roll Bar. Proposed are both robust conventional (integer-type) control approaches and non-conventional (non-integer) schemes with a rigorous investigation of the difficult to achieve deterministic/stochastic tilt trade-off. Optimization has been used extensively for the designs. A by-product of the work is the insight provided into the relevant tilting train model Non Minimum Phase characteristics and its link to uncertainty for control design. Work has been undertaken using Matlab, including proper assessment of tilt ride quality considerations.

Acknowledgements

Alhamdulillah...

I would like to express my greatest gratitude to my supervisor, Dr Argyrios Zolotas for his endless support, supervision and help throughout this PhD journey. Words cannot express how much I feel indebtful towards him. I would also like to thank my second supervisor Dr Rebecca Margetts and the friendly staff of School of Engineering, University of Lincoln.

To my labmate, Sally, thank you for being nice to me and always sharing food with me and for all the useful discussions.

Special dedication to my husband who's been taking care of the kids when I was busy with my PhD work. To my son Farhat, thank you for being a good brother to your sister, Farha. Thank you for listen to me well. To my little daughter Farha, I'm glad you were born during my PhD. Thank you for being so funny. I'm truly sorry for the lack of time being with both of you.

Also to my mom, Jamiah Ahmad and sisters, Widahwati, Salwana and Sarypah back home. Thank you for your financial and emotional support.

To friends who I can disscussed joy and pain during this PhD journey, Iman, Dr Shaharil, Azli, Mader and Chefwan. Last but not least to my thesis proofreader Dr Dilla Duryha, Nurulasyikin and Zamira.

And to everyone who made this thesis possible.

...

Contents

Declaration of Authorship i

Abstract ii

Acknowledgements iii

List of Figures viii

List of Tables xii

Abbreviations xiv

Symbols xvi

1 Introduction 1

1.1 Suspension technology 2

1.2 Tilting technology 4

1.2.1 Tilt mechanical arrangement 5

1.3 Quantifying tilt (vehicle roll) action tilting concept 6

1.4 Tilt control considerations 9

1.5 Motivation for this thesis work 11

1.6 Thesis structure 12

1.7 Publications 13

1.8 Thesis contributions 14

2 Literature study and survey **16**

2.1 A brief encounter of active suspensions in railway vehicles 16

2.2 Tilting control systems 17

2.2.1 Tilt control mechanisms 18

2.2.2 Two actuator based tilt control mechanisms 20

2.3 Optimisation tools in control design 23

2.4 System size reduction 24

2.5 Summary 25

3 Vehicle modeling and control assessment **26**

3.1 ARB tilt vehicle model 26

3.2 A note on track exogenous inputs to the vehicle 29

3.3 Tilt performance assessment utilised in this work 31

3.4 Modelling for control 33

3.4.1 Usefulness of multiplicative uncertainty representation for robust control design 36

3.4.2 On the uncertainty of the original NMP model transfer function 39

3.4.3 A note on use of random plant perturbations 43

3.5 Summary 43

4 Conventional PID design for the ARB tilt system **46**

4.1 Proportional Intergral Derivative(PID) 47

4.2 Frequency response Ziegler-Nichols approach 48

4.3 Alternative conventional PID tuning approach 51

4.4 Performance analysis 54

4.4.1 Nominal performance analysis 55

4.4.2 Robust performance analysis 60

4.5 Summary 61

5 Optimised PID control design for the tilt system **62**

5.1 Optimised modified Z-N PID design 63

5.1.1 Note on optimization tools used for the design 63
5.1.2 Choice of initial conditions for the optimisation process . . . 64
5.1.3 Nominal performance analysis 65
5.2 PID control design based on generic optimisation 66
5.2.1 Choice of initial conditions 68
5.2.2 Nominal performance analysis 69
5.3 Optimised Fractional order PID controller 76
5.3.1 Fractional order introduction 76
5.3.2 Fractional order approximation 79
5.3.3 Nominal performance analysis 80
5.4 Robustness analysis - for the optimised PID control cases 83
5.5 Summary 85

6 Robust loop shaping based tilt control design 88
6.1 Fractional order control with NMP zero shaping 89
6.1.1 Reduced order considerations of the loop-shaping fractional order controller 94
6.1.2 Nominal Performance (nominal plant and controller) 98
6.1.3 Robust performance (plant uncertainty) 100
6.2 $H\infty$ mixed sensitivity loop shaping 101
6.2.1 Mixed sensitivity 101
6.2.2 Nominal performance analysis 104
6.2.3 Controller reduction and robust performance investigation . 110
6.3 Summary 113

7 Comparing proposed SISO nulling-type tilt control to precedence 114
7.1 A note on the precedence controller used 114
7.2 Appraisal of tilt performance 115
7.3 Summary 117

8 Conclusions and future work 120
8.1 Conclusions 120

8.2 Future work recommendation 123

A Vehicle model information **125**

A.1 Vehicle Model Equations 125

A.1.1 Vehicle body (lateral and roll) 125

A.1.2 Vehicle bogie (lateral and roll) 126

A.1.3 Simplified: Airspring, Tilt actuation, Bogie kinematics . . . 126

A.2 Variables and Parameters list 127

A.3 State space matrices 127

A.3.1 17th states space matrices for SISO modelling 127

A.4 Track regularities representation 130

B Tilt assessment PCT factor **132**

C Fractional order controller **134**

C.1 Full order fractional order controller IOR approximation 134

C.1.1 FOPID 134

C.1.2 Loop shaping fractional order controller(full order) 135

C.1.3 7th order controller reduction loop shaping FOC 138

D $H\infty$ Mixed sensitivity **141**

D.1 Full order controller for $H\infty$ Mixed sensitivity 141

D.2 8th order controller reduction for $H\infty$ Mixed sensitivity 144

E Certificate of award **146**

Bibliography **148**

List of Figures

1.1 Conventional railway vehicle mechanical arrangement (Goodall, 1999a) 3
1.2 Passive and active suspension setup 4
1.3 Example of tilting trains, Pendolino train(left), Virgin train(middle) and Zefiro train(right) 5
1.4 Example of tilting trains with different tilt mechanism (Goodall, 1999b) 7
1.5 Non tilt action (a) and Tilt action(b) (Zolotas, 2002) 8
1.6 Partial nulling tilt control set-up 10
1.7 Precedence command driven control 11

3.1 Tilting vehicle end-view (Zolotas, 2002) 27
3.2 Representation of deterministic track profile (Zolotas, 2002). 30
3.3 Ideal and actual lateral acceleration 32
3.4 Ideal and actual absolute body roll velocity 32
3.5 Feedback setup with multiplicative uncertainty 37
3.6 Nominal model MP and multiplicative uncertainty factorisation results 38
3.7 Plant uncertainty plot 40
3.8 Multiplicative uncertainty bound with relative error 42
3.9 Random perturbed plant with 20% change in body mass, secondary vertical suspension and roll suspension damping 44
3.10 Multiplicative uncertainty bound for 20% relative error and fixed perturbed plant relative error 45

4.1 Curve point location by injection of pure gain and phase lead, lag . 50
4.2 Frequency response for all Ziegler Nichols cases. 51
4.3 Complementary Sensitivity and sensitivity plot for all Ziegler Nichols cases. 52

4.4 Ride quality (passive and active) plot for all Ziegler Nichols cases. 52
4.5 Effective cant deficiency (E.C.D) plot for Ziegler Nichols FR, Ziegler Nichols modified Original, Ziegler Nichols modified case 1 to case 4. 53
4.6 Frequency plot for Tyreus-Luyben original, Tyreus-Luyben Detuned and Frequency Response Manual design. 55
4.7 Complementary Sensitivity and sensitivity plot for Tyreus-Luyben original, Tyreus-Luyben Detuned and Frequency Response Manual design. 56
4.8 Ride quality (passive and active) plot for Tyreus-Luyben original, Tyreus-Luyben Detuned and Frequency Response Manual design. . 57
4.9 Lateral acceleration plot for conventional PID methods 58

5.1 Optimised Ziegler-Nichols PID controller design 66
5.2 PID controllers Bode plot. 73
5.3 Deterministic lateral acceleration and nichols plot of designed $L(j\omega)$ results for the different PID controllers 74
5.4 Ride quality TF for different controllers and nominal plant 75
5.5 Sensitivity to Input (disturbance), i.e. Matched uncertainty, (for the different controllers) 75
5.6 Stability region for fractional order system (Chen et al., 2009) . . . 78
5.7 Control frequency plot for FO1, FO2, FO3 and FO4 81
5.8 Frequency (a) and closed loop plot (complementary and sensitivity) for plant with FO1 controller 82
5.9 Frequency (a) and closed loop plot (complementary and sensitivity) for plant with FO2 controller 82
5.10 Frequency (a) and closed loop plot (complementary and sensitivity) for plant with FO4 controller 82
5.11 Frequency (a) and closed loop plot (complementary and sensitivity) for plant with FO4 controller 83
5.12 Lateral acceleration plot for non precedence tilt with FOPID controller (a) and (b) 84
5.13 Closed loop complementary sensitivity bound for (a) Ziegler-Nichols optimised, CF3,CF6,CF7 (b) CF8,FO2,FO3,FO4 86

6.1 The feedback structure for the fractional order shaping controller design 90

6.2 Designed open loop magnitude plot for the fractional order loop shaping case . . . 94
6.3 Reduced-order controller feedback formulation for stability criteria 95
6.4 Controller reduction and performance trade-off (of the rational-order approximated fractional-order based controllers(Approximation of PID + $\tilde{Q}_{n=2}^{-1}$,$\tilde{Q}_{n=5}^{-1}$ and $\tilde{Q}_{n=7}^{-1}$) . . . 97
6.5 Passenger acceler. (determ.) (a) Conventional PID; (b) Optim. PID and Fractional order based control(Optim. PID, IOR-FOPID, PID+$\tilde{Q}_n^{-1}$ (LSC) for $n = 2, \ldots, 7$ (no reduction yet(full order))) . . 98
6.6 Passenger acceleration (determ.) (the precedence scheme uses tilt angle preview information to provide the 60% tilt compensation and integer-order PID for tracking . . . 99
6.7 Reduced-order controller complementary sensitivity(T) with W_δ bound. . . . 100
6.8 Feedback set-up for the tilt related robust H_∞ mixed sensitivity-regulation problem . . . 102
6.9 Loop (a) and closed-loop (b) (complementary sensitivity($T(j\omega)$) and sensitivity($S(j\omega)$) plots for P_{1NMP} case . . . 105
6.10 Loop (a) and closed-loop (b) (complementary sensitivity($T(j\omega)$) and sensitivity($S(j\omega)$) plots for P_{2NMP} case . . . 106
6.11 Loop (a) and closed-loop (b) (complementary sensitivity($T(j\omega)$) and sensitivity($S(j\omega)$) plots for P_{1MP} case . . . 106
6.12 Loop (a) and closed-loop (b) (complementary sensitivity($T(j\omega)$) and sensitivity($S(j\omega)$) plots for P_{2MP} case . . . 106
6.13 Lateral acceleration plot for P_{1NMP} and P_{2NMP} case (a), P_{1MP} and P_{2MP} . . . 107
6.14 Sensivity(S), complementary sensitivity(T) and γ/W_1 plot for (a)$P_{x2NMP}\, W_2 = 0.5$ (b)$P_{x2MP}\, W_2 = 0.1$ . . . 109
6.15 Controller reduction and performance trade-off for H_∞ mixed sensitivity cases . . . 111
6.16 Complementary sensitivity ($T(s)$) for the reduced order controller (a) NMP model (b) MP model with multiplicative bound W_δ,$W_{\delta mp}$ . . . 112

7.1 Precedence approach on curved track for (a) Passenger acceleration (b) Tilt angles (c) Body roll rate . . . 116
7.2 Lateral acceleration responses . . . 118

7.3 Body roll responses 118
7.4 Body gyro responses 119

B.1 Deterministic time-domain assessment elements for P_{CT} and 'ideal tilt' 133

E.1 Best paper award 147

List of Tables

2.1 Classification list of SISO control(tilt only) and MIMO control(tilt with lateral) . . . 22

3.1 Vehicle modal analysis for the ARB Tilt model (Zolotas, 2002) . . 28
3.2 Track profiles used for simulation and assessment (* curved track, † straight track lateral irregularities) . . . 31
3.3 Perturbed plant cases . . . 39
3.4 Pole locations for plant P0-4 . . . 41
3.5 Zero location for plants P0-4 . . . 41

4.1 Ziegler-Nichols controller gains (frequency response method) . . . 49
4.2 Modified Ziegler-Nichols parameter values . . . 50
4.3 PID controller list for Ziegler-Nichols approach . . . 51
4.4 Stability margins for the conventional PID controllers . . . 56
4.5 Performance assessment (P_{CT} / rq(ride quality): PID conventional tuning approaches . . . 59
4.6 Robust performance for P_{CT} standing for all conventional cases . . 60
4.7 Robust performance for ride quality degradation for all conventional cases . . . 60

5.1 Optimised modified Ziegler-Nichols controller performance . . . 65
5.2 Minimization approach identifiers and constraints (Note: rqd denotes ride quality degradation; GM: gain margin; PM: phase margin) . . . 67
5.3 PID controller designed for the different cost functions . . . 70
5.4 PID controller performance assessment with the different time-domain optimisation approaches . . . 71
5.5 Stability margins for the controllers(GM,gain margin:PM,phase margin) . . . 72

5.6 Minimization approach identifiers and constraints for FOPID optimisation (Note: rqd denotes ride quality degradation; GM: gain margin; PM: phase margin) . . . 80
5.7 FOPID optimised parameter values . . . 80
5.8 Stability margins for the conventional PID controllers . . . 81
5.9 FOPID controller performance assessment with the different time-domain optimisation approaches . . . 83
5.10 Robust performance for P_{CT} standing for all conventional cases . . . 85
5.11 Robust performance for ride quality degradation for all conventional cases . . . 85

6.1 Performance assessment (P_{CT} / Ride qual.) under different FO partial cancellation degree (incl. PID) . . . 93
6.2 Stability margins for PID+Q_n^{-1} controller . . . 94
6.3 Robust performance for P_{CT} standing (7th order controller) . . . 100
6.4 Robust performance for ride quality (7th order controller) . . . 101
6.5 Minimization approach identifiers and weight sensitivity parameters(transfer function) for H_∞ Mixed Sensitivity optimization (Note: rqd denotes ride quality degradation) . . . 104
6.6 Minimization approach identifiers and weight sensitivity parameters(transfer function) for H_∞ Mixed Sensitivity optimization for P_{x2NMP} and P_{x2MP} with fixed W_2 and W_3 (Note: rqd denotes ride quality degradation) . . . 104
6.7 H_∞ Mixed sensitivity controller performance assessment with the different time-domain optimisation approaches . . . 105
6.8 H_∞ Mixed sensitivity controller performance assessment with the different W2 values for P_{x2NMP} case. . . . 108
6.9 H_∞ Mixed sensitivity controller performance assessment with the different W_2 values for P_{x2MP} case. . . . 110
6.10 Robust performance for P_{CT} standing for 8th order H_∞ controller . . . 111
6.11 Robust performance for ride quality for 8th order H_∞ controller . . . 113

7.1 Precedence tilt performance . . . 115
7.2 Nominal Performance assessment (P_{CT} / Ride quality (R.Q.)) . . . 117

Abbreviations

APT	**A**dvance **P**assenger **T**rain
ARB	**A**nti **R**oll **B**ar
B/W	**B**andwidth
CT	**C**ontinuous **T**ime
D	**C**ant **D**eficiency
DOF	**D**egree **O**f **F**reedom
FO	**F**ractional **O**rder
FOC	**F**ractional **O**rder **C**ontroller
FOPID	**F**ractional **O**rder **P**roportional **I**ntegrator **D**ifferentiator
F-R	**F**requency **R**esponse
GM	**G**ain **M**argin
GPS	**G**lobal **P**ositioning **S**ystem
HPF	**H**igh **P**ass **F**ilter
IAE	**I**ntegral of **A**bsolute **E**rror
IOR	**I**nteger **O**rder
ITAE	**I**ntegral **T**ime of **A**bsolute **E**rror
LPF	**L**ow **P**ass **F**ilter
MIMO	**M**ulti **I**nput **M**ulti **O**utput
MP	**M**inimum **P**hase
NMP	**N**on **M**inimum **P**hase
NMPZ	**N**on **M**inimum **P**hase **Z**ero
PI	**P**roportional **I**ntegrator
PID	**P**roportional **I**ntegrator **D**ifferentiator
PM	**P**hase **M**argin

rqd	**R**ide **Q**uality **D**egradation
SISO	**S**ingle **I**nput **S**ingle **O**utput
TF	**T**ransfer **F**unction
Z-N	**Z**iegler **N**ichols

Symbols

R	curve radius
g	gravity
δ	actuator position
y_{v}, y_b, y_0	Lateral displacement of body,bogie and railtrack
$\theta_{\mathrm{v}}, \theta_b, \delta_a$	Roll displacement of body,bogie and actuator
θ_0	Rail track cant, curve radius
θ_r	Airspring reservoir roll deflection
v	Vehicle forward speed
m_{v}	Half body mass
i_{vr}	Half body inertia
m_b	Bogie mass
i_{br}	Bogie roll inertia
k_{az}	Airspring area stiffness
k_{sz}	Airspring series stiffness
k_{rz}	Airspring reservoir stiffness
c_{rz}	Airspring reservoir damping
k_{sy}	Secondary lateral stiffness
c_{sy}	Secondary lateral damping
y_w	Bogie kinematics position
f_{t}	Temporal frequency
Ω_l	Lateral track roughness
$\Delta_{(t-i)}$	Ideal control tilt angle
λ_1, λ_2	Tilt percentage compensation

W_Z	Wertungszahl spreling index
W_δ	Multiplicative Uncertainty bound
K_p	PID proportional gain
τ_i,τ_1	PID integrator gain
τ_d,τ_2	PID differentiator gain
N	cut-off frequency
k_u	ultimate gain
T_u,P_u	critical period
α	the ratio of derivative time constant to integral time constant
r_b	gain to introduce by the controller at the given point
φ_b	the phase to introduce by the controller at the given point
λ	integral fractional order PID
μ	derivative fractional order PID
Q_n^{-1}	cancellation fractional order filter
$\tilde{Q}_n^{-1}$	integer order approximation of Q_n^{-1}
Z_u	unstable zero

Dedicated to my beloved children Farhat and Farha...

Chapter 1

Introduction

The history of fast trains in Britain began in early 1899 when Great Central Railway, in one of the early attempts to facilitate higher speed train operation , introduced higher speed trains that used gas turbine engines with a maximum speed of 100 km/h (Parkinson, 2015). From a tilting train viewpoint, British Rail performed substantial research during the 1970s on a prototype train called "Advanced Passenger Train" (APT) (Boocock and Newman, 1976) (although the idea of tilting is older than that,i.e. passive tilting in terms of vehicle coach swing were tried in the 1930s). The APT tilting mechanism involved a tilting bolster that responded to signals from measured lateral acceleration to enable tilt action (the measured signals ultimately being provided by leading vehicles). The maximum tilt angle was 9 degrees (Duffy, 2003). During that time, this type of train was introduced to avoid building new track for higher speed train. The train's maximum speed was about 160mph thus reducing journey time from London to Glasgow by hours. However, due to a number of problems, this project was discontinued in about 1985 (Parkinson, 2015). However, the Italian firm Ferroviaria (acquired by ALSTOM in 2000) bought APT patents and took steps to develop their tilting train called *Pendolino* which is now produced by ALSTOM.

In 2002 Virgin Trains introduced tilting train services in the West Coast line, in particular used Pendolino technology, with top speed of approximately 225 km/h with the service operating to date. SmartRail World presented an article about

the history of the development of tilting trains in UK and Europe (O'Dowd, 2017). Pendolino tilting train evolved to enable CO2 reduction via pollution reduction measures by utilizing advanced energy management (essentially recycling power and distributing subject to demand accordingly) (O'Dowd, 2017).

1.1 Suspension technology

Prior to introducing more technical details relating to tilting trains, some information on generic suspensions for railway vehicles is listed below.

Suspension systems in rail vehicles can be defined as set of elastic elements (usually spring with different materials), dampers and associated component connecting wheel set to the car body (Iwnicki, 2006). Although the concept of suspensions in automotive vehicles and railway carriages is similar, the details are quite different. A particular difference, this being attributed to the evolution of railway vehicles since the 1700s, is that rail vehicles comprise both a bogie (an intermediate mass connected to the wheelsets via primary suspensions that facilitates running safety and guidance) and passenger compartment (connected via secondary suspensions to the bogie and assists to ride quality). As is the case in automotive applications of suspension systems, these in the railway vehicle framework can be also classified into three categories, i.e *passive, semi-active and active*.

Conventional railway vehicles mainly rely on airspring suspensions (passive secondary type) fitted between vehicle bogies and body for ride quality mainly (as these tend to be softer) while primary passive suspension fitted between wheelsets and vehicle bogies for isolation of high frequency motion (Goodall, 1999a). Note that the softer the suspension the better the ride quality (however the worse the suspension deflection which is something that may hinder running safety and gauge limitation violation). For completeness, a typical railway vehicle is shown in Figure 1.1.

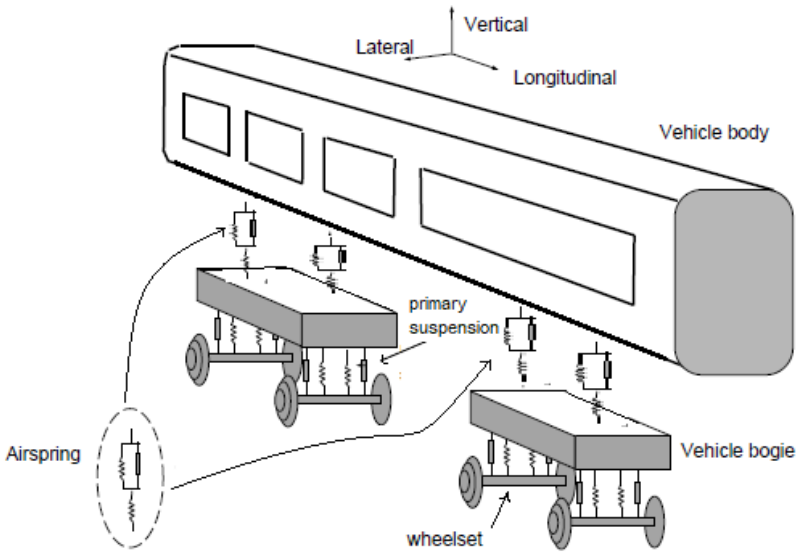

FIGURE 1.1: Conventional railway vehicle mechanical arrangement (Goodall, 1999a)

A passive suspension consists of traditional spring and passive dampers. Conventional passive suspensions are usually configured using coil or leaf springs and viscous damping. Suspensions constrain vehicle motion, the level being defined by how "soft" or "hard" their characteristics are (however, note that vehicle derailment normally occurs at very high speeds or due to cases of suspension failure, hence normally soft suspensions do not necessarily mean higher probability of vehicle overturning but in practice suspensions will not normally be very "soft" in lay terms). The performance of passive suspension solely governed by the values of their system parameters such as damping, spring stiffness and the masses they support. Figure 1.2 shows a schematic diagram of a single suspension illustrating the difference between typical passive and active setups.

A fully active system utilizes the function of sensors, electronic controllers and actuators with an existing mechanical system. The active suspension response of the system is particularly governed by the controller setup and associated control algorithm depending on the application and can be applied to a single or multi-direction, i.e. vertical, lateral, roll, yaw and longitudinal direction. It is widely known that the vehicle dynamic response on curved and straight rail-track can

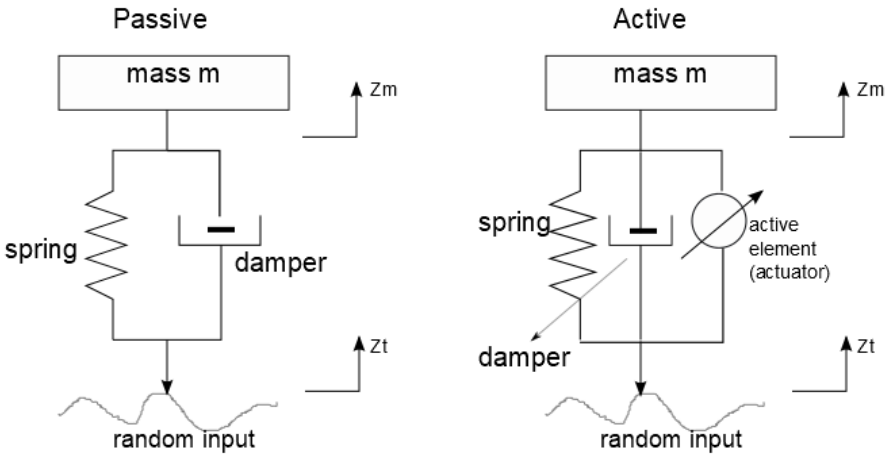

FIGURE 1.2: Passive and active suspension setup

be improved with the introduction of (appropriately designed) active suspensions (Goodall, 1997). A fully actively controlled suspension tends to be complex however the performance is normally better than passive suspension in terms of ride comfort and running safety (assuming that appropriate fault tolerance has been considered) of the high speed train. From a structural point of view, primary active suspension is fitted between wheelsets and vehicle bogie, while secondary active suspension is fitted between vehicle bogies and passenger compartment (vehicle body). Active suspension in the roll direction also known as 'active tilt ' is a form of secondary and acts as means of tilting the vehicle body inwards the rail-track curve. Tilting is the topic of this thesis work and details are discussed next.

1.2 Tilting technology

Tilting is a successful concept of high-speed train operation that offers a solution to enable rail vehicles run faster hence reducing journey times on railway sections with high frequency of corners without the need of substantial change on track infrastructure. The idea is rather straightforward and based on the cycle/motorcycle rider trick of "lean in towards the curve/corner to go faster while still and feeling more comfortable". Similarly, tilting trains lean in towards the railtrack corner

centre (with motion enabled via a tilt mechanism) to reduce passenger lateral acceleration (by emphasizing more gravitational force contribution) thus enabling higher vehicle forward speed. Tilting train technology was highlighted in the 2014 article of BBC future (Moskvitch, 2014) while mentioning the new ZEFIRO tilting train. Tilting trains continue to evolve in terms of their structure and tilt mechanisms (Colombo et al., 2014a) which actually facilitate further exploration of advanced control design.

FIGURE 1.3: Example of tilting trains, Pendolino train(left), Virgin train(middle) and Zefiro train(right)

As mentioned earlier in the thesis, nowadays most tilting trains use a command-driven with precedence tilt control approach devised in the early 1980s as part of the UK-led Advanced Passenger Train development (Boocock and King, 1982). Precedence (or preview) schemes use signals from the vehicle in front to provide preview information which are carefully designed so that the delay introduced by the filtering during communication compensates for the preview time. There have been some further developments of the concept, i.e. use of GPS database and/or additional sensors, but the overall principles essentially remain the same. It is worth noting that achieving a satisfactory local/vehicle tilt control scheme is still an important research question due to facilitating system simplifications and more straightforward fault detection.

1.2.1 Tilt mechanical arrangement

Work in (Zolotas, 2002) discussed on tilting mechanisms rather extensively, however it is important to explain the major points and some details are included here. The

three basic mechanical arrangements for active tilt (active tilt is mainly discussed here, for passive tilt the interested reader can refer to (Zolotas, 2002) and references within) are : *tilt across* (Figure 1.4(a)), *tilt above* (Figure 1.4(c)) and *tilt below* (Figure 1.4(b)) the secondary suspension. The first approach is applying active control to the secondary suspension directly (normally via the Active anti-roll bar setup or control of airsprings) to enable tilt. With tilt across the secondary suspension normally a limited tilt angle is provided i.e. 2-3 degrees of roll action such as in Japanese Series JR-Hokkaido train (Goodall et al., 2000), the case of active anti roll bar(ARB) used in Bombadier's tilting train (Persson et al., 2009) 4 degrees of tilt can be achieved. The ARB is a type of tilt mechanical configuration that is simple to implement and normally added as retrofit to a conventional vehicle (still the tilt amount to be achieved is normally limited). The second approach of mechanical arrangement, tilt above secondary suspension was employed in early Pendolino trains (Goodall et al., 2000). A tilting bolster was fitted above secondary suspension to increase the tilting angle, as a result, the lateral suspension deflection was increased. To avoid this problem, the tilting bolster was moved to below the secondary suspension (i.e. tilt below) is employed together with incline swing link or circular roller beam. This type of tilt mechanism can provide up to 8-10 degrees of tilt (Zolotas, 2002).

This thesis concerns the simple active ARB setup with the assumption that the required tilt angle can be achieved (in fact, the proposed control concepts can be applied to alternative tilt mechanism model setups).

1.3 Quantifying tilt (vehicle roll) action tilting concept

As mentioned earlier, tilting train technology is employed in order to reduce passenger's acceleration during curves hence enable increase of vehicle speed.

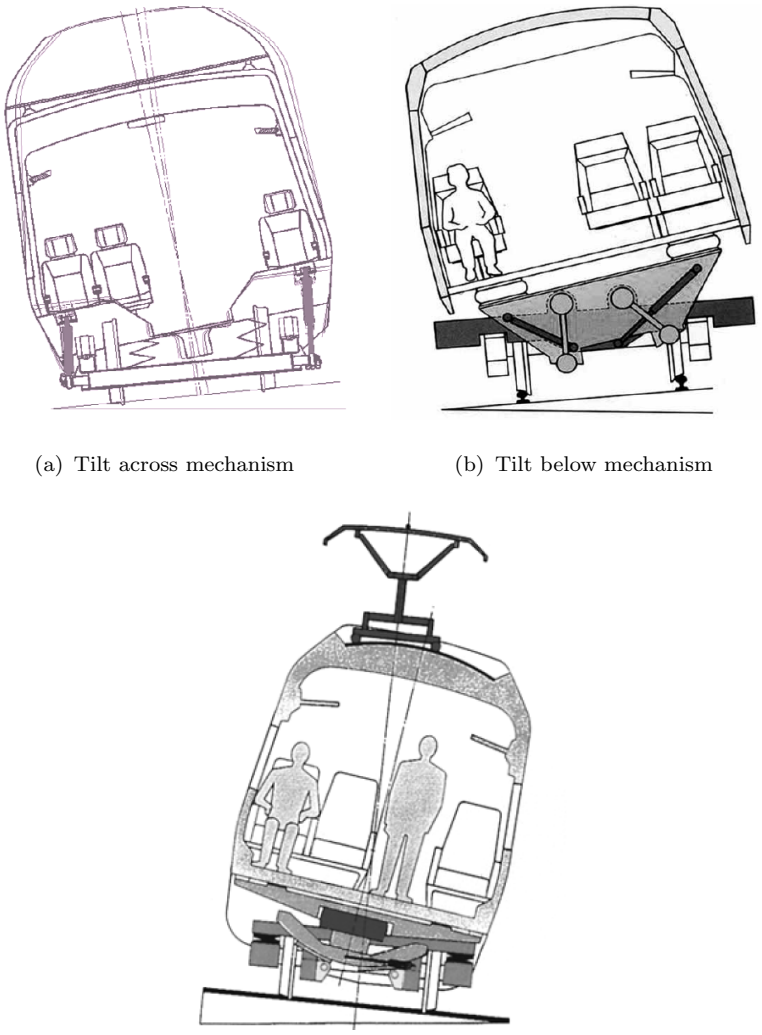

(a) Tilt across mechanism

(b) Tilt below mechanism

(c) Tilt above mechanism

FIGURE 1.4: Example of tilting trains with different tilt mechanism (Goodall, 1999b)

The process of tilting the vehicle body inwards the railtrack curve (corner), towards the curve (virtual) center, includes the concept of "cant deficiency". The term *cant deficiency* refers to a lateral acceleration quantity which defines the difference between the existing degree of cant (track elevation) and the degree required to fully eliminate the effect of centrifugal force at maximum allowable speed of the vehicle (Zolotas, 2002).

Tilting trains can run at higher speeds on curves compared to conventional trains by tilting the vehicle body inwards to compensate the large lateral acceleration. By tilting the vehicle body inwards during curve transition, the amount of lateral force

experienced by the passenger can be reduced and at the same time maintain an appropriate level or improve passenger comfort. (see Figure 1.5 note that θ_v is body roll angle in rad, θ_0 is track cant angle in rad).

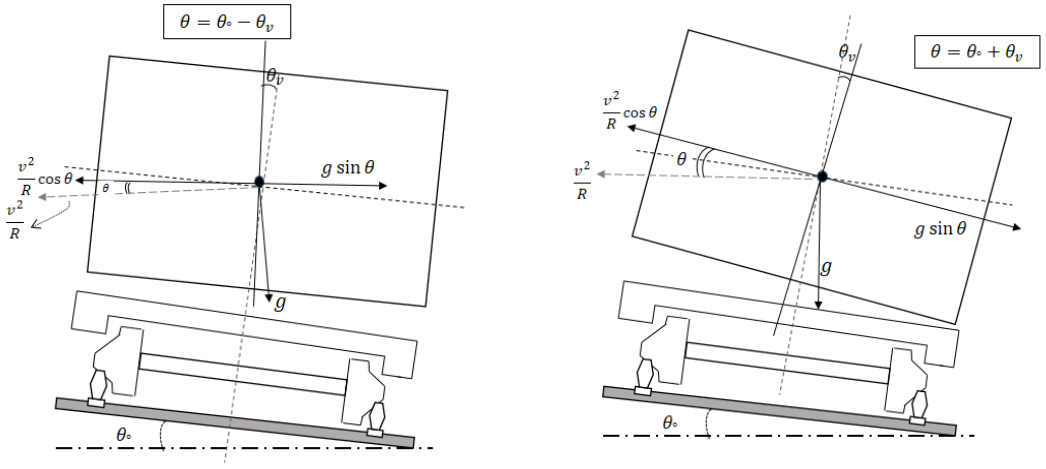

(a) (b)

FIGURE 1.5: Non tilt action (a) and Tilt action(b) (Zolotas, 2002)

Consider a conventional (non-tilting) vehicle, the cant deficiency (D) is given by (Zolotas, 2002),

$$D = \frac{v^2}{R} \times \cos(\theta_0 - \theta_v) - g \times \sin(\theta_0 - \theta_v) \tag{1.1}$$

A way to improve the cant deficiency level is to build rail-tracks with larger cant angle (track elevation) on curved sections of the track (this is followed by an appropriate increase in curve radius). From a geometry point of view, the lateral centrifugal force in Eq. (1.1) is v^2/R where v is vehicle forward velocity in m/s and R is curve radius in m. Increasing vehicle speed, means increase in the lateral force the passenger (and the vehicle) experiences. Examples in this context include, TGV, ICE and bullet trains which include no tilt (or very limited tilt) but run at high speed due to the increased track elevation and in particular the large track curve radius (of the new track infrastructure) (Persson et al., 2009). It has to be noted that for safety (when very low running speed is required due to network incidents, or vehicle stopping on a curved section of the track or parking in stations with track elevated) the track cant angle is limited (not more than 4-6 degrees). Building new

infrastructure can be expensive, and sometimes environmental concerns can bring such a project to a halt. The possibility of using tilting to enable high speed train operation on existing tracks (with an appropriate change in track maintenance due to the increased forces applied to the track, note that tilting trains comprise more advanced bogies that complement the tilt mechanisms) is an attractive alternative solution.

Hence, in the case of a tilting enabled train, the lateral acceleration is given by

$$\ddot{y} = \frac{v^2}{R} \times \cos(\theta_0 + \theta_v) - g \times \sin(\theta_0 + \theta_v) \tag{1.2}$$

Now, θ_v is positive(vehicle rolls inwards the curve), as shown in Figure 1.5. The tilt angle θ_v now adds on the given track cant elevation and this overall action enables, passenger acceleration levels reduction and vehicle speed can be increased (on track corners) (Zolotas, 2002). An example of such improvement is given by (Pearson et al., 1998) where the tilting train in Sweden operating between Stockholm and Gothemburg, has a running time benefit of 10% compared to a non-tilting train. In addition studies performed in Korea by (Rho et al., 2011) have also shown that employing tilting train in Central Line from Cheongnyangni(east Seoul) to Youngju, running time can be reduced to 14%.

1.4 Tilt control considerations

A good tilting system is characterised by its ability to satisfy the challenging trade off of ride comfort and track following during the curved transition (Goodall et al., 2000). Note that some tilting trains comprise systems that switch off the tilt action during straight track sections but this adds extra complexity in the system and is not considered in this work. The tilt control system needs to react quickly to the change of cant deficiency during curve transition while maintaining straight-track ride quality. The tilting process includes: measurement of required tilt angle level and provision of the signal to the controller, the controller commands the tilt

mechanism (via appropriate signal processing and conditioning) and the actuators rotate the vehicle body.

Early tilting trains,comprised the so-called "nulling tilt control" approach based on local vehicle measurements. In particular, an accelerometer was fitted on the vehicle body measuring lateral acceleration and aiming to bring passenger acceleration to zero on steady curve of the rail-track (Goodall, 1999a). Such an approach though increased motion sickness and was found not an appropriate way of providing benefits of tilt (Goodall, 1999a), (Persson et al., 2009). The solution was to also use a portion of the vehicle roll angle(tilt) to enable partial-nulling[1] tilt (normally this is about 60-70%) compensation of lateral acceleration on steady curve. The feedback structure of the partial nulling approach is presented in Figure 1.6. However, the strong lateral/roll model coupling and the inherent delay of feeding the locally measured tilt signals to the controller raised concerns in terms of appropriate (and fast) tilt action at the time (note though that at that time rather basic control methodologies were applied).

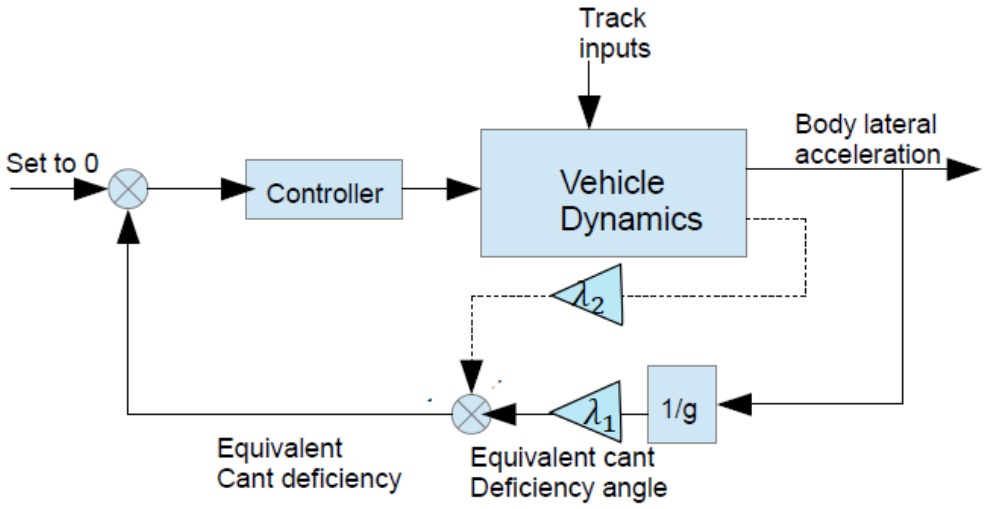

FIGURE 1.6: Partial nulling tilt control set-up

As mentioned earlier, the trend nowadays is to use a command-driven system whereby signal from an accelerometer on a non-tilting part of the previous vehicle

[1] we refer this in the thesis as "nulling" or "nulling-type"

(or front passenger vehicle) commands the required tilting angle, with a straightforward tilt angle feedback controller locally ensuring that each vehicle tilts to the indicated tilt angle (Persson et al., 2009), (Zolotas et al., 2000). The above solution is commonly known as "tilt with precedence" i.e. preview-tilt information from preview vehicle enables a sufficient level of filtering to be applied to remove the effect of track irregularities on the tilt command signal. Although this approach is the currently accepted industrial practice in tilt systems overall tends to be a complex scheme. In particular, amongst other things, it must be reconfigured when the train changes direction and it is also difficult to provide a satisfactory performance for the leading vehicle of the train. It is worth noting that GPS systems, including track database information are used in some cases although issues such as signal, quality communication, delays, and tunnels may affect operation and add to further complexity (Pearson et al., 1998), (Huber, 1998), (Bruni et al., 2007).

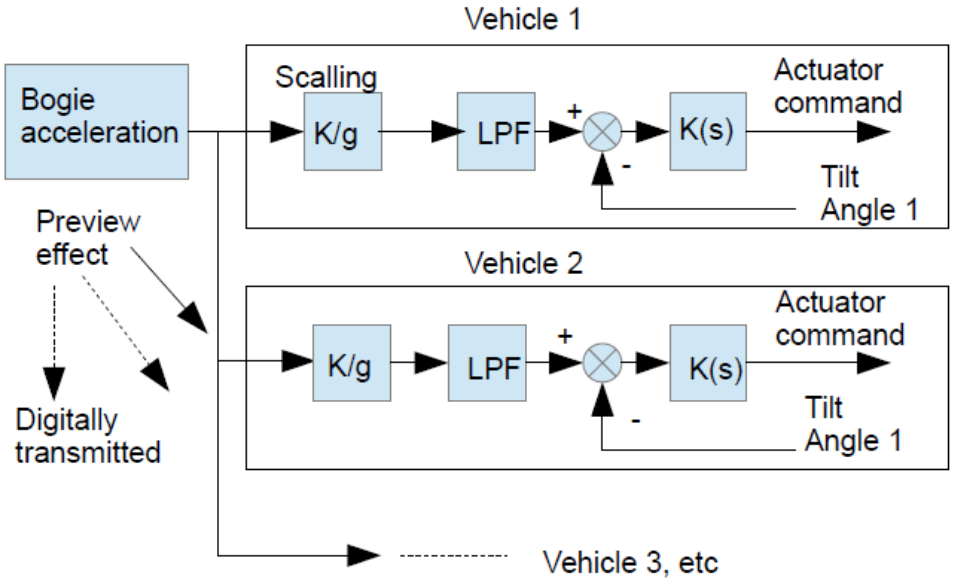

FIGURE 1.7: Precedence command driven control

1.5 Motivation for this thesis work

The work of this thesis is motivated by recent work that illustrated the possibility of utilizing nulling-type tilt control (compared to the more complex precedence

schemes) (Zolotas, 2002), (Zhou, 2010), (Zamzuri, 2008) and further advances in control methodologies. The research question can be summarized as: "Is it possible to provide appropriate tilting action using ONLY single-input-single-output tilt control set-up via advanced control methods and optimization? and what is their impact on the tilt trade-off and relevant robustness?". Essentially, one looks for the simplest tilt control setup but using more elegant control design. This is further supported by the increasing use of non-conventional control methodologies as in the case of *fractional order control* in an increasing number of control applications (details given in the main chapters of the thesis) and alternative considerations of control design for non-minimum phase systems (as is the case of the tilt system in this work) via uncertainty modelling for control.

Therefore main objectives of this thesis are;

- To maintain simple SISO control solution to the active tilt problem.
- To rigorously investigate "modeling for control" taking in account non-minimum phase characteristics in uncertainty considerations.
- To develop advanced robust SISO tilt controllers (including non-rational based solutions) with appropriate stability and tilt performance into account.
- To study robust performance within the tilt control problem.
- To facilitate use of optimization tools in tilt controller design.

1.6 Thesis structure

The structure of this thesis is organized as follows:

- Chapter 2 gives a review of the scientific literature relevant to SISO and MIMO tilt control. The development in controller and different control schemes in local tilt system. Optimisation method and model reduction will also be discussed in this chapter.

- Chapter 3 discussed more on the SISO vehicle modelling and the problem with the existing local tilt with the existence of non minimum phase. It will also investigate the multiplicative uncertainty in the systems.

- Chapter 4 presents a tilt control based on conventional PIDs, i.e Ziegler Nichols, Tyreus Luyben and manually shaped frequency response.

- Chapter 5 presents an optimised PID method via Ziegler Nichols, time domain PID optimisation and Fractional Order PID (FOPID). Robust stability design is also introduced in this chapter.

- Chapter 6 discussed on more robust design of tilt control via loop shaping fractional order controller and H_∞ mixed sensitivity robust design. Due to the nature of the complex controller,reduced order controller is also studied in this chapter. Next,the robustness of the design in investigated in this chapter.

- Chapter 7 presents comparison discussion of the proposed controller designs with precedence tilt.

- Chapter 8 concludes the whole thesis and a description of possible area of research which could be attempted to further this study.

1.7 Publications

A number of outputs have been produced as part of this research study. Published outputs comprise:

Journal papers:

- Hassan, F., and Zolotas, A. C.,*Impact of fractional order methods on optimized tilt control for rail vehicles.* Fractional Calculus and Applied Analysis (FCAA), Deguyter, Volume 20, No 2(2017), pp. 765-789. ISSN 1311-0454, June 2017.

- Hassan, F., Zolotas, A. C., and Margetts, R., *Optimised PID control for tilting trains.* Systems Science & Control Engineering, 5 (1). pp. 25-41. ISSN 2164-2583, January 2017.

- Hassan, F., Zolotas, A. C., and Smith, T., *Optimised Ziegler-Nichols based PID control design for tilt suspension.*[1] Journal of Engineering Science and Technology Review, 10 (5). pp. 17-24. ISSN 1791-2377.

Conference paper:

- Hassan, F., Zolotas, A., and Margetts, R., *Improved PID control for tilting trains.* In Students on Applied Engineering (ISCAE), International Conference for IEEE, pp. 269-274, October 2016. *This paper received the ICSAE 2016 Best Paper award (for the Control Engineering topic).*

1.8 Thesis contributions

This thesis addresses a number of issues concerning SISO tilt system control solutions and the following contributions are listed:

Major:

- The novel idea of employing fractional order control for the nulling-type tilt control problem (this being twofold):

  1. Fractional order based PID solution.
  2. Fractional order based loop-shaping solution.

- Rigorous investigation of optimisation in PID tilt control design and appraisal of its impact to the challenging tilt trade-off.

Minor:

[1] This paper was submitted before the thesis submission, by the time of corrections required after the viva it was an accepted article

- Investigation of the non-minimum phase model characteristics of the SISO tilt system and their mapping to multiplicative uncertainty (i.e. modelling for control).
- Enhanced H_∞ mixed sensitivity design via weight optimization and thorough investigation of the tilt models within this framework (original non minimum phase(NMP) system and the factorised equivalent with uncertainty).
- Investigation of robust performance and robust stability in the framework of SISO tilt control design.

The presented results and outcomes in this thesis, clearly evidence its value in facilitating an effective simple tilt control solution (hence avoiding the more complex structural tilt preview setup) by elegant combination of optimization and robust control design.

Chapter 2

Literature study and survey

2.1 A brief encounter of active suspensions in railway vehicles

As in the case of automotive vehicles, suspensions is an important subsystem of the railway vehicle structure. More importantly when it comes to modern high speed trains, the desire to improve ride quality for passengers facilitates an increased role of designing appropriate active suspensions. A comprehensive discussion on active suspensions in railway vehicles appears in (Goodall, 1997), while more specifically on tilting trains (tilting being classified as a particular form of secondary active suspensions) in (Goodall, 1999c) and (Goodall, 1999b). A furthermore recent study, on more generic discussion in suspensions was performed by (Goodall and Mei, 2006) investigating both active primary and secondary suspension.

From a particular tilting train suspension point of view, a comprehensive review was performed by Zolotas in his thesis (Zolotas, 2002). Moreover, (Zhou et al., 2009) introduced the idea of active lateral secondary suspension to improve tilt performance , essentially forming a MIMO tilt problem, with the aim of attempting to decouple the strongly coupled lateral and roll tilt vehicle modes. (Orvnäs, 2009) developed active lateral suspension system and active vertical secondary suspension system including dynamic control of the lateral/vertical and yaw/roll modes of the

carbody. Both systems are tested on-track and show improvement in ride comfort. The proposed suspension integrated on both active ARB and tilting bolster design model show an improvement in tilt performance. A recent study by (Colombo et al., 2014b) suggested lighter carbody roll using hydraulic actuation as active anti-roll device to replace anti-roll bar (part of active roll suspension) albeit with very tilt angle of 1 to 2 degrees maximum. Whereas, (Qazizadeh et al., 2015) introduced active vertical suspension as part of active secondary suspension on a passenger train to satisfy the need for providing excellent ride comfort with a lighter vehicle carbody.

2.2 Tilting control systems

As mentioned in the introduction of this thesis work, tilting trains lean the body of the vehicle inwards on track corners to reduce lateral acceleration experienced by passengers. Hence, with increased speed (especially on curved sections of the track) journey times are reduced, and the higher the frequency of number of curves in a route the higher the benefits of using tilting trains. (Stribersky et al., 1996) and (Pearson et al., 1998) illustrated the importance of control engineering being the major contributor to modern train vehicle technology, i.e it would be highly challenging to operate efficient tilting train technology without the contributions from control engineering in active tilt. It is of no surprise that nowadays, a large number of modern high speed trains incorporate a form of tilt (Iwnicki, 2006) (Vickerman, 1997) (Fröidh, 2008).

Initial attempts of active tilt control used the so-called nulling-type nature (Zolotas, 2002), a form of economical tilt action as it was based on a SISO control approach. In this context, the tilt action was driven from feedback signal provided by a single lateral accelerometer mounted on the body of the passenger vehicle. Limitations in use and understanding of advanced control techniques at the time and the nature of dynamic coupling constraints in the system, proved to be major challenges for achieving fast tilt response on track corners and maintaining ride quality levels.

The early experience of attempting (full) nulling-type tilt control at the time, necessitated substantial changes which led to the current norm of "tilt with precedence". The latter approach was an intuitive solution to the problem of delayed responses facilitated by the nulling-tilt approach, with the sensor being located on the local-to-tilt vehicle and hence diminish delays in tilt response via use of preview (curve) information. In a nutshell, precedence tilt derives the tilt command signal from the leading vehicle normally with a filter designed in such a way that the delay introduced is compensated by the precedence effect. There has been some development of the concept, including the use of additional sensors (i.e. roll gyroscopes), track database information, GPS signals (Enomoto et al., 2005), (Maki et al., 2003), to further optimise the system response but the overall principles remain the same. Precedence tilt tends to be a complex (in terms of structure) scheme, direction-sensitive, with inter-carriage signal connections required, while the tilt system performance is normally optimised for a specific route operation.

2.2.1 Tilt control mechanisms

Here a brief encounter of tilt control mechanisms is given, although this thesis is solely on SISO tilt systems, listing both SISO type and MIMO type setups.

Active Anti-Roll Bar (ARB). In early studies of single input single output(SISO) tilting control system, (Pearson et al., 1998) on active tilt ARB, both classical and optimal control was presented. Simulations were performed on both a single end-view model and the full vehicle equivalent. Classical control strategies were presented via partial (less than 2.5 degrees of tilt) and full compensation (maximum 2.5 degrees of tilt). The work also discussed on how classical and optimal control approaches dealt with rate responses (i.e. roll rate, jerk levels in acceleration etc.).The need of an estimator was also provided. Furthermore, (Pearson et al., 1998) proposed to combine active lateral suspension with active ARB to achieve higher speeds during curves transition that will be introduced later in MIMO control.

Zolotas in his thesis (Zolotas, 2002) for his tilt model with ARB studied LQR, Estimation-based and H_∞/H_2 robust designs for the nulling-type tilt approach. Illustrated benefits of utilising such advanced control approaches for the tilt control problem and work was disseminated in papers (Zolotas and Goodall, 2000), (Zolotas and Goodall, 2005). A number of open issues with the advanced control methods used in his work were flagged up, and this work is partly motivated by these.

Zamzuri (Zamzuri, 2008), still employing an active ARB setup, followed a rather different approach and investigated the possibility of using intelligent and nonlinear controllers for improved nulling-type tilt control. Work was disseminated in papers i.e. (Zamzuri et al., 2006a), (Zamzuri et al., 2008), (Zamzuri et al., 2010), (Zamzuri et al., 2012). A particular highlight was the proposal of the so-called PID with fuzzy correction (where a fuzzy corrector complemented the effort from the PID controller for the tilting system. As part of this investigated optimised designs via multi-objective genetic algorithm (MOGA and NSGA II) for the tuning of the extra variables. (Zamzuri et al., 2012) also moved to enhance LQG compensators with fuzzy correction for further performance improvement and studied the usefulness of sliding mode controller on tilt control system based on partial nulling tilt control. Results were promising although the complexity of using the complexity of intelligent controller was pointed out.

Tilting mechanism(tilting bolster). (Zolotas, 2002) introduced work on partial nulling tilt control scheme also using an alternative mechanism that of a tilting bolster. This is a tilt mechanism that now allows roll of 10 degrees. The author's work essentially mapped the optimal and estimation control strategies from the ARB setup to that of the above tilt mechanism. In addition, a robust H_∞ loop shaping approach was applied i.e. based on the design process of MacFarlane and Glover (Zolotas, 2002). Once again, improvement and relevant limitations were presented.

Work in (Zhou, 2010) was based on the tilt arrangement (although the author did use this in his ARB setup for completeness as well) of the tilting bolster, and motivated

by suggestions in (Pearson et al., 1998) and proceeded to incorporating a further lateral actuator hence facilitating the use of MIMO-based tilt control designs.

2.2.2 Two actuator based tilt control mechanisms

As suggested in (Pearson et al., 1998), an extra lateral actuator as active lateral secondary suspension is fitted in parallel with secondary damper between vehicle body and bogie. This configuration is employed on both active ARB and tilting mechanism scheme in (Zhou et al., 2009) and (Zhou et al., 2011).From a control point of view now the system has two inputs i.e displacement actuator and lateral actuator which corresponds to a MIMO control setup.

Active ARB+ active lateral secondary suspension. (Zhou et al., 2009) proposed conventional decentralised dual-actuator control(CDAC) on the tilt vehicle with active ARB and extra lateral actuator on 4 DOF vehicle modelling. This approach incorporated skyhook damping strategy with complementary filters, i.e. "Low-pass" + "High-Pass" = "unity". Both high pass and low pass filters, with flat 'Butterworth response', were employed. Partial-nulling tilt was employed to provide 60% compensation (with partial-nulling being the norm in this tilt application for reasons of motion sickness). Genetic algorithm (NSGA_II) is used to tune PI controller in this control scheme. The results via this control scheme showed attenuation in true cant deficiency and body lateral acceleration. To solve this problem, new decentralised dual-actuator control(NDAC) was proposed. Via this approach, Kalman-Bucy filter was employed as estimator in CDAC control scheme. PID controller was combined with first order low pass filter to reduce attenuation at high frequency. The performance trade-off can be achieved. The conventional(classical) decentralised (CD) control strategy was further developed in (Zhou et al., 2010a) employing LQG control and (Zhou et al., July, 2013) with more robust controller, mixed sensitivity H_∞. Tilt performance was improved using both control approaches but the mixed-sensitivity H_∞ classical decentralised approach provided more robust performance. This approach was later embedded in a HIL (Hardware-in-the-Loop)

example and H_∞ controller size was reduced via the Schur method for this implementation.

Tilting bolster with active lateral secondary suspension. A nine DOF full tilting vehicle model with active tilting bolster and active lateral secondary suspension was presented in (Zhou et al., 2010b). Classical decentralised control strategy with 75% partial tilt compensation was employed. A combined PI and phase advance (PA) controller design was used. By applying modal control to the lateral actuator control, lateral and yaw modes interaction was decoupled to facilitate better performance trade-off achievement. The first is CD control strategy based on local tilt control with dual-actuator. The second scheme is Command-Driven decentralised dual-actuator control with precedence solution. The former approach essentially mimicking nulling tilt control strategy as in SISO tilt control system, the latter one mimicking aspects of precedence tilt. More advance control strategies were also introduced in (Zhou et al., 2011), i.e MIMO optimal control and Estimator-Based decentralised. Non-dominated Genetic Algorithm (NSGA_II) was used to optimize PID controller design for the tilt control. Estimator-based decentralised strategy later extended in (Zhou et al., 2014) via robust estimation approach i.e. that of H_∞ filter to deal with system uncertainty.

For completeness, the comparison of feedback control structure between tilt control mechanisms(SISO) and two actuator based tilt control mechanisms(MIMO) presented in Table 2.1.

Although, work on MIMO tilt appears in the literature and raises a number of interesting points for further investigation, still a number of issues to achieve better SISO tilt control remain open and the current thesis aims to contribute to these aspects.

TABLE 2.1: Classification list of SISO control(tilt only) and MIMO control(tilt with lateral)

SISO control	MIMO control
Conventional strategy	
Partial nulling tilt strategy	Classical decentralised control strategy
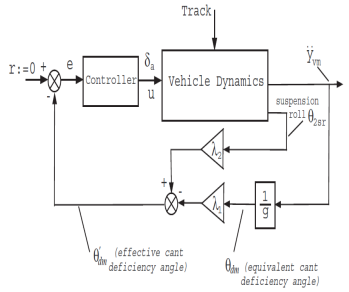	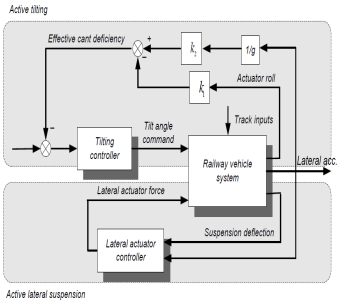
Command driven precedence (precedence)	Classical decentralised precedence
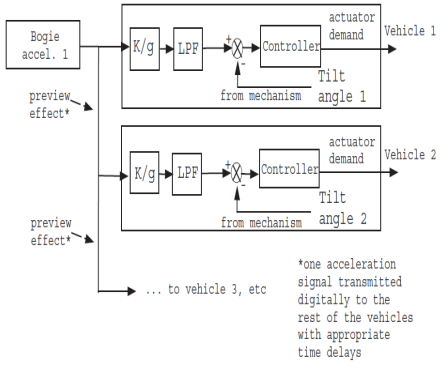	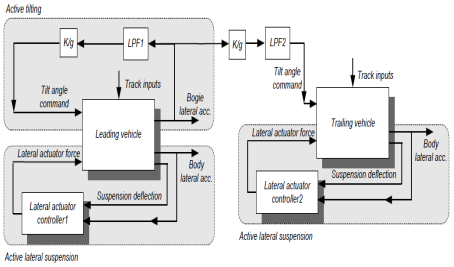
Estimator based control strategy	
Model-based estimator	Estimator based decoupling control
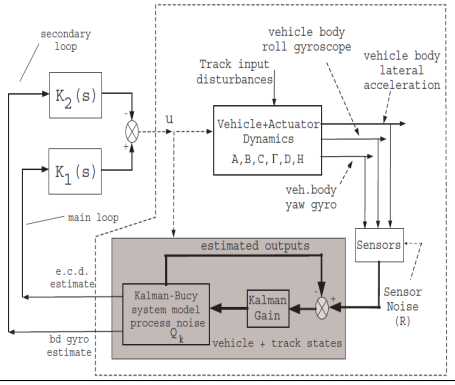	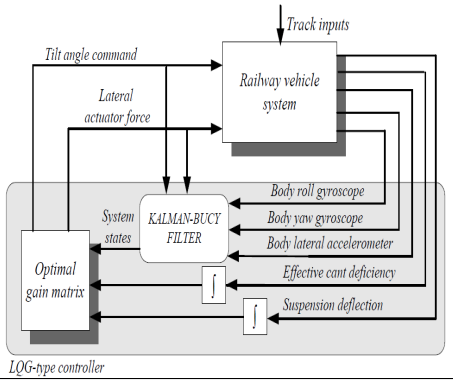

2.3 Optimisation tools in control design

Optimisation tools are used in this thesis work, and as a result a brief discussion is presented here.

There are a number of studies on controller optimisation methods. Some widely used meta-heuristic algorithm i.e Genetic algorithm(GA), Particle Swarm Optimisation(PSO), Simulated Annealing(SA), and others rely upon nonlinear optimization methods such as Nelder-Mead (NM) method. These have been successfully applied in many fields and the results prove that better performance can be achieved compared to manually tuned (classical) controller design. Substantial research has been done on comparison of the popular optimisation methods, for example, comparison in different meta-heuristic method is investigated in (Sabir and Khan, 2014) to find optimal design of PID controller for the speed control of DC motor.

GA optimisation mimicked biological evolution where parents are selected at random population and produce children for the next generation. Constrained and unconstrained population can be solved via this method. Heuristic optimisation methods such as Genetic algorithm(GA) have been used in many railway vehicle research before. Examples of GA applications in railway include the optimisation of wheel profiles in (Persson and Iwnick, 2004) , railway scheduling in (Tormos et al., 2008) and more recent studies on energy-saving train coasting-control in (Lin et al., 2017). In local tilt SISO control studies, GA were used to optimised PID controller parameters with fuzzy correction in (Zamzuri et al., 2006b), (Zamzuri et al., 2008) and (Zamzuri et al., 2012). Moreover, (Zhou et al., 2011) adopted GA in tuning cut off frequency, skyhook damping coefficient, centering control coefficient and PID parameters in MIMO local tilt control.

Simulated Annealing(SA) inspired from process of annealing metallurgy in thermodynamic process where the material is annealed then cooled slowly to produce perfect high-quality end product. SA run random search by finding better neighbour after better neighbour in a given amount of time. The search will stop when no better neighbour can be found. The search outcome may become stuck to a local

minimum though. It needs to run for much longer time to find a global minimum solution. SA has been used in minimizing energy in train operation in recent studies by (Keskin and Karamancioglu, 2017) and (Xie et al., 2012).

Nelder-Mead is a simplex method used to search for a local minimum of a function several variables originally introduced in 1965 by Nelder and Mead (Nelder and Mead, 1965). Simplex is a triangle and pattern search which compares function values of $f(x, y)$ at vertices of triangle. New vertex is replaced when $f(x, y)$ is large. New triangle is generates until the solution shrinkage towards smallest $f(x, y)$. In MATLAB, this non linear searching method is implemented in $fmincon()$ (Yang et al., 2005). This searching method is used in tilting train application for derailment analysis of tilting railway vehicles with wind loads in (Cheng et al., 2012).

2.4 System size reduction

In addition to optimization tools, this thesis presents some aspects of controller reduction and hence it is appropriate to briefly mention this aspect here (the section refers to system size reduction as this can be mapped to both model and controller reduction).

When it comes to advanced control methods in control design, especially robust H_∞ based, or multivariable LQR, LQG or estimator-based, the controller size that results from the design process can be high to very high (relative to the design application that is). Direct examples in the tilt control topic can be seen in (Zolotas, 2002) and (Zhou, 2010).

Early research on model reduction design was done for NASA by (Enns, 1985), the author's work introduced high order controller reduction with appropriate weighting and LQG synthesis based on model reduction attained with appropriate weighting.

Moving to a controller reduction point of view two main approaches can be noted (Obinata and Anderson, 2001)

1. Direct controller reduction design, whereby an approximate reduced order controller is obtained that preserves the required closed loop properties (optimization is used in many cases).

2. Indirect controller-reduction design, whereby first a reduced model of the system is obtained (capturing the important dynamic characteristics of the model) and then a controller is designed using that model version.

For controller reduction purposes in this thesis, a closed-loop controller reduction approach is followed (where the desired closed-loop properties are maintained).

In local tilt vehicle model, physical-based and mathematical-based model reduction are utilised in (Zolotas et al., 2006) on vehicle plant with LQG optimal controller. In physical-based model, the vehicle states are reduced down to 5th and 4th order. Modelling reduction via indirect design is introduced in (Zolotas et al., 2008). The purpose of the design is to minimize complexity and eliminate unnecessary system modes by approximating the dynamic model of the plant using lower order system. It utilizes, system size reduction for control system design suggested in (Obinata and Anderson, 2001). Hardware in the loop design also benefits from system size reduction as seen in (Zhou et al., July, 2013) by reducing controller order down to 5th order H_∞ controller using Schur method (Safonov and Chiang, 1988) for efficient embedded implementation onto FPGA controller.

2.5 Summary

This chapter presented a survey and literature study on suspensions, tilting related system work, a brief encounter on optimization tools and system size reduction. The above form important background information sets that directly linked to aspects presented in this thesis.

Chapter 3

Vehicle modeling and control assessment

3.1 ARB tilt vehicle model

This section will briefly introduce the ARB tilt vehicle model, which will be used for control design. This is a tilt only model, as no lateral actuator is included. The model is based on the work presented in (Zolotas, 2002). The active anti roll bar(ARB) is connected between bogies and the body frame in Figure 3.1 configured by transversely-mounted torsion tube and provides the mechanism for active tilt across the secondary suspension. Please note that the assumption here is that (i) the required tilt angle for the tilt compensation used in this thesis will be provided by the ARB, (ii) there is no hard constraints on secondary suspension lateral deflection. Note that this thesis work does not contribute to the core modeling of the ARB system (as this is already presented before), rather enhances it by investigating "modeling for control" and how the NMP zero characteristics of the plant TF are mapped to relevant uncertainty.

The set of equations for the end-view model can be seen in Appendix A.1.

In fact, this is included to incorporated realistic actuator bandwidth capability. Note that the actuator dynamics parameters are selected to provide damping of

50% and a bandwidth of 3.5Hz (the usually expected dynamic behaviour in railway actuator systems).

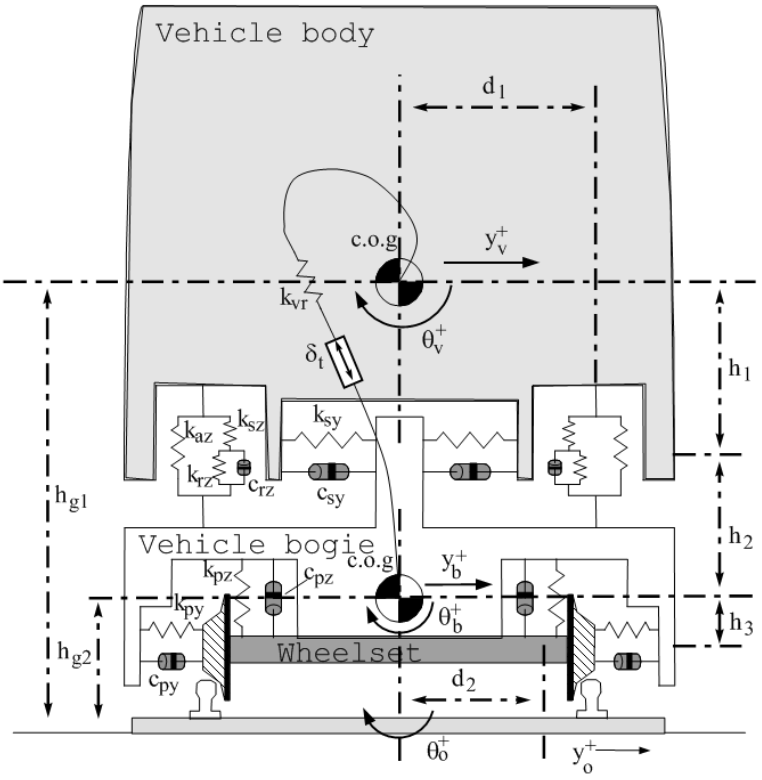

FIGURE 3.1: Tilting vehicle end-view (Zolotas, 2002)

Although in practice the model will be nonlinear, a linearised version on a curved track is a good approximation for analysis and sufficient for designing robust controllers. Note that the overall roll angle from the horizon (track elevation + expected tilt) does not exceed ≈ 14 degrees. The mathematical model (with equations presented in Appendix A.1) can be arranged in the usual state-space form with state equation.

$$\dot{x}(t) = \mathbf{A}x(t)t + \mathbf{B_u}u(t) + \mathbf{B_w}w(t) \tag{3.1}$$

With the state vector, control input and exogenous input vectors being -(t) dropped for simplicity-

$$x = \left[\begin{array}{cccccccccccc} y_{\mathrm{v}} & \theta_{\mathrm{v}} & y_b & \theta_b & \dot{y}_{\mathrm{v}} & \dot{\theta}_v & \dot{y}_b & \dot{\theta}_b & \theta_r & \delta_t & \dot{\delta}_t & y_w & \dot{y}_w \end{array} \right]^T \tag{3.2}$$

$$u = [\delta_{ti}], \quad w = \left[\begin{array}{ccccccc} R^{-1} & \dot{R}^{-1} & \theta_0 & \dot{\theta}_0 & \ddot{\theta}_0 & y_0 & \dot{y}_0 \end{array} \right]^T \tag{3.3}$$

Note that the definition (and values) of parameters/ constants/ variables are presented in Appendix A.2).

The modal analysis is presented in Table 3.1. The percentage of damping represent the ratio between actual and critical damping. Due to the interaction of coupling between lateral and roll modes, resulting upper sway and lower sway modes in Table 3.1. Upper sway mode is sway node appears above the vehicle body c.o.g while lower sway mode located below the vehicle body c.o.g (Zolotas, 2002).

TABLE 3.1: Vehicle modal analysis for the ARB Tilt model (Zolotas, 2002)

Mode	**Damping**	**Frequency**
Body lower sway	16.5%	0.67Hz
Body upper sway	27.2%	1.50Hz
Bogie lateral	12.4%	26.8Hz
Bogie roll	20.8%	11.1Hz
Bogie Lateral kinematics (wheelset filtering)	20.0%	5.00Hz
Air spring	100.0%	3.70Hz
Actuator	50.0%	3.50Hz

From the vehicle equations, a (nominal) design model transfer function (TF), $G_p(s)$ is given by (3.4). This represents the dynamic relationship between effective cant deficiency $Y_{(e.c.d)}$ (for 60% tilt compensation) and the control input $\Delta_{(t-i)}$ (ideal control tilt angle). In fact, the effective cant deficiency is the indicator on how much tilting the train requires to provide the reduction in the passenger acceleration at higher speed. Essentially, the effective cant deficiency maps "partial-tilt".

$$\begin{aligned} G_p(s) = & \frac{27531(s+26.18)(s+40.73)}{(s+23.2)(s^2+1.38s+17.44)(s^2+5.11s+88)} \\ & \cdots \frac{(\mathbf{s-29.36})(\mathbf{s-6.02})}{(s^2+22s+483.6)(s^2+29.15s+4888)} \\ & \cdots \frac{(s^2+7.65s+24.44)}{(s^2+4.825s+15870)(s^2+41.73s+28440)} \end{aligned} \tag{3.4}$$

The effective cant deficiency of the feedback signal is given by

$$\theta'_{dm} = \left(-\lambda_1 \frac{\ddot{y}_{\text{vm}}}{g} + \lambda_2 \theta_{2sr} \right) \tag{3.5}$$

where $\ddot{y}_{\mathrm{vm}}$ is the lateral acceleration felt by the passengers as measured from an accelerometer on the body c.o.g (3.6), and θ_{2sr} is the secondary suspension roll angle (3.7).

$$\ddot{y}_{\mathrm{vm}} = \frac{v^2}{R} - g\left(\theta_o + \theta_{\mathrm{v}}\right) + \ddot{y}_{\mathrm{v}} \tag{3.6}$$

$$\theta_{2sr} = \theta_{\mathrm{v}} - \theta_b \tag{3.7}$$

The parameters λ_1, λ_2 are selected to provide 60% tilt compensation on steady curve (typically $0.6, 0.4$ respectively, under bogie roll-out angle being neglected).

3.2 A note on track exogenous inputs to the vehicle

The excitation (exogenous) inputs that excite the train are the low frequency track disturbance (deterministic track input) and the lateral track irregularities (straight track misalignments in the lateral direction- termed as stochastic track input). In particular, the stochastic track input velocity spectrum is represented by (3.8) (note v is the vehicle speed (m/s) and f_{t} the temporal frequency (this was converted from spatial frequency f_{s} for dynamic analysis)) (Pratt, 1996). The equation 3.8 is derived from approximation expression of spatial spectra of lateral track S_{s}. The full expression and derivation is included in Appendix A.4.

$$\dot{S}_{\mathrm{T}}(f_{\mathrm{t}}) = \frac{(2\pi)^2 \Omega_{\mathrm{l}} v^2}{f_{\mathrm{t}}} \qquad (m/s)^2 (Hz)^{-1} \tag{3.8}$$

Hence, the lateral track velocity represents a coloured noise input and has a steady roll-off as frequency increases. The lateral track roughness used for simulation purposes is $\Omega_l = 0.33 \cdot 10^{-8}$m (representing a typically medium-quality rail track). It is worth noting that for ride quality purposes, we assess the weighted lateral acceleration of passengers by Wertungszahl(W_Z) Sperling index(human factor index

for ride quality) transfer function as given Eq. (3.9) see (Orvnäs, 2009). This filter can be applied to both vertical and lateral motions.

$$W_{Z_{lateral}} = 0.737 \frac{\frac{0.25}{(2\pi)^2}s^2 + \frac{\sqrt{1.911}}{2\pi}s}{\frac{0.0368}{(2\pi)^3}s^3 + \frac{0.277}{(2\pi)^2}s^2 + \frac{1.563}{2\pi}s + 1} \tag{3.9}$$

The deterministic track (curved track) arises from the intended geometrical layout of the rail-track. This is designed by civil engineers to ensure that the effect upon the passengers meets defined comfort requirements. In particular, for tilting trains the deterministic track relates to (curved sections) track segments with measurable curvature (R^{-1}, R being the curve radius from a virtual inwards curve centre). In addition, the track is leaned inwards or "canted" in order to rotate the vehicle inwards (hence, minimise the effect of the centrifugal forces experienced by the passengers). Note that the rates of cant and curvature are changing linearly during the curve transitions, while settling on their steady-state values on steady-state see Figure 3.2.

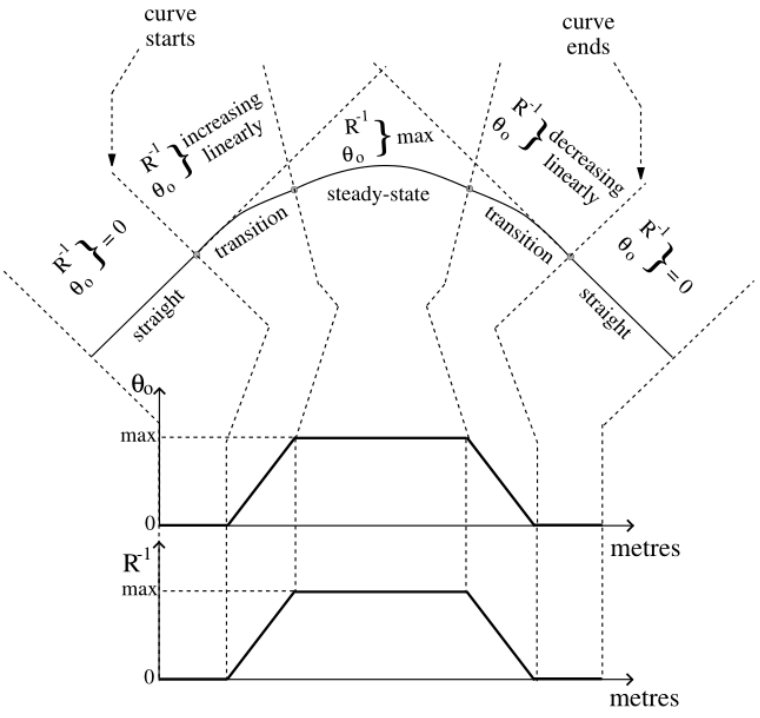

FIGURE 3.2: Representation of deterministic track profile (Zolotas, 2002).

The misalignment characteristics appear at a higher frequency compared to the deterministic input characteristics. Moreover, the control input is the ideal tilt command (processed via the actuator servo). More details on these track characteristics can be found in (Zolotas, 2002). For completeness, the track test case information used for simulation and assessment can be seen on Table 3.2. We note that the (non-tilting) nominal vehicle speed is 45m/s and the (tilting) high speed is 58m/s.

TABLE 3.2: Track profiles used for simulation and assessment (* curved track, † straight track lateral irregularities)

Tilt compensation		**60%**	units
*deterministic track**			
maximum cant angle	$\theta_{o_{\{\max\}}}$	**6.00**	(degrees)
maximum curve radius	$R_{\max}$	**1000.00**	(m)
transition length		145.00	(m) @ each end
track length		1200.00	(m)
stochastic track†			
track roughness	Ω_l	0.33e-8	(m)
track spatial spectrum	S_T	Ω_l/f^3	$\left(\frac{\text{m}^2}{(\text{cycle/m})}\right)$
track length		1200.00	(m)

**Note that work in (Zolotas, 2002) did not concern W_z lateral

3.3 Tilt performance assessment utilised in this work

For tilting trains there is a rather challenging trade-off i.e. deterministic (tilt following response) and stochastic (straight track response/ ride quality). This is assessed via the method proposed in (Goodall et al., 2000). In summary, the following apply

- Investigation of the fundamental tilting response based upon the P_{CT} factor. P_{CT} factor specifies the percentage of seated and standing passengers on a tilting trains feeling uncomfortable on curve transition (based on European standard) (Goodall et al., 2000). The calculation of this percentage value is included in Appendix B.

- Investigation of the transitional dynamic suspension effects via comparison to the *ideal tilting* response are calculated between time interval of 1s before it starts and 3.6s after it ends of the curve transition as follows:

  1. $|\ddot{y}_m - \ddot{y}_{mi}|$, where $\ddot{y}_m$ is actual lateral acceleration [2] and $\ddot{y}_{mi}$ is ideal lateral acceleration. The r.m.s value of deviation $\ddot{y}_m$ from $\ddot{y}_{mi}$. (see Figure 3.3)

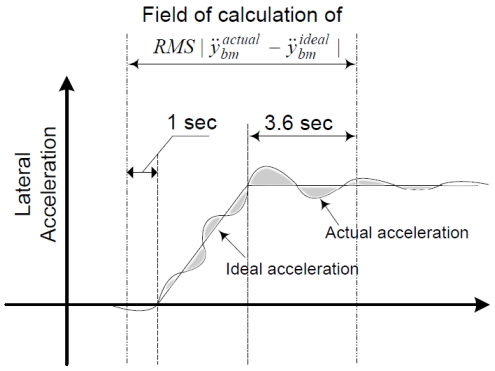

FIGURE 3.3: Ideal and actual lateral acceleration

  2. $|\dot{\theta}_m - \dot{\theta}_{mi}|$, where $|\dot{\theta}_m$, where $\dot{\theta}_m$ is actual absolute roll velocity and $\dot{\theta}_{mi}$ is ideal value of absolute roll velocity. (see Figure 3.4).

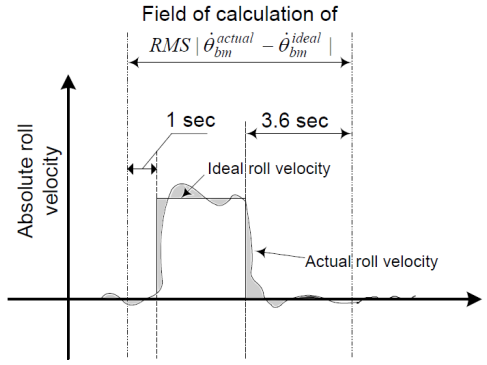

FIGURE 3.4: Ideal and actual absolute body roll velocity

In the case of the stochastic criterion(straight track response), the degradation of lateral ride quality, compared to that of the non-tilting train (done at the same speed) must not exceed 7.5% degradation level (in some cases this is up to 10% but the more constrained case is used here).

[2] Note that a finite jerk level is associated with a typical lateral acceleration profile due to the nature of the railtrack corners (i.e. no discontinuity appears between end of transition and start of steady-state, including ideal acceleration profile)

3.4 Modelling for control

In this section, two aspects of modelling enhancement for control are investigated. The first look into the NMP characteristics of the SISO design transfer function, then moves to factorisation of the original TF into a minimum-phase part and the mapping of the NMP zeros to multiplicative uncertainty. The second aspect is the presentation of parametric uncertainty for the actual NMP model and how this maps to multiplicative uncertainty.

The nature of the NMP zeros of the SISO transfer function is due to the location of the suspension-relative to the centre of gravity of the vehicle body (c.o.g) and the centre of tilt- as well as the roll angle contribution (from portion of the gravitational force) measured by the lateral accelerometer. Due to the complexity of the 17th order design plant(this will be presented in Appendix A.1), symbolic analysis is meaningful on a simpler (physically reduced) 8th order model with air-spring. This result is approximate as it includes only the secondary suspension dynamics (while disregarding bogie, airpring and kinematics contribution). However, the validity of the analysis stands as the neglected modes do not largely affect the NMP zero locations. The 4th order model state equation matrices (state and control respectively) are:

$$A_2 = \begin{bmatrix} 0 & 0 & 1 & 0 \\ 0 & 0 & 0 & 1 \\ -\frac{2\,k_{\mathrm{sy}}}{m_{\mathrm{v}}} & \frac{2\,h_1\,k_{\mathrm{sy}}}{m_{\mathrm{v}}} & -\frac{2\,c_{\mathrm{sy}}}{m_{\mathrm{v}}} & \frac{2\,c_{\mathrm{sy}}\,h_1}{m_{\mathrm{v}}} \\ \frac{2\,h_1\,k_{\mathrm{sy}}+g\,m_{\mathrm{v}}}{i_{\mathrm{vr}}} & -\frac{2\,k_{\mathrm{sy}}\,{h_1}^2+k_{\mathrm{vr}}}{i_{\mathrm{vr}}} & \frac{2\,c_{\mathrm{sy}}\,h_1}{i_{\mathrm{vr}}} & -\frac{2\,c_{\mathrm{sy}}\,{h_1}^2}{i_{\mathrm{vr}}} \end{bmatrix} \tag{3.10}$$

$$B_2 = \begin{bmatrix} 0 & 0 & 0 & \frac{k_{\mathrm{vr}}}{i_{\mathrm{vr}}} \end{bmatrix}^T \tag{3.11}$$

$$C_2 = \begin{bmatrix} \frac{6\,k_{sy}}{5\,g\,m_{\mathrm{v}}} & -\frac{6\,h_1\,k_{sy}-5\,g\,m_{\mathrm{v}}}{5\,g\,m_{\mathrm{v}}} & \frac{6\,c_{sy}}{5\,g\,m_{\mathrm{v}}} & -\frac{6\,c_{sy}\,h_1}{5\,g\,m_{\mathrm{v}}} \end{bmatrix}. \tag{3.12}$$

The state space is used here to illustrate transmission zeros. The state vector includes $\left[y_{\mathrm{v}}, \theta_{\mathrm{v}}, \dot{y}_{\mathrm{v}}, \dot{\theta}_{\mathrm{v}}\right]$ (i.e. body: lateral, roll, lateral rate, roll rate, response).

The output matrices for the output signal refers to the effective cant deficiency for 60% tilt compensation on steady-state curve. For a minimal state space realization invariant and transmission zeros coincide. From a practical point of view, the system zeros refer to the case of a zero output for some non-zero input acting on the system. In fact, the zeros are the solution of $\det\left(RSM(s)\right) = 0$.

Given the simplified 4-state model, the determinant of the above $RSM(s)$ system matrix results to:

(a) a cubic polynomial in s if damping parameter $c_{\mathrm{sy}} \neq 0$

(b) a quadratic polynomial in s if damping parameter $c_{\mathrm{sy}} = 0$

(a) For case $c_{\mathrm{sy}} \neq 0$ the characteristics of the system give negative cubic discriminant, and its roots comprise a real root and a complex pair. The real root is positive (reflecting the location of the slow NMP zero) and, after tedious calculations (and extended symbolic analysis), given by

$$\begin{aligned} z_p = \ldots \\ \ldots + \sqrt[3]{\sqrt{r_{fc}} - \frac{\left(\frac{k_{\mathrm{sy}}}{c_{\mathrm{sy}}} - \frac{5\,g\,m_{\mathrm{v}}}{6\,c_{\mathrm{sy}}\,h_1}\right)^3}{27} - \frac{5\,g\,\left(\frac{9\,k_{\mathrm{sy}}}{c_{\mathrm{sy}}} - \frac{15\,g\,m_{\mathrm{v}}}{2\,c_{\mathrm{sy}}\,h_1}\right)}{162\,h_1} + \frac{5\,g\,k_{\mathrm{sy}}}{6\,c_{\mathrm{sy}}\,h_1}} \\ \ldots + \sqrt[3]{-\sqrt{r_{fc}} - \frac{5\,g\,\left(\frac{9\,k_{\mathrm{sy}}}{c_{\mathrm{sy}}} - \frac{15\,g\,m_{\mathrm{v}}}{2\,c_{\mathrm{sy}}\,h_1}\right)}{162\,h_1} - \frac{\left(\frac{k_{\mathrm{sy}}}{c_{\mathrm{sy}}} - \frac{5\,g\,m_{\mathrm{v}}}{6\,c_{\mathrm{sy}}\,h_1}\right)^3}{27} + \frac{5\,g\,k_{\mathrm{sy}}}{6\,c_{\mathrm{sy}}\,h_1}} + \\ \ldots + \frac{5\,g\,m_{\mathrm{v}}}{18\,c_{\mathrm{sy}}\,h_1} - \frac{k_{\mathrm{sy}}}{3\,c_{\mathrm{sy}}} \end{aligned} \tag{3.13}$$

with

$$\begin{aligned} r_{fc} = \frac{\left(\frac{2\left(\frac{k_{\mathrm{sy}}}{c_{\mathrm{sy}}} - \frac{5\,g\,m_{\mathrm{v}}}{6\,c_{\mathrm{sy}}\,h_1}\right)^3}{27} + \frac{5\,g\left(\frac{9\,k_{\mathrm{sy}}}{c_{\mathrm{sy}}} - \frac{15\,g\,m_{\mathrm{v}}}{2\,c_{\mathrm{sy}}\,h_1}\right)}{81\,h_1} - \frac{5\,g\,k_{\mathrm{sy}}}{3\,c_{\mathrm{sy}}\,h_1}\right)^2}{4} \ldots \\ - \frac{\left(\frac{\left(\frac{k_{\mathrm{sy}}}{c_{\mathrm{sy}}} - \frac{5\,g\,m_{\mathrm{v}}}{6\,c_{\mathrm{sy}}\,h_1}\right)^2}{3} + \frac{5\,g}{3\,h_1}\right)^3}{27} \end{aligned} \tag{3.14}$$

Note that finding the complex pair of roots is not necessary as, for the tilt system, these naturally reflect the stable complex zero location (which do not impose particular design concerns).

(b) For the case $c_{\mathrm{sy}} = 0$ the state matrix becomes

$$A_2|_{(c_{\mathrm{sy}}=0)} = \begin{bmatrix} 0 & 0 & 1 & 0 \\ 0 & 0 & 0 & 1 \\ -\frac{2\,k_{\mathrm{sy}}}{m_{\mathrm{v}}} & \frac{2\,h_1\,k_{\mathrm{sy}}}{m_{\mathrm{v}}} & 0 & 0 \\ \frac{2\,h_1\,k_{\mathrm{sy}}+g\,m_{\mathrm{v}}}{i_{\mathrm{vr}}} & -\frac{2\,k_{\mathrm{sy}}\,{h_1}^2+k_{\mathrm{vr}}}{i_{\mathrm{vr}}} & 0 & 0 \end{bmatrix} \tag{3.15}$$

(the remaining state space matrices change accordingly) and the result greatly simplifies to a set of real roots. The positive root relates to the aforementioned NMP zero, i.e.

$$z_p|_{(c_{\mathrm{sy}}=0)} = \sqrt{\frac{10\,g\,k_{\mathrm{sy}}}{6\,h_1\,k_{\mathrm{sy}} - 5\,g\,m_{\mathrm{v}}}}$$

The contribution of the suspension location and lateral-roll dynamic coupling can be clearly seen (note that a torque providing positive roll will reflect to an opposite lateral motion of the body).

Remark: The location of the lower frequency NMP zero, with respect to symbolic parameters presented in this analysis, is an approximation of that of the actual model TF (it is expected that bogie, airspring, actuator, kinematics introduce minor secondary effects). For completeness, results are also given numerically here i.e.

$$z_p|_{(c_{\mathrm{sy}}=0)} \approx 7.35 \quad \text{(4-state model, no damping)} \tag{3.16}$$

$$z_p|_{(c_{\mathrm{sy}}\neq 0)} \approx 5.47 \quad \text{(4-state model, with damping)} \tag{3.17}$$

$$z_p = 6.02 \quad \text{(13th order model)} \tag{3.18}$$

Note that the simplified 4th order model with no damping reflects a slightly slower NMP zero location. This analysis refers to the NMP zero closer to the origin as this is the major obstacle regarding achievable bandwidth for the designed system. The simplified model used here is not employed for design purposes, however the

analysis presented here enables discussion in the robustness assessment using the full order TF (i.e. how parameter change impacts dynamic characteristics).

3.4.1 Usefulness of multiplicative uncertainty representation for robust control design

Representing system uncertainty in a lumped, multiplicative in nature, setup greatly simplifies robust control design. It is very well suited to H_∞ design schemes, although does introduce some conservativeness in the design (as it represents uncertainty by a disk relative to the chosen nominal model at each frequency in the frequency domain (Skogestad and Postlethwaite, 2007). Despite the conservativeness, and regarding the topic presented in this thesis, it offers a natural way of including a frequency domain bound (esp. for robust stability) within the constrained optimization schemes for the tilt controller design. For a number of uncertainty representations the interested reader is referred to (Skogestad and Postlethwaite, 2007) and references within.

Below, three alternative plant families are presented for the particular model used in this thesis (in the of factorised model form with multiplicative uncertainty).

$$\mathbf{\Pi_i}: \quad G_{pp}(s) = G_{nmp}(s)\left(1 + W_i(s)\Delta_i(s)\right) \tag{3.19}$$

$$\mathbf{G_p}: \quad G_{nmp}(s) = G_{mp}(s)\left(1 + W_\Delta^{uz}(s)\Delta^{uz}(s)\right) \tag{3.20}$$

$$\mathbf{\bar{\Pi}_i}: \quad \bar{G}_{pp}(s) = G_{mp}(s)\left(1 + \bar{W}_i(s)\bar{\Delta}_i(s)\right) \tag{3.21}$$

Here we look into the way of factorising the nominal NMP model into a MP part and the NMP zeros as multiplicative uncertainty bound. Referring to Eq. (3.21) above, the transfer function plant with Non minimum phase zeros in 3.4 can be rearranged as follows,

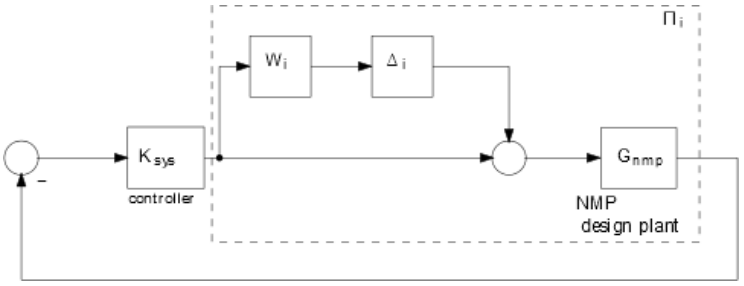

(a) The plant family $\mathbf{\Pi_i}$ for the NMP system model

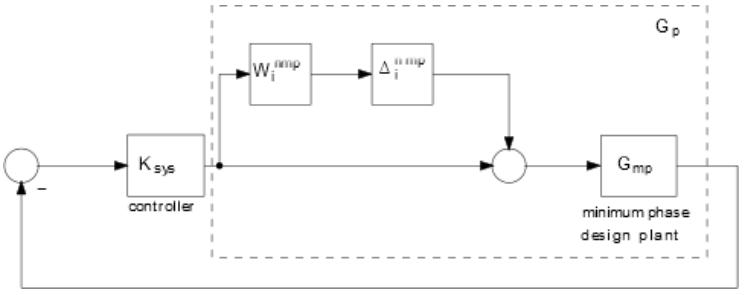

(b) The factorized nominal NMP model

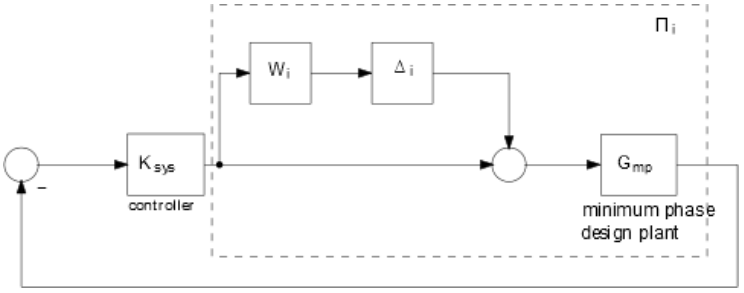

(c) The overall uncertainty when considering the nominal MP model

FIGURE 3.5: Feedback setup with multiplicative uncertainty

$$G_p(s) = G_{mp}(s)G_{allp}(s) \tag{3.22}$$

where $G_{allp}(s)$ is an all-pass transfer function (comprising the NMP zeros). This can be represented in the form of multiplicative uncertainty, as in (3.20), quite straightforwardly.

$$G_{nmp}(s) = G_{mp}(s)\left(1 + W_\Delta(s)\Delta(s)\right) \tag{3.23}$$

Recall that $\Delta^{uz}(s)$ is any stable transfer function where $\Delta^{uz}(j\omega) \leq 1$. In this

particular case, the following multiplicative uncertainty bound covers the NMP zeros of the system with its magnitude plot shown in Fig. 3.6(a),

$$W_{\Delta}^{uz}(j\omega) = \frac{-j70.76\omega}{(176.7 - \omega^2) + j35.38\omega} \tag{3.24}$$

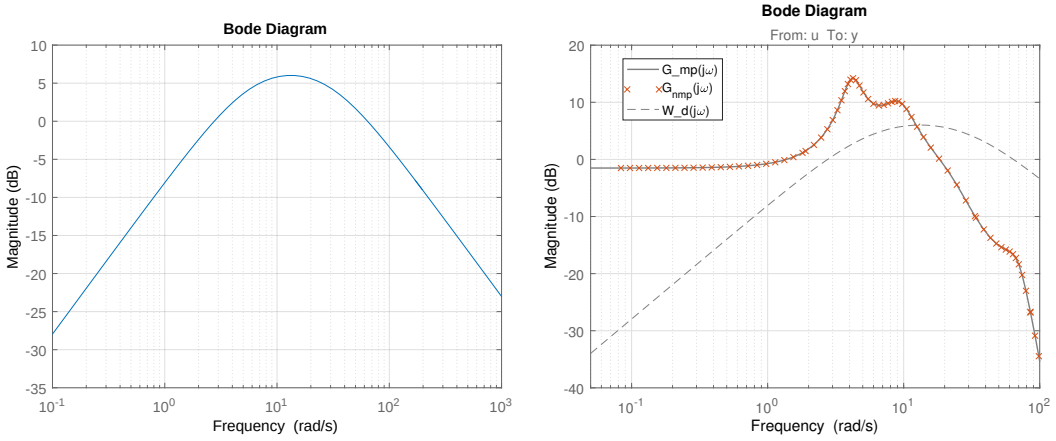

(a) NMP portion shown as multiplicative uncertainty bound

(b) Design models and uncertainty bound

FIGURE 3.6: Nominal model MP and multiplicative uncertainty factorisation results

By introducing some conservativeness with the NMP zeros represented in the form of multiplicative uncertainty, the design model (nominal) is denoted $G_{mp}(s)$. Note how the uncertainty is mainly located in the band-pass of the two NMP zero frequencies. $G_{mp}(s)$ transfer function is,

$$G_{mp}(s) = \frac{27531(s + 40.73)(s + 29.36)(s + 26.18)(s + 6.019)}{(s + 23.21)(s^2 + 1.376s + 17.44)(s^2 + 5.112s + 88.02)} \\ \frac{(s^2 + 7.651s + 24.44)(s^2 + 4.825s + 1.587 \times 10^4)}{(s^2 + 21.99s + 483.6)(s^2 + 29.15s + 4888)(s^2 + 41.73s + 2.844 \times 10^4)} \tag{3.25}$$

This also illustrates the clear challenge on fast tilt responses for the nominal model from an analytical point of view.

3.4.2 On the uncertainty of the original NMP model transfer function

An alternative representation of the nominal design TF in a factorised (MP+multiplicative uncertainty bound for the NMP zeros) was presented. Here, we discuss few points on general uncertainty on the actual design TF (including NMP zeros).

In order to ensure the robustness in the performance of the system, the controller must satisfy both nominal and robust stability (in fact, to achieve the control specifications one should strictly talk about performance rather than just stability- here though we only refer to bounds for stability). We present a simple way to represent the parametric uncertainty on the actual design TF (including NMP zeros) in the form of multiplicative uncertainty. Although the case in the previous subsection was easy to get in an analytical way, here the bound is obtained in the form of an envelope covering the multitude of frequency responses.

First we commence with the choice of 4 plant perturbations (in addition to the nominal one noted P0), i.e. see Table 3.3.

TABLE 3.3: Perturbed plant cases

Plant ID	**Perturbation**
P1	20% body mass increase [3]
P2	20% body mass decrease
P3	20% decrease in dynamic body mass and 40%(20%) decrease (increase) in secondary suspension damping (stiffness)
P4	20% increase in dynamic body mass and 30%(20%) decrease (increase) in secondary suspension stiffness (damping)

The rationale behind the parameter perturbation choice is as follows: the variation of vehicle body mass serves as a mechanism to affect (vehicle dynamics) but in particular NMPZ locations, while the variation of the listed secondary suspension parameters will affect vehicle dynamics (but not the NMPZ locations). Hence,

3 In nominal model, body mass is measured when the vehicle is full with seated passengers

offering a wider level of assessing performance under uncertainty (rather than just linking to non-minimum phase location uncertainty).

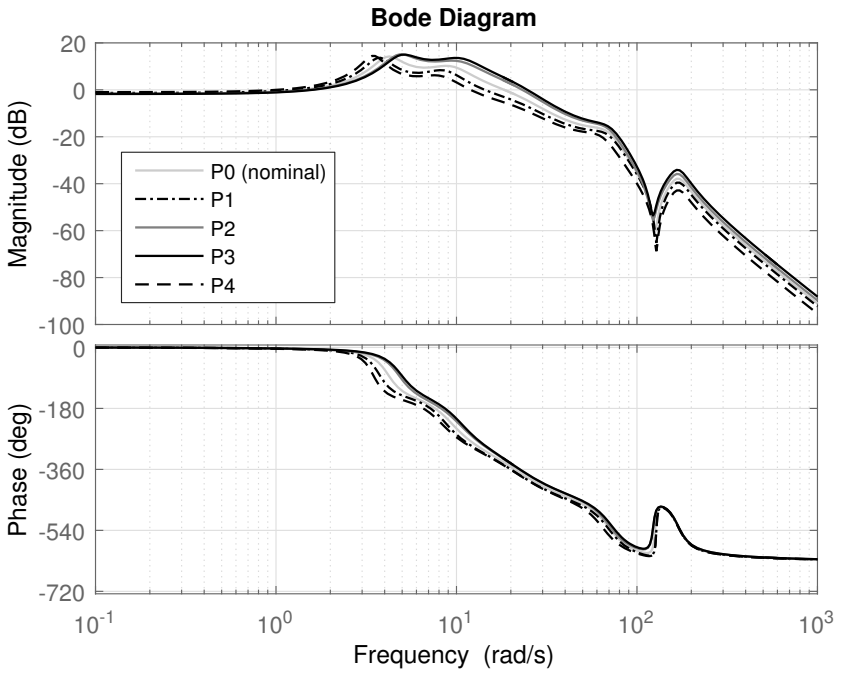

FIGURE 3.7: Plant uncertainty plot

Pole and zero locations for the perturbed plant cases for G_{pert} (nominal plant with non minimum phase zeros-P1,P2,P3 and P4) are displayed in Table 3.4 and Table 3.5. The following are noted: (i) varying vehicle body mass affects NMP zero locations of the perturbed plant, (ii) increase on body mass of the vehicle (cases P1 and P4) forces a 13% increase in the frequency of the "slow" NMPZ and a 25% decrease in the frequency of the "faster" NMPZ compared to the nominal plant case P0, (iii) decrease in vehicle body mass (cases P2 and P3) forces a 9% decrease in the frequency of the "slow" NMPZ and a 36% increase in the frequency of the "faster" NMPZ compared to the nominal plant case P0, (iv) varying secondary suspension (airpsring and roll) damping and/or stiffness does not affect the unstable zero locations as expected (note that only the lateral suspension characteristics have an impact on NMPZ locations).

Here, in obtaining the multiplicative uncertainty bound, both perturbed plant for G_p and G_{mp} is considered. W_δ must covered relative bound(relative error) as in Eq.

TABLE 3.4: Pole locations for plant P0-4

P4	**P3**	**P2**	**P1**
$-20.84 \pm 167.39j$	$-20.88 \pm 167.24j$	$-20.86 \pm 167.23j$	$-20.87 \pm 167.42j$
$-14.03 \pm 63.36j$	$-15.56 \pm 70.77j$	$-14.51 \pm 68.47j$	$-14.62 \pm 68.32j$
$-2.258 \pm 7.89j$	$-3.03 \pm 10.17j$	$-3.167 \pm 9.864j$	$-2.15 \pm 8.37j$
$-0.45 \pm 3.44j$	$-0.97 \pm 4.83j$	$-0.892 \pm 4.714j$	$-0.56 \pm 3.68j$
-13.578	-47.28	-23.13	-23.27
$-11 \pm 19.05j$	$-11 \pm 19.05j$	$-11 \pm 19.05j$	$-11 \pm 19.05j$

TABLE 3.5: Zero location for plants P0-4

P4	**P3**	**P2**	**P1**
$-1.67 \pm 127.97j$	$-3.54 \pm 122.83j$	$-3.54 \pm 122.83j$	$-1.67 \pm 127.97j$
22.08	**39.9**	**39.9**	**22.08**
6.823	**5.465**	**5.466**	**6.823**
-39.516	-43.51	-43.51	-39.516
$-3.45 \pm 3.285j$	$-4.24 \pm 2.89j$	$-4.24 \pm 2.89j$	$-3.45 \pm 3.285j$
-15.273	-52.364	-26.182	-26.182

(3.26).

$$\left| \frac{G_{pert}(jw) - G_{nom}(jw)}{G_{nom}(jw)} \right| \leq |W_\delta(w)| \tag{3.26}$$

The multiplicative bound W_δ is actually given by is,

$$W_\delta = \frac{0.5481s^4 + 10.31s^3 + 143.7s^2 + 228s + 186.3}{s^4 + 9.505s^3 + 240.8s^2 + 454.3s + 2555} \tag{3.27}$$

The 4th order bound in (3.27) is sufficient to cover the perturbations, see Figure 3.8(a).

We also take one step further to establish a more conservative multiplicative robustness bound if the nominal plant now changes to the factorised MP model given in (3.28). In such case the perturbed plant covers the actual NMP plants P0-P4. A 6th order bound is required to cover the responses (see Figure 3.8(a), and is given below

$$W_{\delta MP} = \frac{0.9231s^6 + 76.16s^5 + 388s^4 + 7882s^3 + 1.388 \times 10^4 s^2 + 9.361 \times 10^4 s + 1.332 \times 10^4}{s^6 + 28.85s^5 + 394.6s^4 + 3470s^3 + 2.438 \times 10^4 s^2 + 4.888 \times 10^4 s + 2.179 \times 10^5} \tag{3.28}$$

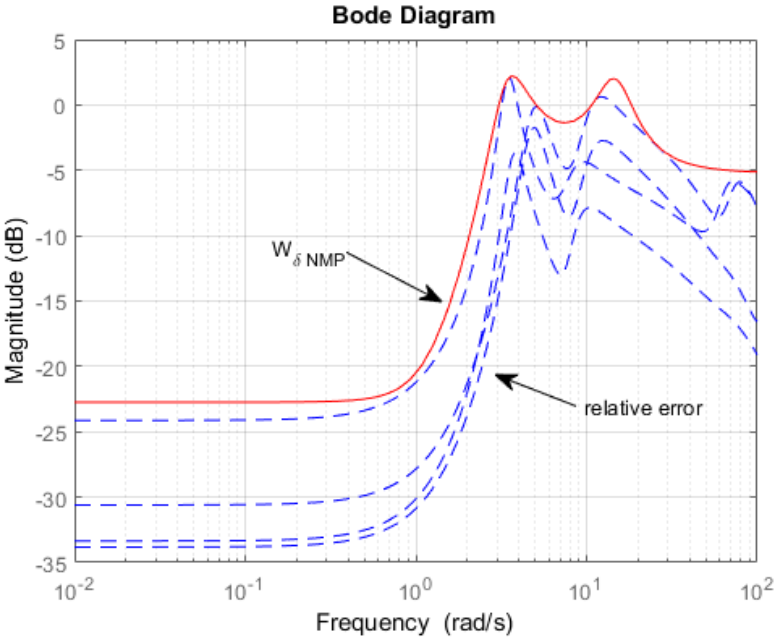

(a) Multiplicative bound $W_{\delta_{NMP}}$ for G_p plant case

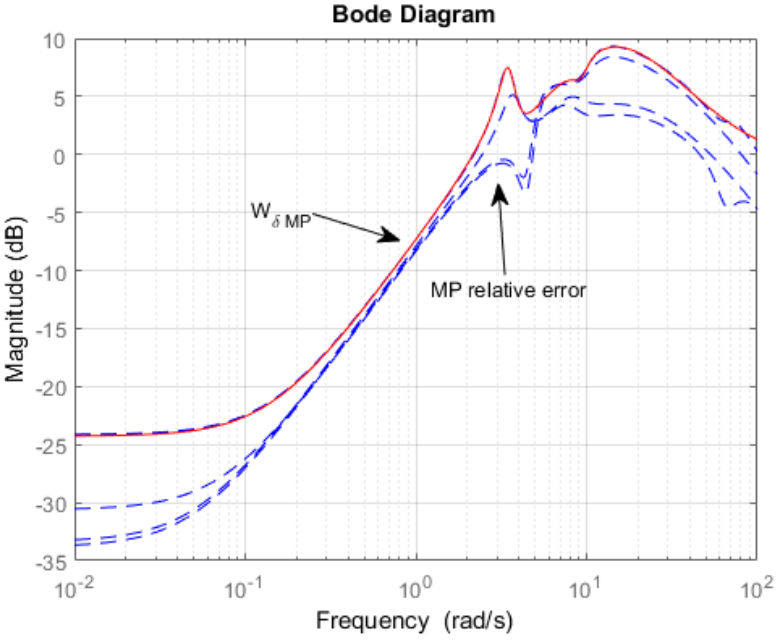

(b) Multiplicative uncertainty bound $W_{\delta_{MP}}$ for $G_m p$ plant case

FIGURE 3.8: Multiplicative uncertainty bound with relative error

With the latter representation we illustrate the increasing conservativeness depending on which nominal model can be utilised for attempted robust control designs. These models are actually revisited in the robust H-infinity design later on in this thesis.

3.4.3 A note on use of random plant perturbations

Recently, an increasing number of robust control designs uses random perturbations on the plant. In fact, Matlab has dedicated functions that cater for this type of representation of uncertainty. Here, we present a brief encounter of such representation and how it relates to the fixed ones presented above.

Here, plant with random perturbation is presented as follows, 20% (upper and lower) change in body mass, 20% change in secondary vertical suspension (stiffness) and 20% roll suspension damping (stiffness). The frequency plot for this random 20% perturbed plant is shown in Figure 3.9.

Multiplicative uncertainty $W_{\delta rand}$ for this random perturbed plant can bee seen in Figure 3.10 alongside the bound obtained for the fixed perturbed cases previously. Although, the randomized plant perturbations can increase in percentage this will also affect the reality of the uncertainty scenario in the railway vehicle application. Hence, the representation using fixed set of plant perturbations present a more realistic scenario for analysis purposes in this thesis.

3.5 Summary

This chapter introduces the SISO vehicle modelling for local vehicle tilt control. An insight into the NMP characteristics of the design TF was included. In addition, the chapter presented information on track inputs, control assessment followed and modeling for control aspects (plant uncertainty) as well as a brief note on system size reduction.

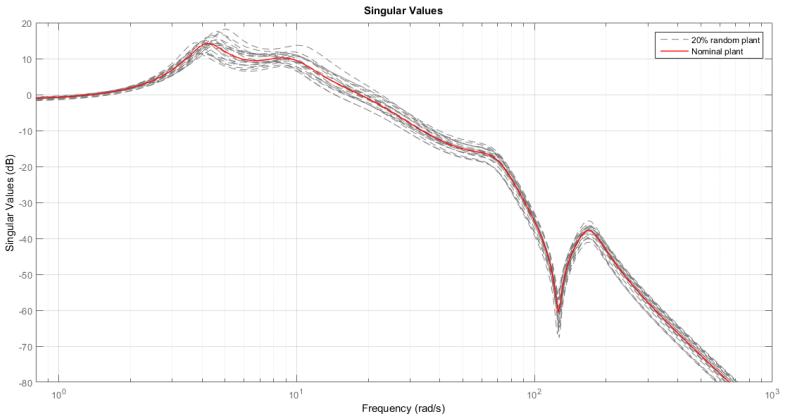

(a) Bode frequency plot of 20% random plant(grey –) and nominal plant (red)

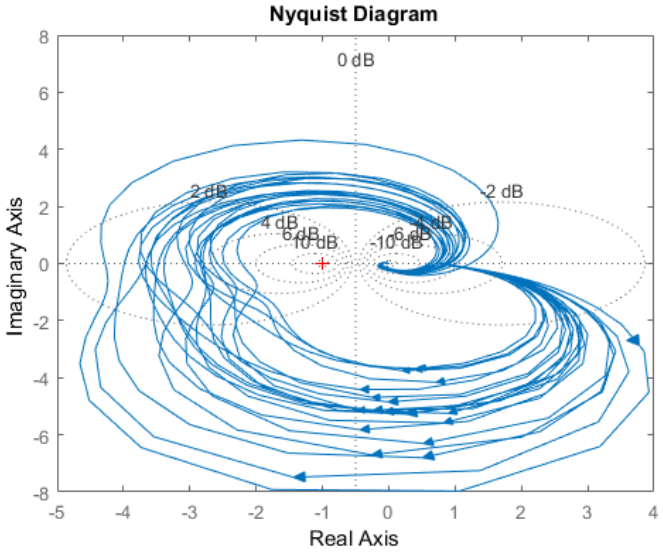

(b) Nyquist plot for 20% random plant

FIGURE 3.9: Random perturbed plant with 20% change in body mass, secondary vertical suspension and roll suspension damping

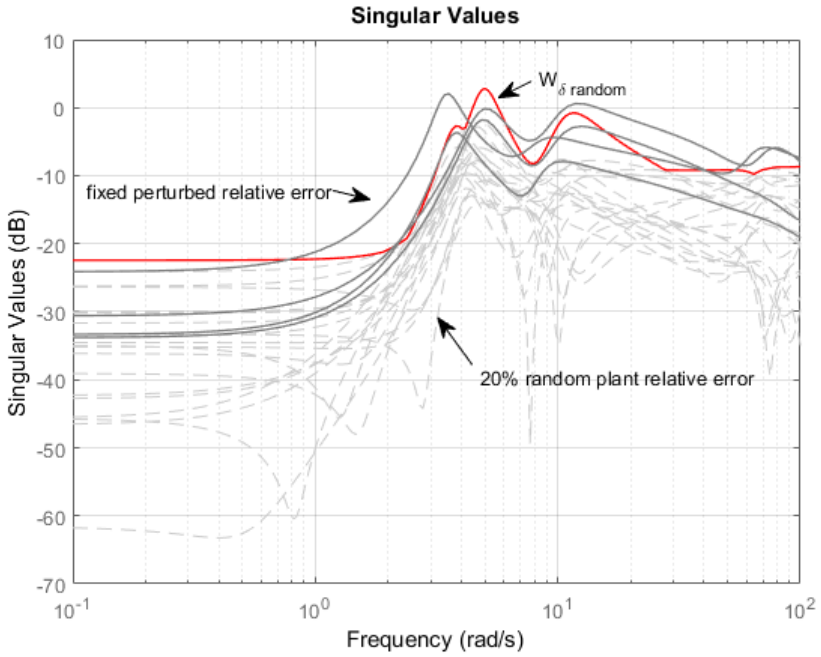

FIGURE 3.10: Multiplicative uncertainty bound for 20% relative error and fixed perturbed plant relative error

Chapter 4

Conventional PID design for the ARB tilt system

This chapter discusses conventional PID control design of nulling-type nature (as is the nature of the problem addressed in this thesis work). Basic conventional PID nulling-type control is revisited (preliminary work has appeared in (Zolotas, 2002)) and a more detailed analysis is performed (including discussion on alternative PID control manual tuning rules). The purpose is to demonstrate the performance limitations of basic (non-optimisation based) PID nulling-tilt control approach and to pave the way towards the optimization approaches and alternative control design approaches that follow on in the next chapters. As mentioned previously in the thesis, using the ARB vehicle model, to allow for the application of full tilt angle for partial compensation purposes it is assumed that:

(a) The active anti-roll bar is able to provide full tilt angle action, i.e. no limitation on tilt angles is imposed by suspension clearance (this can be possible in practice by having a single central airspring, rather than two airsprings) and allows tilt angles up to 8-10 degrees).

(b) No bumpstop limits arise within the required interval of tilt action. In reality, this depends upon available loading gauge applied to a given route in order to ensure that a railway vehicle will not collide with a lineside or overline structure (such as

station platforms, canopies, overhead power supplies (catenary) overbridges, tunnels) (Zolotas, 2002).

4.1 Proportional Intergral Derivative(PID)

P+I+D (Proportional +Integral + Derivative) controllers are a popular simple classical type of controllers used in a large number of industrial applications (Rocco, 1996) (Quevedo and Escobet, 2000) (Chen et al., 2015) (Diba et al., 2014) (Gopi Krishna Rao et al., 2014) including some simple quarter-car suspension systems (Popovic et al., 2000). It is of no surprise that it also forms the simplest conventional controller for the tilting active control application, as it offers both the integral action required to force zero effective cant deficiency on steady-curve and the proportional/derivative action to limit phase lag at higher frequencies (compared to the crossover frequency). In this context, conventional P+I and fuzzy P+I+D controllers have been investigated in tilt control previously (Zolotas et al., 2000), (Zamzuri et al., 2008), (Zamzuri et al., 2006b).

The usual PID controller expression with approximate derivative is employed here, with the derivative cut-off at 1000 rad/s (well above the frequency range of interest for the tilt application). We have chosen such a high level cut-off frequency to set a PID controller structure as close to the pure PID as possible (relative to the given tilt model dynamics).

$$K_{PID} = k_p \left(1 + \frac{1}{\tau_i s} + \frac{\tau_d s}{\frac{s}{N} + 1} \right) \tag{4.1}$$

The remainder of the parameters is the usual set of: k_p the proportional gain, τ_i the integral time constant and τ_d the derivative time constant. The PID controller is designed to achieve tilt control performance requirements on straight and curved track essentially as discussed in Section 3.3. Essentially, tilt control systems are required to maintain a straight track (stochastic) ride quality degradation performance of about 7.5% (Förstberg, 2000) while keeping the comfort response of passengers during curve transition (deterministic) in terms of appropriate P_{CT}

factor (it is noted that a number of tilting control resources (Goodall et al., 2000), refer to achieving P_{CT} factor as good as the non-tilting case. It is noted though that once the hard control specifications are applied to the design, it is more appropriate to appraise by how much the P_{CT} factor of the tilting system can reduce). More explanation on P_{CT} factor can be found in Appendix B. Of course this is co-called deterministic(track following) vs stochastic(ride quality) trade-off. On curved track sections, lateral acceleration perceived by the passengers should be reduced. The full assessment for tilt control can found in (Goodall et al., 2000).

4.2 Frequency response Ziegler-Nichols approach

Work in (Zolotas, 2002), introduced very basic and manual design of a conventional PID controller. Some preliminary NMP zero analysis was also shown. Here the design is tackled in an alternative way, i.e. by commencing design via a simple conventional PID tuning rule i.e. the Ziegler-Nichols. Noting that the tilt control design is not a typical process control type application, the frequency-response Ziegler-Nichols method is employed.

The Ziegler-Nichols method is still a rather popular choice in PID design and normally used as basis to comparing other tuning techniques. As mentioned above, we employ the Z-N frequency response method, which is based on the knowledge of the point of the systems Nyquist curve that intersects the negative real axis. In fact, this point of intersection is called ultimate point as it refers to the ultimate gain and ultimate period. In particular, (the ultimate gain) is the proportional gain before system instability and (the ultimate period) is the critical period at inverse of frequency of $-180deg$.

For completeness, Table 4.1 refers to a set of recommended gain parameters to achieve a decay ratio of 1/4. Nominal plant is used in this chapter. Full transfer function of this nominal plant can be seen in Eq. (3.25). Note that Ziegler-Nichols

originally made the recommendations, based on an extensive set of simulations on different processes, mainly to achieve good load disturbance performance. Their systems were ones typified in the process control industry (Åström and Hägglund, 2006).

TABLE 4.1: Ziegler-Nichols controller gains (frequency response method)

Controller type	K_p	$\tau_1(\tau_i)$	$\tau_2(\tau_d)$
P	$0.5k_u$		
P+I	$0.4k_u$	$0.8T_u$	
P+I+D	$0.6k_u$	$0.5T_u$	$0.125T_u$

Normally Z-N tuning produces closed-loop systems with insufficient damping, hence re-tuning is a necessity. A well-known modified tuning approach is based on the graphical interpretation of the frequency response method, i.e. design a controller to move any arbitrary point of the frequency response curve (e.g. Nichols curve etc.) to a suitable location. If the arbitrary point is the ultimate point, as mentioned before, it is known as **Modified Z-N (M/Z-N)** method (Åström and Hägglund, 2006).

The limitation of the method is that it relocates on point and performance will depend on the nature of the overall compensated curve, its slope etc., albeit is a very simple method of tuning in its manual form. The derivation of the M/Z-N tuning parameter equations for a PID controller are actually given in Eq. (4.2), hence we only list the resulting equations for moving the ultimate point on the frequency response:

$$\begin{cases} k_p = k_u r_b \cos\varphi_b \\ \tau_1 = \frac{P_u \tan\varphi_b}{4\alpha\phi}\left(1 + \sqrt{\frac{4\alpha}{\tan^2\varphi_b} + 1}\right) \\ \tau_2 = \alpha\tau_1 \end{cases} \tag{4.2}$$

Where, α is the ratio of derivative time constant to integral time constant for the PID controller, r_b the gain introduced by the controller at the given point, φ_b is the phase to be introduced by the controller at the given point. In the common Z-N rule it is set to 1/4 but this is not the case in this section. It is worth noting that

for the tilt system with the nominal values given in this thesis, the ultimate gain is $k_u = 0.325$ and period is $T_u = 0.825s$.

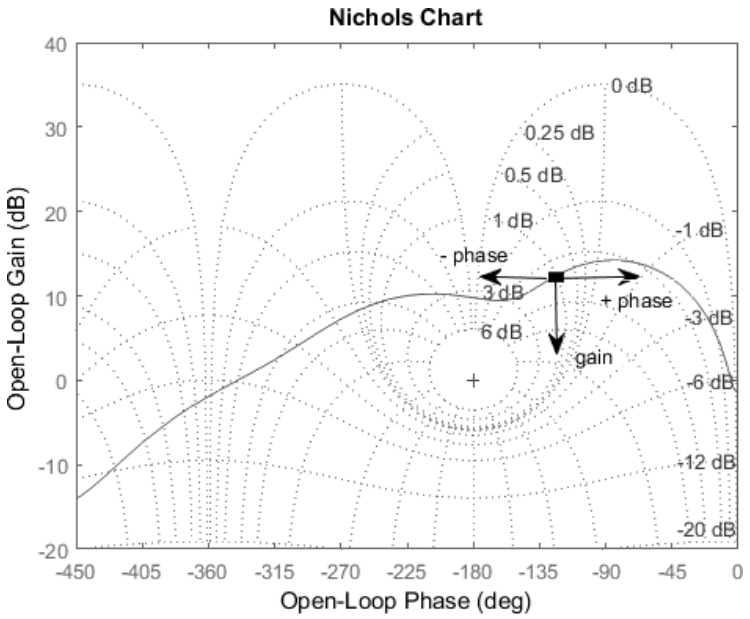

FIGURE 4.1: Curve point location by injection of pure gain and phase lead, lag

The design follows a manual approach i.e. manually changing the M/Z-N parameters and investigating the trend of responses of the closed-loop system. The parameter values start from the recommended ones as discussed and proceeds by varying mainly the ratio and the phase. The parameter variation trend (manually) is shown in Table 4.2 and the actual PID controller for each case in Table 4.3. Note that the controller of the first row in Table 4.3 follows the original Ziegler-Nichols controller gains shown in Table 4.1.

TABLE 4.2: Modified Ziegler-Nichols parameter values

Z-N modified	α	r_b	$\varphi_b(deg)$
original	0.25	0.5	20
case 1	0.5	0.5	20
case 2	0.7	0.5	20
case 3	0.9	0.5	20
case 4	0.9	0.4	10

The comparison frequency domain plot for the designed modified Ziegler-Nichols for all cases are shown in the set of Figure 4.2 to Figure 4.4. Figure 4.5shows the effective cant deficiency response (if it is zero then the required amount of tilt on steady-curve

TABLE 4.3: PID controller list for Ziegler-Nichols approach

Design	k_{PID} **controller**
ZN freq resp orig	$\frac{8.377s^2+80.57s+194.7}{0.4129s^2+412.9s}$
ZN modified orig	$\frac{0.7321s^2+7.344s+19.16}{0.3754s^2+47.17s}$
ZN modified case 1	$\frac{0.5871s^2+4.745s+19.16}{0.2397s^2+30.13s}$
ZN modified case 2	$\frac{0.5392s^2+3.887s+19.16}{0.1949s^2+24.49s}$
ZN modified case 3	$\frac{0.52s^2+3.364s+19.16}{0.1676s^2+21.06s}$
ZN modified case 4	$\frac{0.3534s^2+2.569s+16.06}{0.152s^2+19.1s}$

is achieved).The dotted line presents the same response if a pseudo-reference E.C.D step input of unity amplitude was applied (with all rail-track inputs set to zero). Increasing makes the response more aggressive for the effective cant deficiency and degrades ride quality level. Decreasing the phase contribution also complements aggressiveness of response due to the move of the curve closer to the Nichols plot point (0 dB, -180deg). The analysis here clearly identifies the contribution to the response (from the modified ZN approach) and the related limitations in the tilt control trade-off.

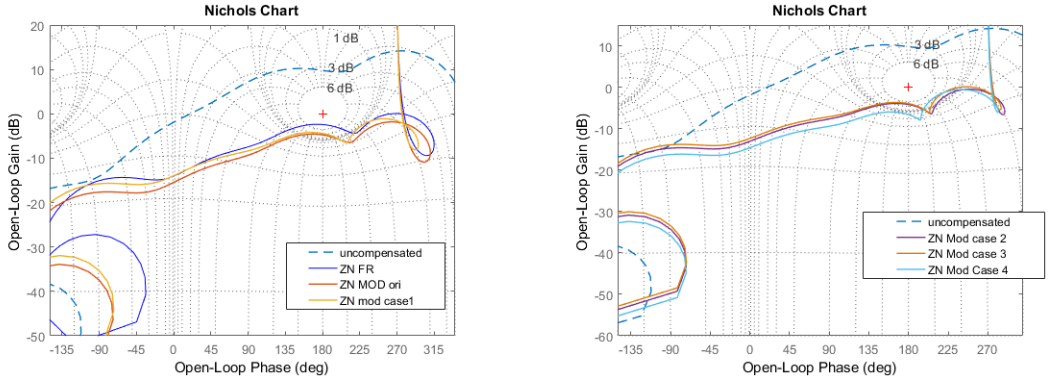

(a) Frequency plot for Ziegler Nichols FR, ZN-Modified(original) and ZN-Modified case 1

(b) Frequency plot for ZN-Modified case 2, ZN-Modified case 3 and ZN-Modified case 1

FIGURE 4.2: Frequency response for all Ziegler Nichols cases.

4.3 Alternative conventional PID tuning approach

Here, we apply a couple of alternative PID conventional tuning methods mainly for completeness in the design (as the previously presented tuning approach is

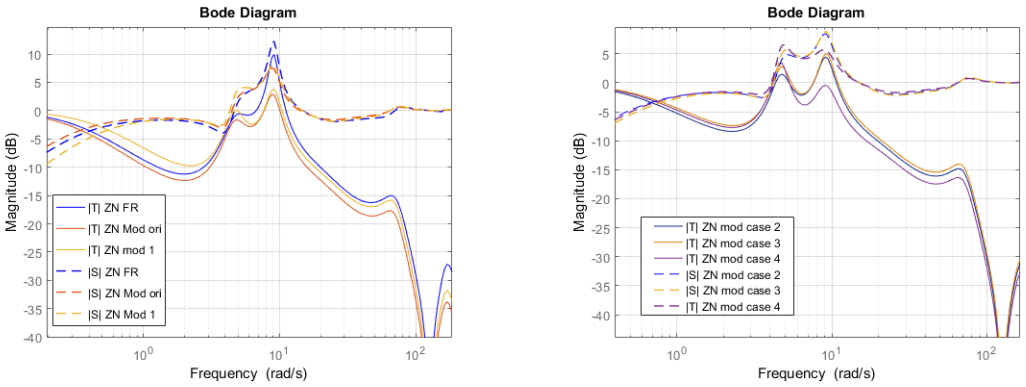

(a) Complementary Sensitivity and sensitivity plot for Ziegler Nichols FR, ZN-Modified(original) and ZN-Modified case 1

(b) Complementary Sensitivity and sensitivity plot for ZN-Modified case 2, ZN-Modified case 3 and ZN-Modified case 1

FIGURE 4.3: Complementary Sensitivity and sensitivity plot for all Ziegler Nichols cases.

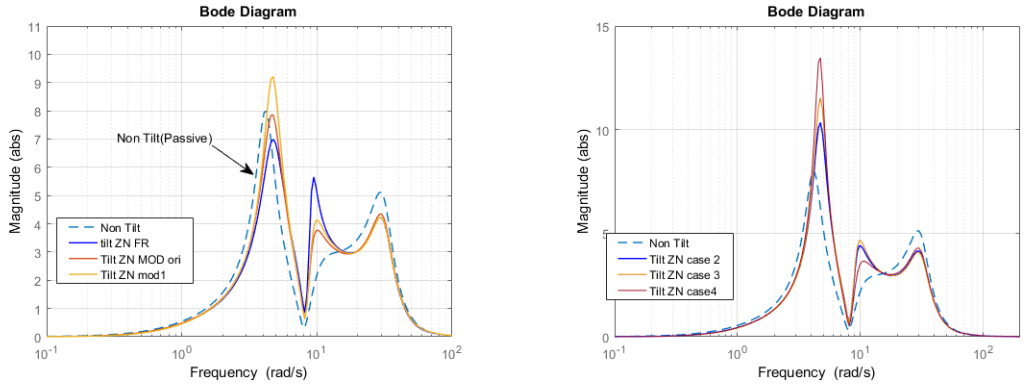

(a) Ride quality (passive and active) plot for Ziegler Nichols FR, ZN-Modified(original) and ZN-Modified case 1

(b) Ride quality (passive and active) plot for ZN-Modified case 2, ZN-Modified case 3 and ZN-Modified case 1

FIGURE 4.4: Ride quality (passive and active) plot for all Ziegler Nichols cases.

not the only possible one). Hence, we present two classical PID design rules ie. Tyreus-Luyben (original and detuned) and frequency-response gain/phase margins and overall guaranteeing an acceptable performance level of tilt deterministic vs tilt stochastic trade-off. Note that "detuned" in this context means a PID controller which emphasizes more integral action.

The following approaches are utilised here;

- Tyreus-Luyben approach (mainly because it was based on the Z-N original but aims to less oscillatory response and reduced sensitivity in process conditions),

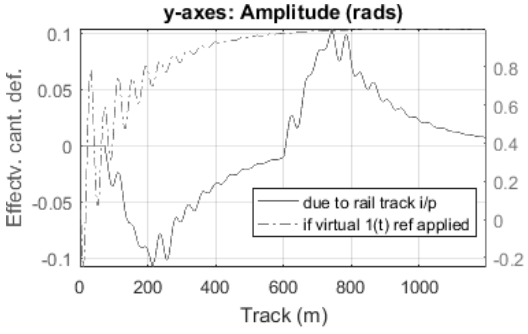

(a) E.C.D for Ziegler Nichols FR

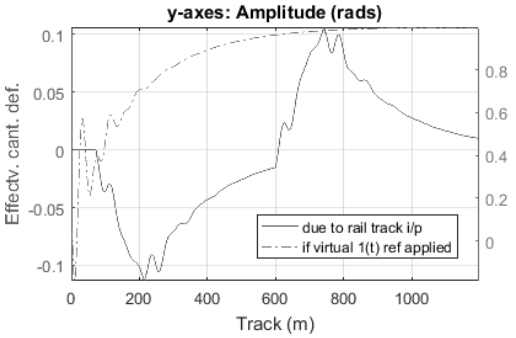

(b) E.C.D for ZN-Modified(original)

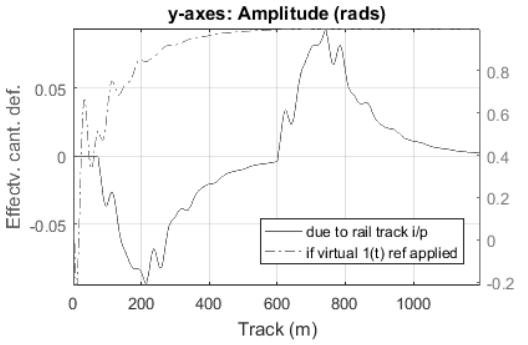

(c) E.C.D for ZN-Modified case 1

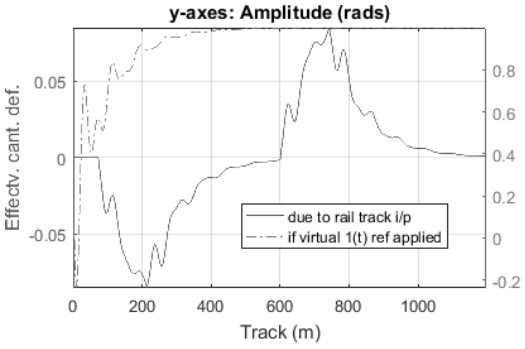

(d) E.C.D for ZN-Modified case 2

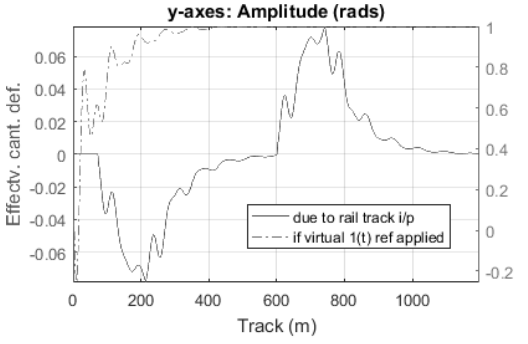

(e) E.C.D for ZN-Modified case 3

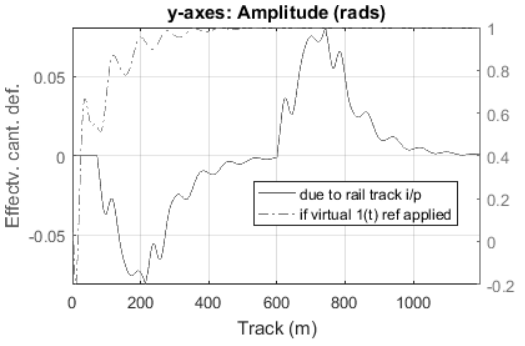

(f) E.C.D for ZN-Modified case 4

FIGURE 4.5: Effective cant deficiency (E.C.D) plot for Ziegler Nichols FR, Ziegler Nichols modified Original, Ziegler Nichols modified case 1 to case 4.

Tyreus-Luyben detuned (to emphasize more integral action), and

- Frequency response design (F-R manual) providing GM approx. 5dB, PM approx. 45 deg, b/w approx. 1 rad/s. The manual designs are quite straightforward (Åström and Hägglund, 2006), (Hassan et al., 2016). In addition, the F-R response done here also serves as a preamble manual loop-shaping approach.

The controller gains achieved from the manually designed PIDs approach via manually shaping Tyreus-Luyben and frequency response are:

$$\begin{aligned}
\text{T-L original:} \quad & k_p = k_u/2.2, \quad \tau_i = 2.2T_u, \quad \tau_d = T_u/6.3 \\
\text{T-L detuned:} \quad & k_p = k_u/2.2, \quad \tau_i = 0.19T_u, \quad \tau_d = T_u/6.3 \\
\text{F-R manual:} \quad & k_p = 0.1256, \quad \tau_i = 0.122, \quad \tau_d = 0.1829
\end{aligned}$$

where the ultimate gain (gain at which the closed-loop system is marginally stable) and period of such oscillations for the nominal transfer function are $k_u = 0.325$ and $T_u = 0.825$s, respectively as mention previously.

Tyreus-Luyben original method used larger gain and phase margin compare to Ziegler-Nichols tuning. The conservativeness of the original Tyreus-Luyben design shows in frequency and time domain results in Figure 4.6 and 4.9(a). By tuning τ_i in Tyreus-Luyben design to $0.19T_u$, more satisfactory performance can be achieved. Manually frequency response(FR manual) tuning design show almost similar results as Tyreus-Luyben detuned in frequency domain. The comparison of frequency domain performance for these three proposed design can be seen in Figure 4.6, 4.7 and 4.8.

The two methods above presented here are sufficient to complement the modified ZN approach presented before. There is of course a plethora of PID control tuning approaches, i.e. Cohen-Coon and IMC(Internal Model Controller) but these will not be discussed in this thesis.

4.4 Performance analysis

Here we look into a more detailed performance PID designs. Both nominal and robust performance is studied. For the uncertainty employed in the vehicle model the reader is referred to Section 3.4.1.

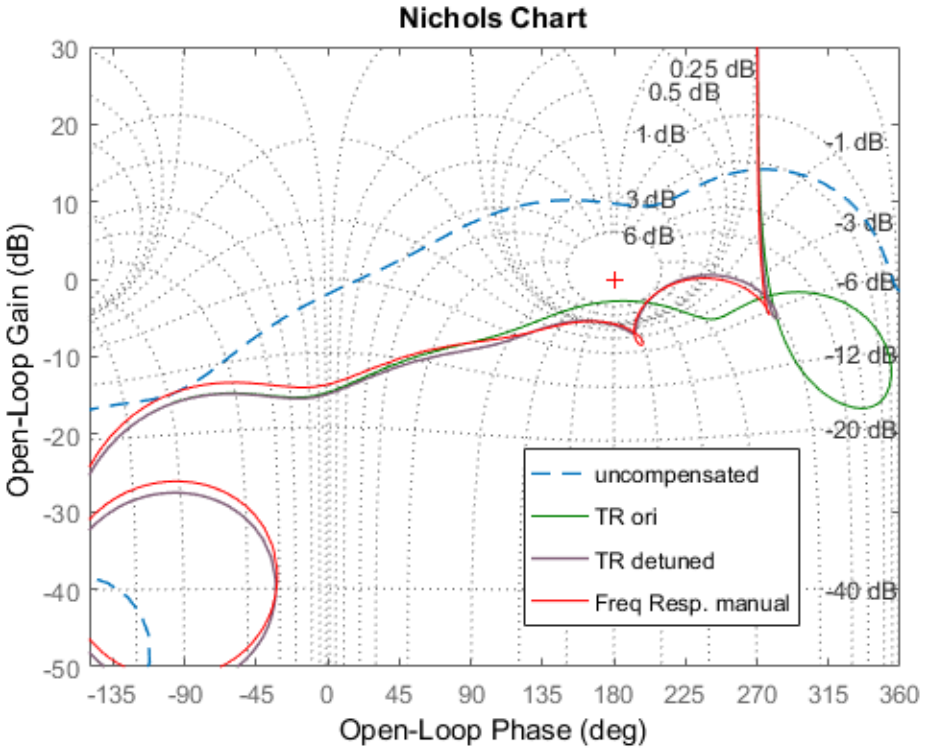

FIGURE 4.6: Frequency plot for Tyreus-Luyben original, Tyreus-Luyben Detuned and Frequency Response Manual design.

4.4.1 Nominal performance analysis

The achievable (nominal) performance for P_{CT} standing and ride quality degradation for conventional PID method is shown in Tables 4.5 and 4.4. Satisfied ride quality degradation and P_{CT} standing performance can be seen in Ziegler-Nichols modified case 4 although the frequency response(FR) manual design and offers improvement (but requires few design iterations to accomplish the design and produce acceptable tilt control performance results), still the achieved ride quality is slightly higher than the industrially accepted norm of 7.5% degradation (although slightly elevated value still acceptable in this case).

Since the manual design for the conventional PID controller only considers phase and gain margin nominal stability, clearly the NMP zero characteristic of the plant imposes hard bandwidth constraints (Skogestad and Postlethwaite, 2007), while achieving a low value for the module margin $\|S\|_\infty$ which is a challenging task with the manually designed controllers. It is proved difficult to achieve less than

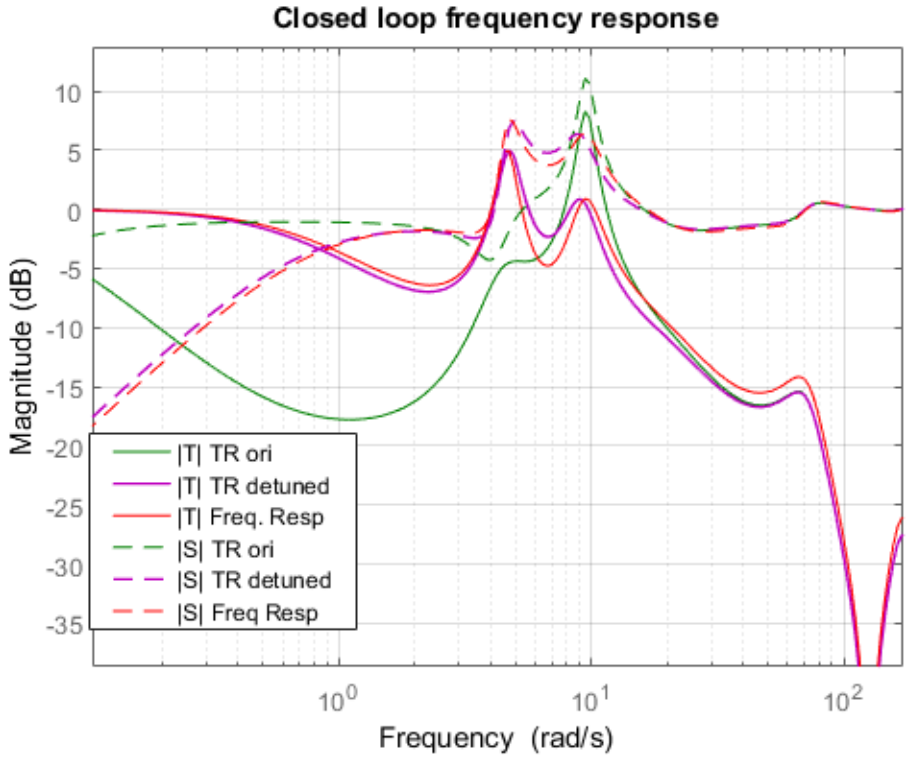

FIGURE 4.7: Complementary Sensitivity and sensitivity plot for Tyreus-Luyben original, Tyreus-Luyben Detuned and Frequency Response Manual design.

the typical value of 2 in term of the infinity norm(i.e. peak) of 2(6dB) magnitude $||S(jw)||$, see Table 4.4.

TABLE 4.4: Stability margins for the conventional PID controllers

PID rule	**GM(dB)**	**PM(deg)**	**B/W(rad/s)**	$\|S\|_\infty$
Tyreus-Luyben	2.83	96.89	0.08	3.6
Tyreus-Luyben (detune)	5.88	43.28	0.93	2.36
Freq.-Resp. (manual)	5.75	48.29	1	2.4
ZN freq resp	2.403	80.832	5.57	4.09
ZN mod orig	4.749	96.3	4.31	2.38
ZN case 1	4.412	95.75	4.05	2.53
ZN case 2	4.176	95.42	3.91	2.65
ZN case 3	3.963	57.29	3.79	2.77
ZN case 4	6.594	94.0	3.77	2.13

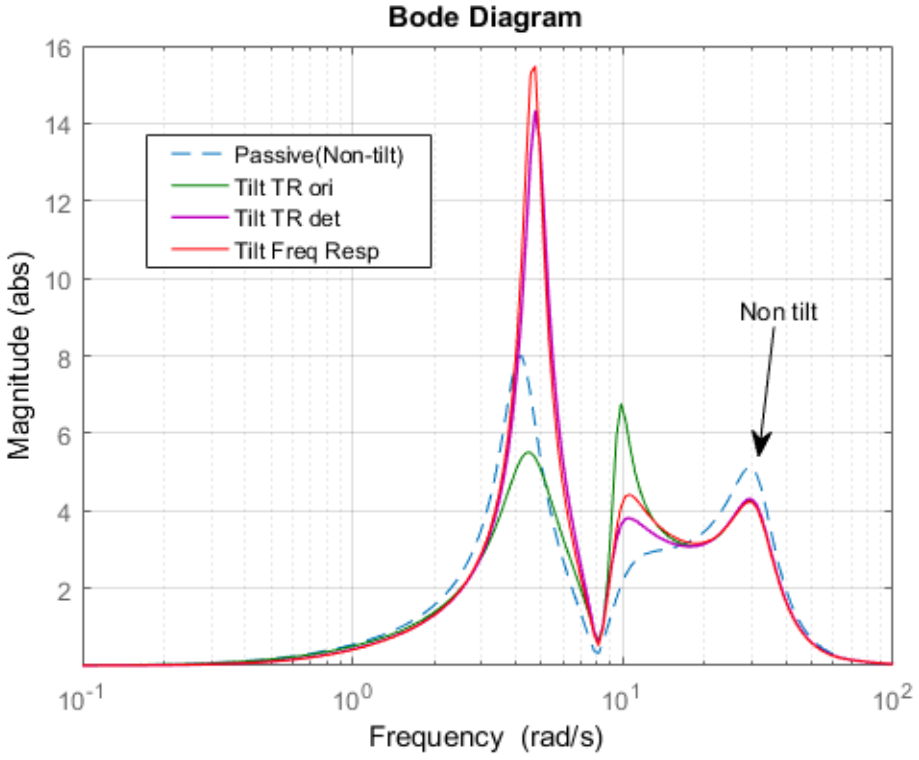

FIGURE 4.8: Ride quality (passive and active) plot for Tyreus-Luyben original, Tyreus-Luyben Detuned and Frequency Response Manual design.

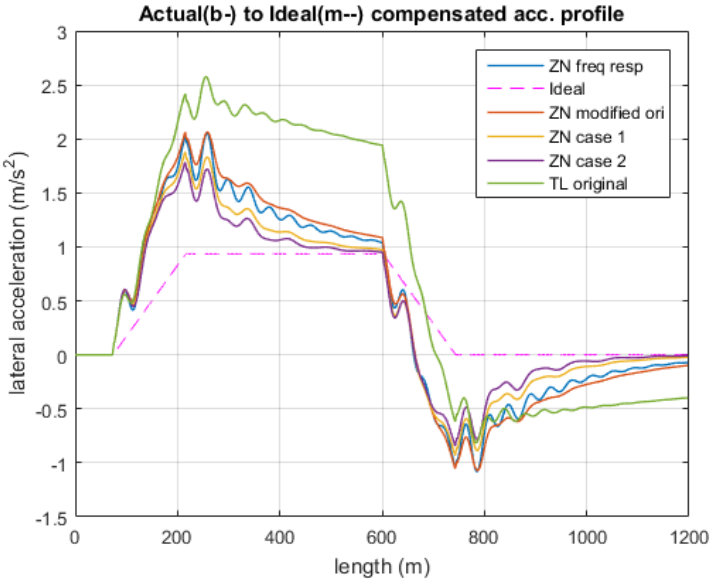

(a)

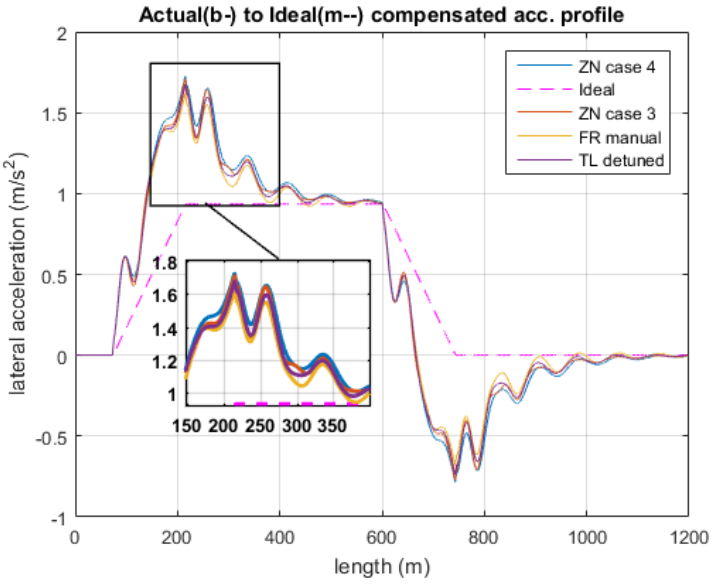

(b)

FIGURE 4.9: Lateral acceleration plot for conventional PID methods

TABLE 4.5: Performance assessment (P_{CT} / rq(ride quality): PID conventional tuning approaches

PID control.:		**Tyreus-Luyben**	**Tyreus-Luyben** (detune)	**F-R** manual	**ZN** freq resp original	**ZN** modified original	**ZN** case 1	**ZN** case 2	**ZN** case 3	**ZN** case 4
P_{CT}	Stand. (% psg.)	92.16	64.50	63.12	76.192	75.208	69.896	67.627	66.077	65.553
P_{CT}	Seated (% psg.)	30.42	20.05	19.46	24.698	24.423	22.343	21.356	20.648	20.527
Stochastic (acceleration %g) @58m/s **										
rq	r.m.s active ($\%g$)	2.719	3.042	3.110	2.709	2.696	2.758	2.813	2.874	2.969
rq	Degrad.(%)	-4.520	6.8	9.194	-4.887	-5.347	-3.166	-1.229	0.915	4.246

% psg. = % of passengers

4.4.2 Robust performance analysis

The perturbation of the plant characteristics used here follow plant perturbation proposed in Section 3.4.2 in Table 3.3.

Table 4.6 and Table 4.7 presented robust performance for 4 selected cases ; Tyreus-Luyben detune, Frequency response manual, Ziegler-Nichols modified original and Ziegler-Nichols case 4 for comparison. It is seen that the P_{CT} standing is maintained around the nominal value given by the designs (relative to each design of course). However, it is seen that in terms of ride quality the performance degrades fast (for the "extreme" uncertainty cases). The latter is a realistic outcome and further highlights the difficult trade-off to achieve (in addition the ride quality constraint is that of a stochastic nature).

TABLE 4.6: Robust performance for P_{CT} standing for all conventional cases

PID rule	**Nominal**	**P1**	**P2**	**P3**	P4
Tyreus-Luyben (detune)	64.50	63.218	67.231	71.603	65.350
Freq.-Resp. (manual)	63.12	61.952	65.657	72.034	64.162
ZN mod orig	75.208	74.758	80.977	83.513	77.164
ZN case 4	65.553	64.962	67.857	70.475	67.146

TABLE 4.7: Robust performance for ride quality degradation for all conventional cases

PID rule	**Nominal**	**P1**	**P2**	**P3**	P4
Tyreus-Luyben (detune)	6.8	15.391	0.817	1.856	43.002
Freq.-Resp. (manual)	9.194	20.219	5.134	20.962	70.535
ZN mod orig	-5.347	-2.769	-7.771	-4.848	-0.131
ZN case 4	4.246	11.681	-1.878	-2.560	29.766

It is worth mentioning the use of Sensitivity represented by $S(s)$ function in the design, as it directly relates to robust performance (and forms an important function for robustness analysis). The peak of the Sensitivity function's magnitude plot, i.e. $||S||_\infty$ is of paramount interest in robust control analysis and design. Greatly used within the remit of robust H-infinity control design methods (as will be seen in the next chapters of this thesis work), it also relates to the system's module margin which is a more appropriate robustness metric (compared to gain and/or phase margins).

4.5 Summary

This chapter discusses manually designed conventional (integer-type) PID control design. In particular revisits basic PID control design and details the design via Ziegler-Nichols, Tyreus-Luyben, and a manual frequency-domain design for the tilt control system. Limitations and performance achievement are highlighted, while the way for the next chapter that deals with optimisation-based PID approaches is paved.

Chapter 5

Optimised PID control design for the tilt system

The previous chapter has mainly introduced a SISO classical control design flavour for the ARB tilt setup. The design challenge for the tilt control trade-off and the limitations of the manually designed SISO PID controller makes use of advanced optimization tools imminent. This chapter presents exactly that, i.e. constrained optimisation based SISO controller design (of PID nature). In particular, the following approaches are studied rigorously:

- Optimised modified Z-N
- Generic optimisation applied to PID design
- Optimised Fractional order PID (FOPID) design

The last method forms a major contribution in this thesis (i.e. that of a non-conventional non-integer PID design for the tilt control system). In the best knowledge of the author this is very novel in the railway tilt control application.

5.1 Optimised modified Z-N PID design

The manual tuning analysis reveals trends of parameter variation in the Z-N modified approach, see Section 4.2, their mapping into PID gains and impact on tilt performance. We utilise an optimization framework to improve tuning of the PID controller given the cumbersome performance trade-off and the non-minimum phase characteristics of the design plant. Here, we focus on minimization given by (5.1).

$$\begin{aligned} \underset{r_b\,\varphi_b\,\alpha}{\text{minimize}} \quad & f(x) = P_{CT}\,standing \\ \text{subject to} \quad & < \mathbf{constraint} = \mathbf{rqd} \leq \mathbf{7.5}\%,\ \| \mathbf{S(jw)} \|_\infty \leq \mathbf{2.4} > \end{aligned} \tag{5.1}$$

Note that rqd refers to the ride quality (Hassan et al., 2017) degradation of the tilting system compared to the non-tilting system at the higher speed ($58m/si.e.30\%$ higher than the non-tilting speed) and r_b, φ_b, α refer to Eq.(4.2) in Section 4.2. The sensitivity peak bound imposed a basic level of robustness (note that we do not consider a core robust control scheme explicitly in this section). Normally for the sensitivity peak a bound of no more than 2 is used (Skogestad and Postlethwaite, 2007) but as the system is non-minimum phase and a very simple controller is employed, a slightly higher bound is allowed. R+ is the set of positive real numbers.

5.1.1 Note on optimization tools used for the design

It is noted that this thesis does not contribute to the theory of optimization methods for control design. Rather, optimization is used as a tool to achieve the control specifications required for the tilt control problem. However, we propose a variety of minimisation problems that impact the tilt control design in different ways (something of particular interest to the practising control engineer). In this context, we employ (nonlinear optimisation) implemented in Matlab i.e. *fminsearch()* with violation constraints implemented manually or *fmincon()* which implements constrained optimisation directly.

Following nonlinear optimisation, it is appreciated that initial conditions can affect final solution. Hence, we opt to utilise randomised multi-start approach for the initial conditions (in an iterative way) and select the best result. The obtained result is then passed through a neighbourhood search for completeness. A few more details on this are listed below.

5.1.2 Choice of initial conditions for the optimisation process

The optimization process commences with parameter conditions for the optimized modified Z-N design process, especially for the practising control engineer, that stem from the original suggestion in (Iwnicki, 2006), i.e. $r_b^0 = 0.5$, $\varphi_b^0 = 20deg$, $\alpha^0 = 0.25$.

Different initial conditions will impact the non-linear optimization outcome due to the existence of local minima. A way to prevent the optimisation process getting stuck in local minimum is to add more iterations. We utilise multi-start to perturbing initial conditions in the optimisation procedure (about 10 iterations with a random initial value generation in the interval $[0.25\overline{x},\ 5\overline{x}]$, where is the row vector of initial parameters (r_b^0, φ_b^0, α^0 as discussed above). Note that unrealistic parameter bounds for the initial conditions would normally result to unrealistic optimization. Note, that once the best optimisation outcome is obtained, the result is passed through a further stage of neighbourhood search for completeness. The problem can be implemented in Matlab software using either $fminsearch()$, with appropriate violation constraints, or $fminbnd()$ functions. Note that the former optimisation function implements the Nelder-Mead algorithm (Nelder and Mead, 1965), while the latter implements a number of alternative constrained optimisation algorithms such as Trust region, Active set, SQP, Interior point (MathWorks, 2017).

5.1.3 Nominal performance analysis

Details on designing PID controllers via the modified Z-N approach have been shown in the previous chapter, and we thus avoid replicating these here. Table 5.1 presents the results from the optimized modified Z-N design process. The value of ratio α and that of the phase are substantially increased relative to the original recommended values, while the value of the gain decreased. The parameters value achieved from the optimization are, α=4.69, $r_b = 0.293$ and $\Phi_b = 41.1deg$. The overall PID controller transfer function can be seen in (5.2).The optimization process essentially aims to satisfy the required constraints and the P_{CT} minimization by moving one point on the Nichols plot, i.e. inherited by the modified Z-N approach (Åström and Hägglund, 2006) and Section 4.2. Here we use the same cut-off frequency N as in Eq. (4.1). The results are shown on Figure 5.1.

$$k_{sys} = \frac{0.2372s^2 + 0.739s + 9}{0.0741s^2 + 9.316s} \tag{5.2}$$

TABLE 5.1: Optimised modified Ziegler-Nichols controller performance

Deterministic(as per given units)		**Ziegler-Nichols parameter optim**
Lateral accel.	RMS Deviation (%g)	4.07
	Peak value (%g)	16.68
Roll gyro.	RMS deviation(rad/s)	0.029
	Peak value (rad/s)	0.091
	Peak jerk level(%g/s)	9.247
P_{CT} related	Standing (% of passengers)	62.465
	Seated (% of passengers)	19.334
Stochastic (acceleration %g) @58m/s **		
**Ride quality of non-tilt. train if running @ high speed = 2.848%g		
Ride quality	Tilting train	3.062
	Degradation (%)	7.485
Performance Margins		
Freq. resp.	Gain margin (linear)	1.91
	Phase margin (deg)	90.86
	$\|\|S(j\omega)\|\|_\infty$	2.1

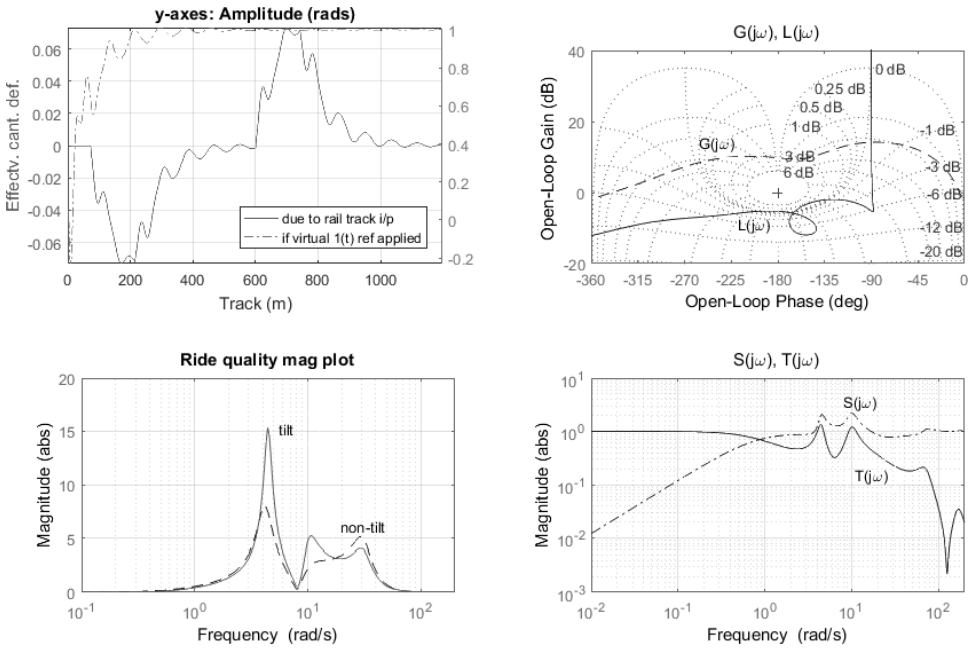

FIGURE 5.1: Optimised Ziegler-Nichols PID controller design

5.2 PID control design based on generic optimisation

Here, a more generically based optimisation approach is studied for the PID tilt control design. Contrary to the optimised modified Z-N approach, here the approach is not based on moving a single point on the compensated system frequency response. The approach stems from the well studied PID optimisation approaches especially in the process control industry, whereby a number of time-domain based cost-functions have been also used. In most time domain optimisation based PID works four typical and widely popular performance indices for PID design in the time domain appear (Åström and Hägglund, 2006) (ÅStröm and Hägglund, 2004) (Hypiusová and Kajan) (Gude and Kahoraho, 2010).

There are four typical and widely popular performance indices for PID design in the time domain widely used in the PID control literature, and a natural set of metrics in process control applications, (Panagopoulos et al., 2002), (Ho et al., 1998). Namely the ISE (integral of squared error), IAE (integral of absolute error), ITSE (integral of time multiply squared error) and ITAE (Integral time of absolute

error). Other ways of setting up PID controller design via global optimization with generic additional constraints can be seen in (Ozana and Docekal, 2016). In this thesis we focus on IAE and ITAE, since these are the ones used more frequently in PID tuning (Zamzuri et al., 2006b) (Ho et al., 1998). We follow the usual formulae for ITAE and IAE costs:

$$J_{(itae)} = \int_0^\infty t|e(t)|dt \tag{5.3}$$

$$J_{(iae)} = \int_0^\infty |e(t)|dt \tag{5.4}$$

respectively, where $e(t)$ represents an error signal in the feedback control framework, i.e. minimisation of a form of error in the closed-loop system. For the tilt control application this is the effective cant deficiency, i.e. the signal that establishes partial-tilt compensation on curved track. The ITAE and IAE cost functions are set up in the usual constrained optimisation approach given by,

$$\begin{aligned} &\underset{K_{pid}}{\text{minimize}} \quad f(x) \\ &\text{subject to} \quad < \textbf{constraints} > \end{aligned} \tag{5.5}$$

For the tilt application, a number of constraints are included and given in Table 5.2. The different constraints emphasize the increasingly stringent tilt performance speed of response.

TABLE 5.2: Minimization approach identifiers and constraints (Note: rqd denotes ride quality degradation; GM: gain margin; PM: phase margin)

Minimization ID	**f(x)**	**<constraints>**
CF1	ITAE	at least absolute stability
CF2	IAE	at least absolute stability
CF3	ITAE	rqd $\leq 7.5\%$
CF4	ITAE	$GM \geq 1.45$, $PM \geq 45^0$
CF5	ITAE	$GM \geq 1.45$, $PM \geq 45^0$, rqd $\leq 7.5\%$
CF6	P_{CT} (standing)	$GM \geq 1.45$, $PM \geq 45^0$, rqd $\leq 7.5\%$
CF7	P_{CT} (standing)	rqd $\leq 7.5\%$, $\|S(j\omega)\|_\infty \leq 2$
CF8	P_{CT} (standing)	rqd $\leq 7.5\%$, $\|S(j\omega)\|_\infty \leq 2$, $\|W_\delta(j\omega)T(j\omega)\|_\infty \leq 1$

The above minimisation procedure can be set-up in a straightforward manner in one of the currently available software tools. In this section, Matlab was employed via use of function *fmincon()* (an alternative approach is via use of *fminsearch()* with appropriate constraints). The optimization problem can also be implemented via Pattern Search and Genetic Algorithm(GA) with longer process time compared to *fmincon()*. Few remarks: (i) in CF1 and CF2 "at least absolute stability" essentially constrained by a least bound of (gain margin) GM = 1.2, and (phase margin) PM = 20 deg., (ii) CF8 introduces a bound on multiplicative uncertainty to guarantee robust stability (details on this will be shown in later sections), (iii) We opt to using minimization of P_{CT} (standing) as this forms the worst-case P_{CT} factor metric.

It is worth noting that the allowed GM and PM bounds represent a typical set of accepted design margins for railway vehicle suspensions, i.e. a gain margin of not less than 3dB and a phase margin of not less than 45deg. The bound for the peak of the sensitivity function $S(j\omega)$ attempts to maintain a level of allowed worst case performance degradation (values of less than 2 (6dB) can be tried but will impose a hard design constraint for the tilt control application given the NMP zeros. A value of 2 (6dB) is still acceptable to provide a minimum level of damping also see (Skogestad and Postlethwaite, 2007)). Similarly the one for the peak of the robust stability $W_\delta(j\omega)T(j\omega)$ function is imposed by robust control theory (essentially driven by choice of W_δ) (Skogestad and Postlethwaite, 2007). The choice of weighting function W_δ in this work characterises the multiplicative nature of model uncertainty for the tilt vehicle model (details presented in Section 3.4.1).

5.2.1 Choice of initial conditions

This subsection is included for completeness (as in the case of the optimised modified Z-N method) to list consideration of initial conditions in the optimisation process. A natural choice of initial PID gain conditions for the optimization process, especially for the practising control engineer, can stem from the ultimate gain Ziegler-Nichols method, refer to Table 4.1 whereby k_u is the ultimate gain (i.e. maximum gain before instability occurs) and T_u is the critical period (i.e. the period of sustained

oscillations being the inverse of the crossover frequency. For the case presented in this paper, k_u and T_u value as previously mentioned in Section 4.2. The Z-N (original) PID gains are given as

$$K_{p_{(z-n)}} = 0.195, \quad K_{i_{z-n}} = \frac{K_{p_{(z-n)}}}{\tau_{i_{(z-n)}}} = 0.472, \quad K_{d_{z-n}} = \frac{K_{p_{(z-n)}}}{(\tau_{d_{(z-n)}})^{-1}} = 0.02;$$

Ziegler-Nichols is not the only classical tuning rule that can be used (Veselỳ, 2003), however it suffices for the purposes of the work presented here as well as been one of the most popular simplified PID tuning rules. The authors has looked into a number of classical PID tuning rules, amongst other approaches, for the tilt control problem in (Hassan et al., 2016).

As in the previous optimisation based control design, we also utilise multi-start to perturbing initial conditions in the optimization procedures for completeness (about 10 iterations with a random initial value generation in the interval $[0.01\vec{x}_0, 2\vec{x}_0]$, where $\vec{x}_0$ is a row vector of initial gains given by Z-N rules on the original design model TF). Note that again unrealistic gain bounds for the initial conditions would normally result to unrealistic optimization.

5.2.2 Nominal performance analysis

The tilt performance results via different optimizations and constraint identifiers are shown on Table 5.4, and discussed further in this section. For completeness the designed PID controllers for the different cost functions can be seen on Table 5.3.

With reference to results from Table 5.4 on the use of minimization of the conventional ITAE (CF1) and IAE (CF2) (with at least absolute stability) these offer improvement in deterministic tilt performance (i.e. see Table 5.4) but largely degraded ride quality (stochastic). This type minimization will only work well with the system that need to minimize error unlike tilt control system where P_{CT} is important to minimize to maintain tilt performance. The aforementioned kind of

TABLE 5.3: PID controller designed for the different cost functions

Design approach	**K_{PID} controller TF**
CF1	$\frac{4.254s^2+20.56s+186.3}{0.1093s^2+109.3s}$
CF2	$\frac{4.253s^2+20.55s+186.3}{0.1093s^2+109.3s}$
CF3	$\frac{5.305s^2+43.43s+243.6}{0.1773s^2+177.3s}$
CF4	$\frac{2.468s^2+6.957s+93.67}{0.07328s^2+73.28s}$
CF5	$\frac{3.828s^2+18.97s+145.5}{0.1294s^2+129.4s}$
CF6	$\frac{2.675s^2+8.778s+92.37}{0.09404s^2+94.04s}$
CF7	$\frac{2.098s^2+7.161s+80.63}{0.08781s^2+87.81s}$
CF8	$\frac{1.328s^2+2.533s+44.84}{0.05548s^2+55.48s}$

minimization does provide controllers that drive the system closer to instability (being optimization on time-domain signal), hence the results are not surprising. The performance indices above could be used as a starting point for the PID design, but offer no advantage in the overall tilt performance.

TABLE 5.4: PID controller performance assessment with the different time-domain optimisation approaches

Deterministic(as per given units)		**CF1**	**CF2**	**CF3**	**CF4**	**CF5**	**CF6**	**CF7**	**CF8**
Lateral accel.	RMS Deviation ($\%g$)	2.775	2.775	3.291	3.325	3.612	3.997	4.204	4.625
	Peak value ($\%g$)	15.370	15.367	16.199	15.081	16.290	16.660	16.979	17.749
Roll gyro.	RMS deviation(rad/s)	0.027	0.027	0.031	0.026	0.027	0.028	0.029	0.031
	Peak value (rad/s)	0.119	0.119	0.108	0.099	0.099	0.090	0.090	0.088
	Peak jerk level($\%g/s$)	9.857	9.857	9.824	8.962	9.603	9.313	9.307	9.280
P_{CT} related	Standing (% of passenger)	66.833	66.829	66.141	58.98	63.68	62.3	63.1	64.834
	Seated (% of passenger)	19.724	19.722	20.025	17.895	19.570	19.342	19.604	20.198
Stochastic (acceleration %g) @58m/s **									
**Ride quality for non-tilting train if running at the higher speed = 2.848$\%g$									
Ride quality	Tilting train	3.642	3.642	3.062	3.373	3.062	3.062	3.061	3.031
	Degradation (%)	27.873	27.88	7.5	18.448	7.5	7.5	7.49	6.412

CF3 minimizes ITAE while constraining ride quality to being up to 7.5% degraded. The minimization process provides controller values that attempt to address the trade-off (the ITAE being related to the deterministic side, while the ride quality constraining the allowed stochastic side degradation). The CF3 results show that increasing the PM improves damping, which gives improved ride quality performance and deterministic improvement due to the reduced peak value of the roll gyroscope signal.

The overall situation is largely improved once more direct stability margin constraints are included, i.e. GM and PM bounds to achieve. We then note the amount of module margin (i.e. the H-infinity norm of the designed system sensitivity transfer function) the proposed minimization process provides (as with only a PID controller it is rather challenging to constrain the sensitivity peak for the tilt control design without substantially affecting speed of response).

TABLE 5.5: Stability margins for the controllers(GM,gain margin:PM,phase margin)

Design approach	**GM(dB)**	**PM(deg)**	**CL B/W (rad/s)**	$\|S(j\omega)\|_\infty$
CF1	1.45	15.0	3.95	6.16
CF2	1.42	10.0	4.16	7.7
CF3	1.44	21.9	4.15	6.68
CF4	3.22	44.9	1.2	3.22
CF5	3.23	45.1	1.12	3.23
CF6	4.1	91.8	0.9	2.63
CF7	6	91.45	0.84	2
CF8	6.01	89.9	0.71	1.99

Figure 5.2 presents the bode plot for the designed PID controllers, whereby small differences may be seen however this supports that refined tuning does have a substantial impact on the tilt performance. Moreover, Figure 5.3(c) and 5.3(d) present frequency and time domain results for CF3, CF4, CF5. The slower response due to the improved stability margins is evident (compared to Figure 5.3(a) and 5.3(b) for CF1, CF2). The lateral acceleration response is improved for CF6, CF7 and CF8 cases with larger phase margin (5.3(e), 5.3(f)). In the compensated open-loop figures the cumbersome nature of finely shaping the module margin with only a PID controller is shown.

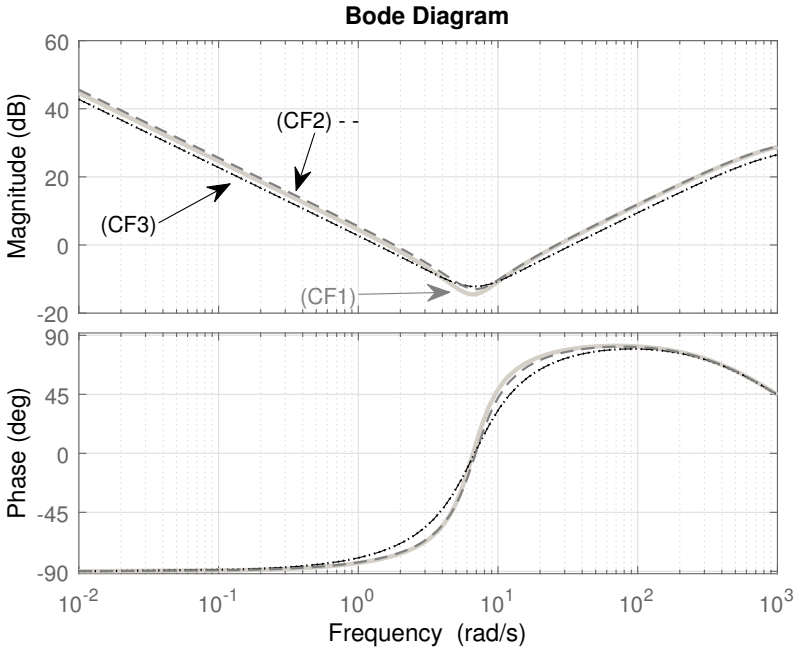

(a) CF1, CF2, CF3

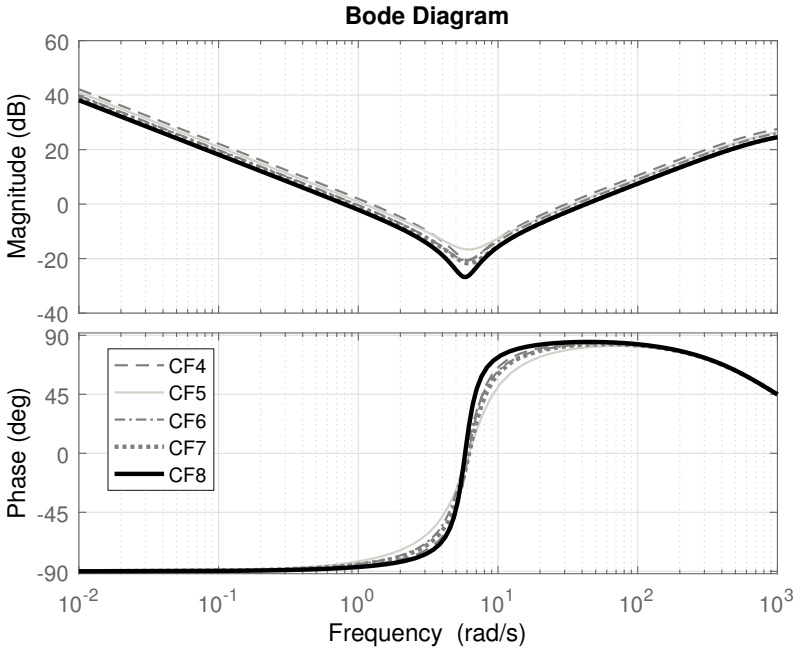

(b) CF4-8

FIGURE 5.2: PID controllers Bode plot.

For completeness, Figure 5.5 presents the sensitivity of the system (nominal plant and listed controllers in the Figure 5.2) to the stochastic track input disturbance (rate of lateral track irregularity to filtered lateral acceleration for passenger comfort). The noted region on the Figure 5.4 indicates changes that have an impact

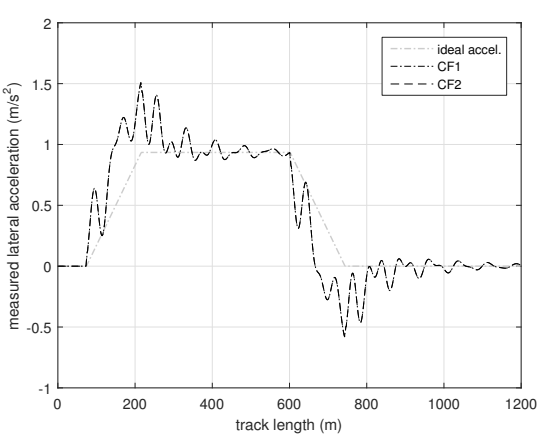

(a) Lateral acceleration

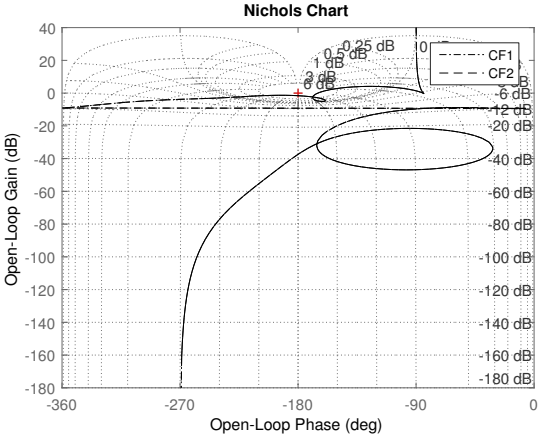

(b) Compensated open-loop freq. resp.

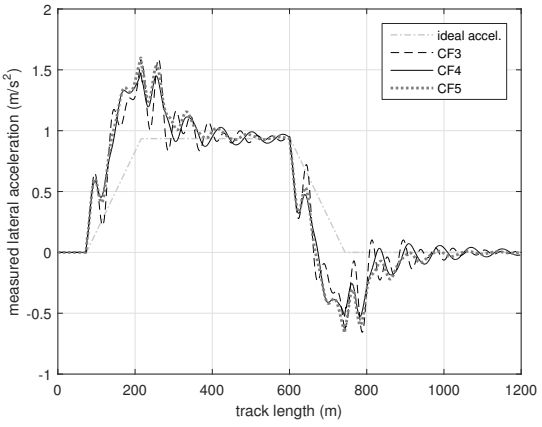

(c) Lateral acceleration

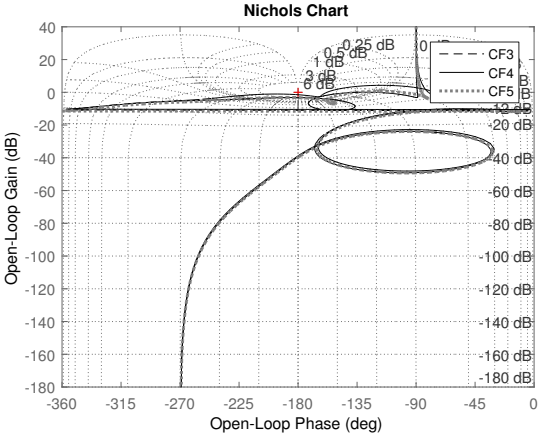

(d) Compensated open-loop freq. resp.

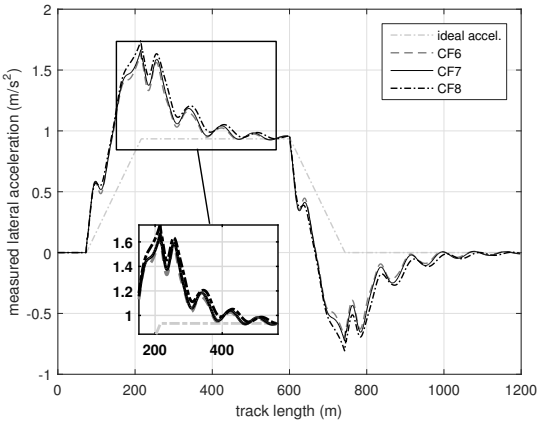

(e) Lateral acceleration

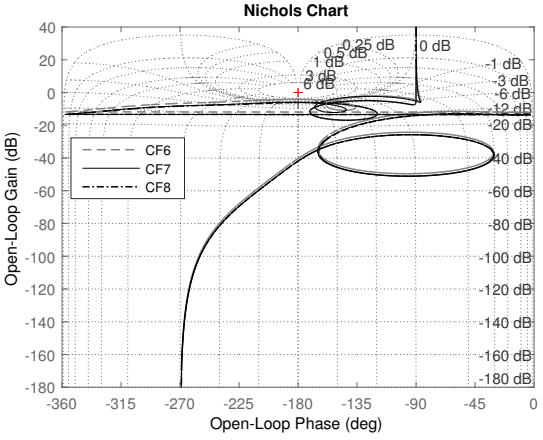

(f) Compensated open-loop freq. resp.

FIGURE 5.3: Deterministic lateral acceleration and nichols plot of designed $L(j\omega)$ results for the different PID controllers

on the ride quality value. Recall that active tilt will tend to degrade the ride quality (thus, the industrially accepted bound of 7.5% worst as discussed previously) (Goodall et al., 2000). We also present the result on sensitivity to matched uncertainty (see Figure 5.5).

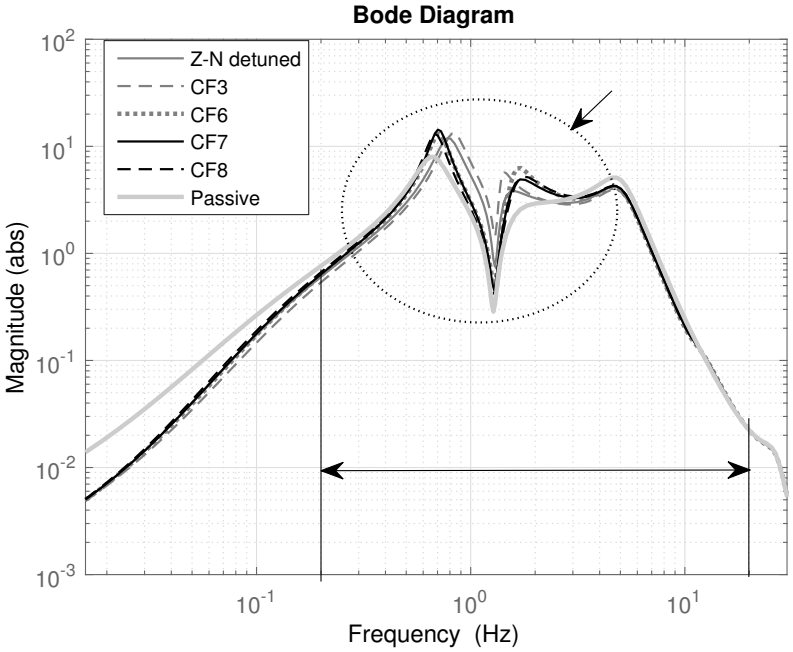

FIGURE 5.4: Ride quality TF for different controllers and nominal plant

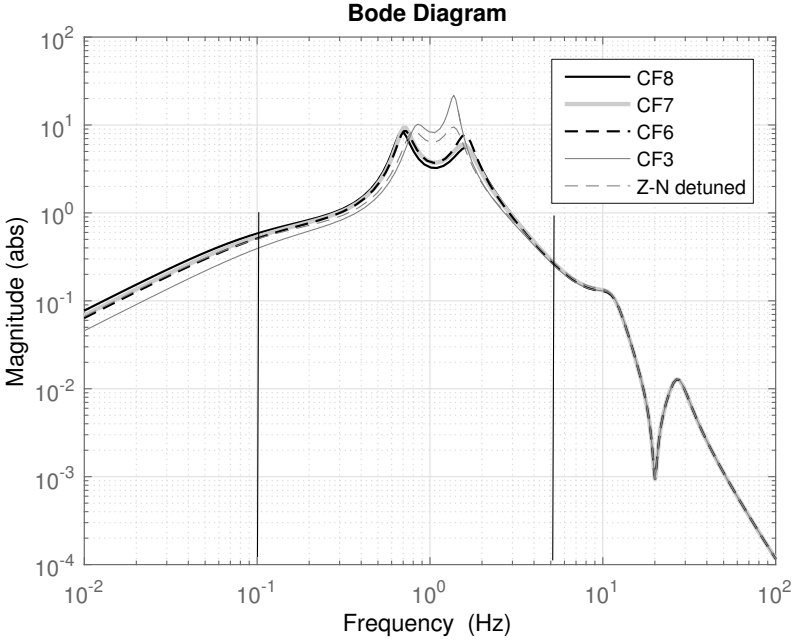

FIGURE 5.5: Sensitivity to Input (disturbance), i.e. Matched uncertainty, (for the different controllers)

5.3 Optimised Fractional order PID controller

This section introduces, fractional order PID design. Note that this thesis proposes two alternative versions of fractional order PID control design for the tilt problem. First a direct fractional order PID equivalent (discussed here) and referred to as FOPID, and in the next chapter a more loop-shaping related fractional order PID type controller. First, we introduce few details about fractional order systems in general.

5.3.1 Fractional order introduction

The birth date of Fractional order calculus seems to be in 1695 with a letter sent by L'Hospital to Leibniz on the topic of derivatives, which excited replies on the concept of 'non-integer' order i.e. a more generalized version of differentiation and/or integration. (e.g. Riemann-Liouville definition, Caputo's definition etc.), with Caputo's approach offers the advantage of linking fractional order to physical realization and given by

$$ {}_a^C D_t^\alpha f(t) = \frac{1}{\Gamma(\alpha - n)} \int_a^t \frac{f^{(n)}(\tau)}{(t-\tau)^{\alpha+1-n}} d\tau, \tag{5.6} $$

where $(n-1 < \alpha < n)$ and $\Gamma(.)$ is the *Gamma function*. In addition its Laplace transform is (Podlubny, 1999)

$$ \int_0^\infty e^{-st} \left\{ {}_0^C D_t^\alpha f(t) \right\} dt = s^\alpha F(s) - \sum_{k=0}^{(n-1)} s^{\alpha-k-1} f^{(k)}(0), \tag{5.7} $$

where $F(s) = \mathcal{L}\{f(t)\}$, $(n-1 < \alpha \leq n)$ and s is the Laplace operator.

Without a doubt fractional order calculus enables more flexible analysis and design on dynamical systems and controller solutions. It has proven a mechanism of great benefits in the area of control theory, and Fractional order PID control illustrates such benefits very delicately. Fractional order control design has gained, especially

recently, popularity in the control literature and a number of control design cases can be seen related to industry applications (Monje et al., 2008) (Bohannan, 2008) (Petráš and Vinagre, 2002) (Xue and Chen, 2002). The approach is quite straightforward, i.e. instead of the classical case of integer powers of s, fractional powers are utilised. Hence, additional flexibility in tuning controller parameters arise (note that the fractional controllers can be approximated by appropriate IOR functions and a number of techniques to achieve these approximations exist). There are four well known fractional order controllers: CRONE(Commande Robuste d'Ordre Non Entier) (Oustaloup et al., 2000), Fractional order PID(FOPID) (aka $PI^{\lambda}D^{\mu}$), Fractional Order Lead-Lag compensator (Monje et al., 2004) (Monje et al., 2005) , and Fractional Order Phase shaper (Chen et al., 2004). The work presented here stems from utilising an FOPID and also utilising (Merrikh-Bayat, 2013) which proposes an FOC method that reduces the effect of unstable poles and zeros within a feedback control design framework.

It is well known that in integer order LTI system, the system is stable if there are no real or complex roots located on the right hand plane of the complex plane. This case is differ for fractional order LTI system where the system may stable even with the existence of right have of the complex plane as long as it follows the condition in (5.8) (Chen et al., 2009). The stability region for fraction order system can be seen in Figure 5.6).

$$|arg(eig(A))| > q\frac{\pi}{2} \tag{5.8}$$

As mentioned earlier, the contribution of FOC on PID control in this thesis is twofold: (i) via design of a fractional PID while maintaining the original NMP model in 5.3, (ii) via design of an integer order PID + fractional order-based shaping filter partially cancelling the NMP zeros characteristics of the original model will be discussed in Section 6.1. The former design is discussed here.

Fractional order PID (FOPID) also identified as $PI^{\lambda}D^{\mu}$ introduces two extra variables to tune i.e. the integral (fractional) order (λ) and derivative (fractional) order

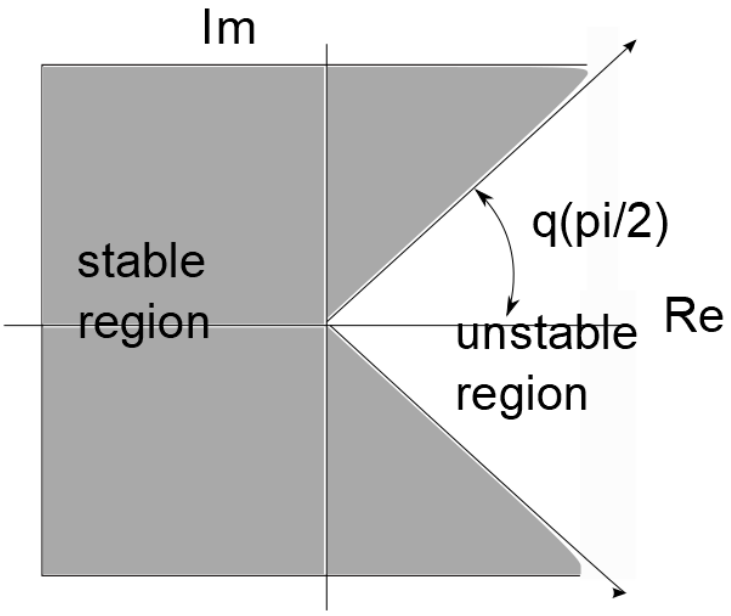

FIGURE 5.6: Stability region for fractional order system (Chen et al., 2009)

(μ). Hence, FOPID enables a much refined shaping of the compensated open-loop in terms of gain/phase with the fractions of orders introduced (but at the expense of tuning five controller parameters). Its transfer function (with limited fractional derivative) is given by

$$K_{FOPID}(s) = k_p \left(1 + \frac{1}{\tau_i s^{\lambda}} + \frac{\tau_d s^{\mu}}{N^{-1} s^{\gamma} + 1}\right) \tag{5.9}$$

where $k_p, \tau_i, \tau_d \in \mathbb{R}^+$ and also $\lambda, \mu, \gamma \in \mathbb{R}^+$ ($\mathbb{R}^+$ the set of positive real numbers). It is normal to set $\gamma = \mu$ for bi-properness (and hence not necessary to tune this parameter in the design process). The parameter N is the derivative cut-off frequency similar to the case of integer order PID.

The introduction of two extra tuning terms in the FOPID adds extra complexity, albeit advanced software tools and available processing power (as well as advances in hardware) nowadays offer a rather trouble-free way of designing. Ultimately FOPID control is possible to implement (via appropriate IOR approximation) although normally its structure will be more complex compared to the conventional PID. FOPID provides a clear advantage on more flexible control design in terms of stability margins and hence open and closed loop shaping (Lanusse et al., 2014). In addition,

while similar to conventional PID, FOPID enables shaping closer to Bode's ideal transfer function. Still FOPID is not the panacea of all solutions as there may be cases where it does not offer better performance compared to a conventional PID, e.g. see issues of rejection of input disturbance to the plant (Lanusse et al., 2014).

5.3.2 Fractional order approximation

After tuning the FOPID (Petráš, 2012) an IOR approximation using one of the accepted methods in the literature (Vinagre et al., 2000), (Xue et al., 2006), can be obtained. One of the most popular techniques is the *Oustaloup recursive method* (provides a recursive approach in approximating the fractional terms) (Vinagre et al., 2000). In fact, the IOR approximation is a key fact that could make FOPID largely attractive to the practising control engineer i.e. offering a more direct way of designing a "refined" PID (on top of any integral or derivative action, injecting a set of lead-lag networks), hence fine shaping the frequency response of the compensated open loop. The notion of frequency shaping via a number of lead-lag networks is also met in more conventional control methodologies such as Quantitative Feedback Theory (Horowitz, 1993).

For its rational order implementation, the Oustaloup (5th order per fractional term) recursive approximation is utilised.

$$\begin{aligned} &H(s) = s^{\mu}, \quad \mu \in \mathbb{R}^{+}, \ \text{ approximated by} \\ &\widehat{H}(s) = C \prod_{k=-M}^{M} \frac{1 + s/\omega_k}{1 + s/\omega'_k} \end{aligned} \tag{5.10}$$

where $C, M, \omega_k, \omega'_k$ are parameters given by the approximation procedure in (Vinagre et al., 2000).

Regarding tuning of the FOPID the same optimization process to the conventional PID is followed, i.e. (5.5), although the optimization runs on all fractional order PID controllers now. Also, the variables to tune are five, and the consideration for initial conditions (given the global optimization) are similar to the case of the

conventional PID (however in this case include the extra two tuning variables of fractional order). A note regarding the order of the integral and derivative terms, i.e. bounds need to be set such that the optimization has a meaning (for example one cannot have an excessive integral or derivative action as these will offer no advantage to the control design). A bound for the fractional order of the integral term between 0.5 and 2 as well as a bound for the derivative term between approx. 0 and 1.25 suffice. Although direct fractional stability can be followed, note that for stability check we employ the integer order approximation of the designed FOPID controller (as papers do follow such an approach (Chen et al., 2009)).

5.3.3 Nominal performance analysis

FOPID optimization cost function set up in this section, follows Eq. (5.5). The aim is to minimize P_{CT} factor as much as possible while satisfied the given constraints. The minimization ID with different constraints is shown in Table 5.6.

TABLE 5.6: Minimization approach identifiers and constraints for FOPID optimisation (Note: rqd denotes ride quality degradation; GM: gain margin; PM: phase margin)

Minimization ID	**f(x)**	**<constraints>**
FO1	P_{CT} (standing)	$GM \geq 1.45$, $PM \geq 45^0$
FO2	P_{CT} (standing)	$GM \geq 1.45$, $PM \geq 45^0$, rqd $\leq 7.5\%$
FO3	P_{CT} (standing)	rqd $\leq 7.5\%$, $\|S(j\omega)\|_\infty \leq 2$
FO4	P_{CT} (standing)	rqd $\leq 7.5\%$, $\|S(j\omega)\|_\infty \leq 2$, $\|W_\delta(j\omega)T(j\omega)\|_\infty \leq 1$

The tuned FOPID controller parameters values that satisfied all the constraints Table 5.6 can be seen in Table 5.7 below,

TABLE 5.7: FOPID optimised parameter values

	K_p	τ_i	τ_d	λ	μ
FO1	0.2863	0.0925	0.0607	1.5064	1.2500
FO2	0.2703	0.1087	0.0532	1.5557	0.8140
FO3	0.2174	0.0801	0.0425	1.6589	1.0663
FO4	0.2217	0.0843	0.029	1.673	0.913

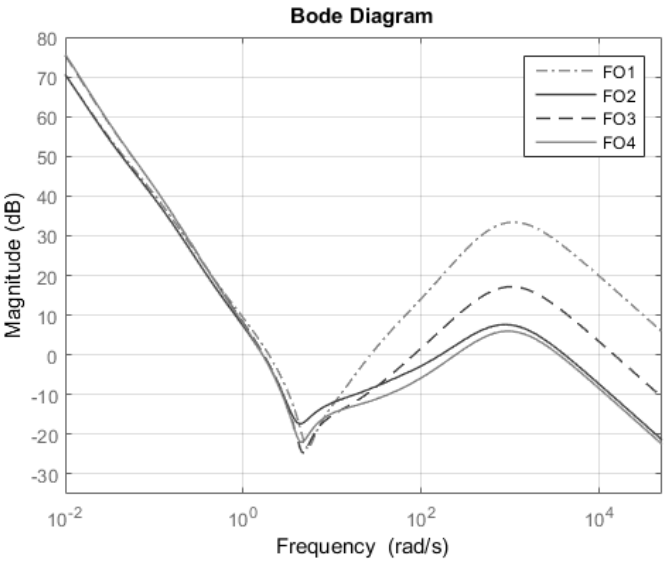

FIGURE 5.7: Control frequency plot for FO1, FO2, FO3 and FO4

The rational order controller approximation is of 12th order after minimal realization. The full order controller approximation in Appendix C.1. Table 5.9 and Table 5.8 presents the FOPID results (for the nominal plant and, in this case, using the 12th order controller IOR approximation).

TABLE 5.8: Stability margins for the conventional PID controllers

PID rule	**GM(dB)**	**PM(deg)**	**B/W(rad/s)**	$\|S\|_\infty$
FO1	3.203	45.00	1.32	3.872
FO2	3.499	44.993	1.06	3.224
FO3	6.258	30.669	1.05	1.986
FO4	6.49	30.45	1.02	2.00

In term of nominal performance in tilting train, P_{CT} factor for both standing and seating are definitely better than normal PID optimisation and Ziegler-Nichols method while ride quality degradation can be maintained within acceptable limit. Plant with FOPID controller also show some robust performance by keeping the sensitivity (S) and complementary sensitivity(T) peak as in Figure and acceptable gain and phase margin for robust stability.

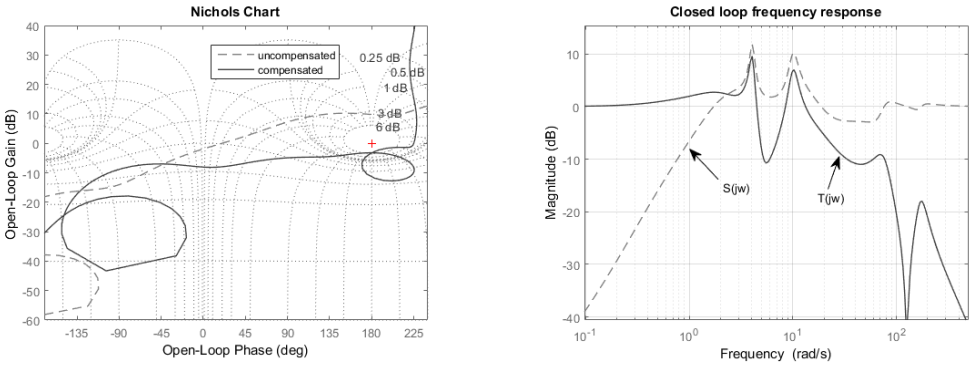

(a) Frequency plot (b) Closed loop sensitivity plot

FIGURE 5.8: Frequency (a) and closed loop plot (complementary and sensitivity) for plant with FO1 controller

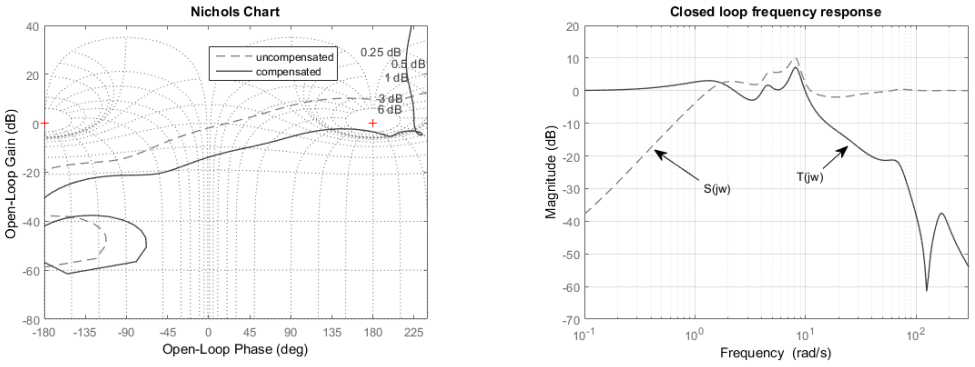

(a) Frequency plot (b) Closed loop sensitivity plot

FIGURE 5.9: Frequency (a) and closed loop plot (complementary and sensitivity) for plant with FO2 controller

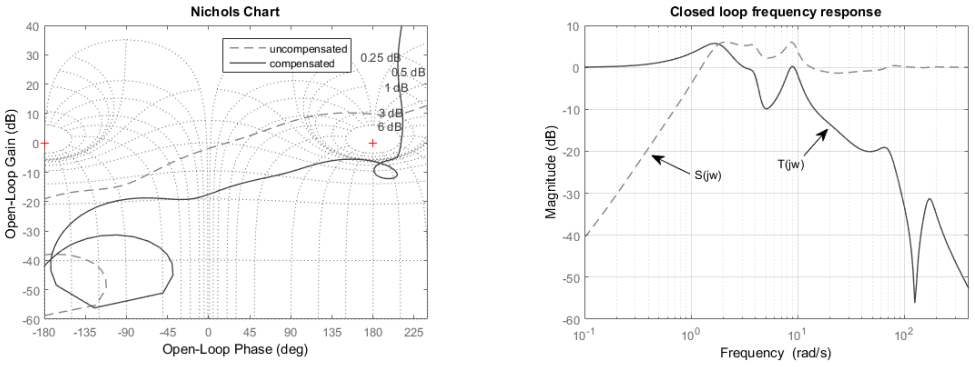

(a) Frequency plot (b) Closed loop sensitivity plot

FIGURE 5.10: Frequency (a) and closed loop plot (complementary and sensitivity) for plant with FO4 controller

TABLE 5.9: FOPID controller performance assessment with the different time-domain optimisation approaches

Deterministic(as per given units)		**FO1**	**FO2**	**FO3**	**FO4**
Lateral accel.	RMS Deviation (%g)	1.998	2.412	2.474	2.609
	Peak value (%g)	10.725	10.133	10.803	10.884
Roll gyro.	RMS deviation(rad/s)	0.023	0.028	0.029	0.031
	Peak value (rad/s)	0.123	0.133	0.138	0.140
P_{CT} related	Peak jerk level(%g/s)	6.210	6.776	6.923	6.652
	Standing (% of passenger)	44.895	50.275	51.030	51.454
	Seated (% of passenger)	11.516	12.736	12.710	12.621
Stochastic (acceleration %g) @58m/s **					
**Ride quality for non-tilting train if running at the higher speed = 2.848%g					
Ride quality	Tilting train	3.936	3.062	3.063	3.063
	Degradation (%)	38.193	7.499	7.533	7.543

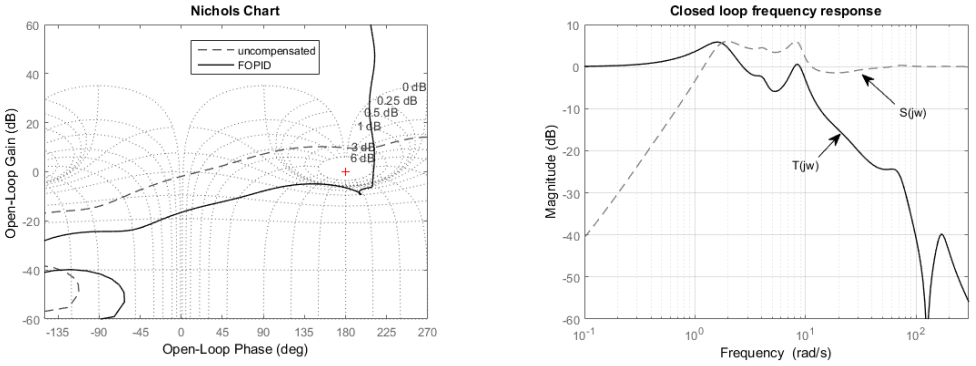

(a) Frequency plot

(b) Closed loop sensitivity plot

FIGURE 5.11: Frequency (a) and closed loop plot (complementary and sensitivity) for plant with FO4 controller

5.4 Robustness analysis - for the optimised PID control cases

In this section, we briefly discuss fundamental robust performance consideration for the proposed controller designs. The robustness analysis is based on the uncertainty consideration discussed in Section 3.4.1. For robust performance analysis 6 cases

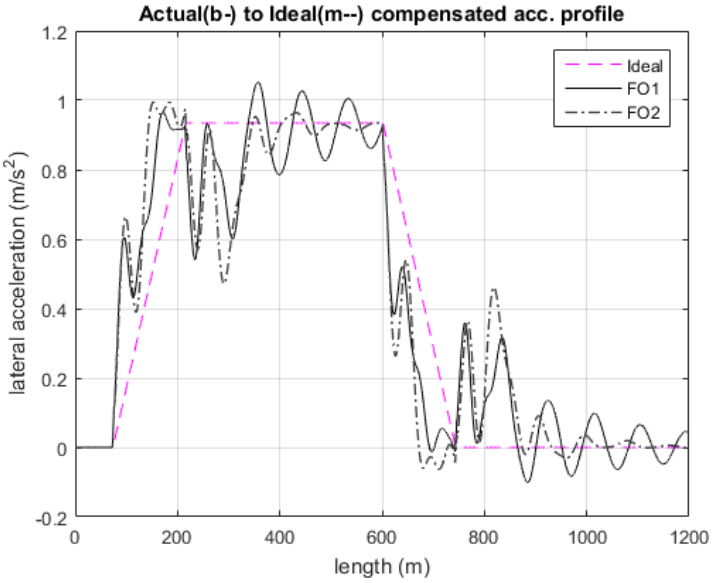

(a) Lateral acceleration plot for FO1 and FO2

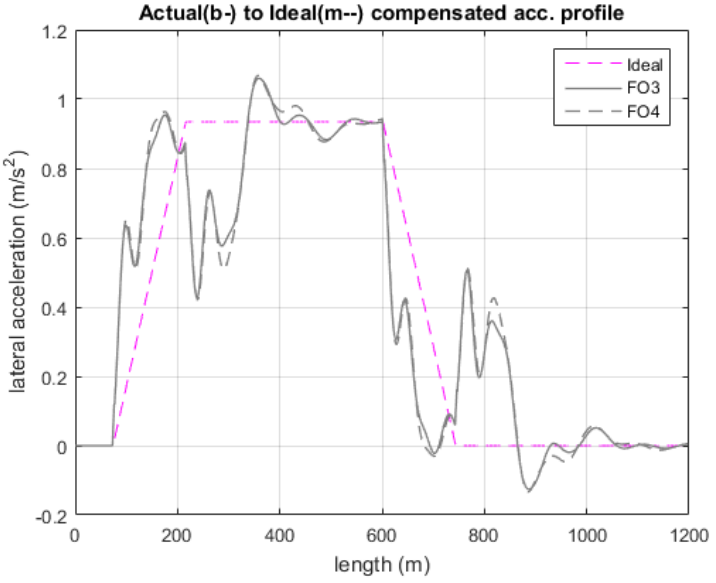

(b) Lateral acceleration for FO3 and FO4

FIGURE 5.12: Lateral acceleration plot for non precedence tilt with FOPID controller (a) and (b)

are selected according to their satisfied nominal performance as following, Ziegler-Nichols Modified optimisation, CF7, CF8 ,FO3 and FO4.

Closed loop robust performance can be seen in complementary sensitivity plot (T) with W_δ bound (introduced in Section 3.4.1) in Figure5.13. For CF8 and FO4 case, the robustness in guaranteed in design process where the complementary sensitivity for both cases is expected to be constrained below multiplicative uncertainty bound (W_δ).

TABLE 5.10: Robust performance for P_{CT} standing for all conventional cases

PID rule	**Nominal**	**P1**	**P2**	**P3**	P4
ZN optimised	62.47	62.97	65.09	71.73	66.70
CF7	63.10	63.68	65.01	69.54	67.11
CF8	64.83	66.10	66.00	67.47	70.12
FO3	51.03	50.10	53.23	58.50	52.61
FO4	51.44	51.31	53.19	59.44	52.64

TABLE 5.11: Robust performance for ride quality degradation for all conventional cases

PID rule	**Nominal**	**P1**	**P2**	**P3**	P4
ZN optimised	7.49	17.79	8.55	64.87	55.98
CF7	7.49	15.45	9.07	33.65	40.35
CF8	6.41	11.61	12.10	40.83	24.96
FO3	7.53	27.74	-2.034	-3.48	182.04
FO4	7.48	23.51	-0.80	-1.90	82.99

5.5 Summary

This chapter discusses optimised PID control design. In particular it extends the modified Z-N based PID controller via constrained optimization, moves to a more generic type of optimization based PID design and introduces a non-conventional (non-integer) PID optimized control design. It is clear that the introduction of optimization benefits achieving improved tilt control performance compared to the manually designed cases. In addition, the optimization based approach helps in terms of robustness (robustness related constraints can be included in the design as required). From a performance point of view, it is seen that the FOPID tilt control

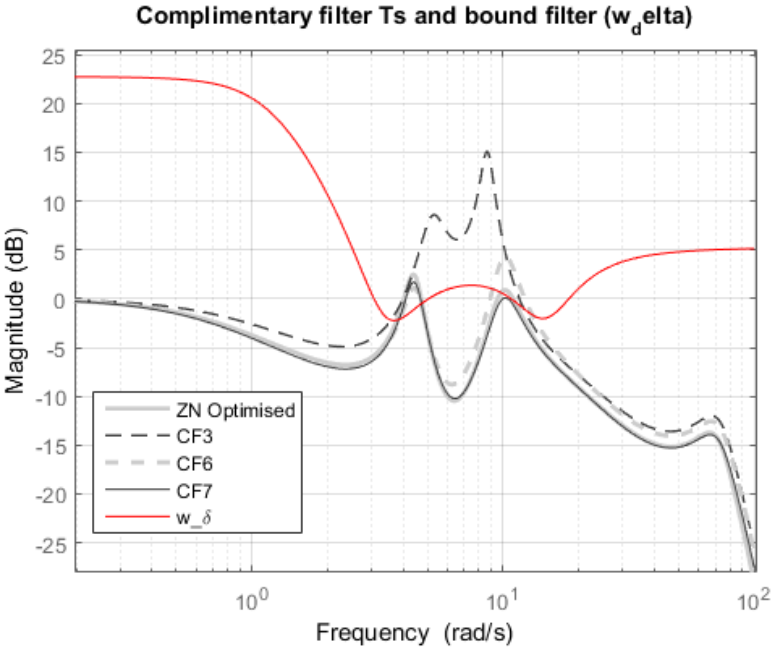

(a)

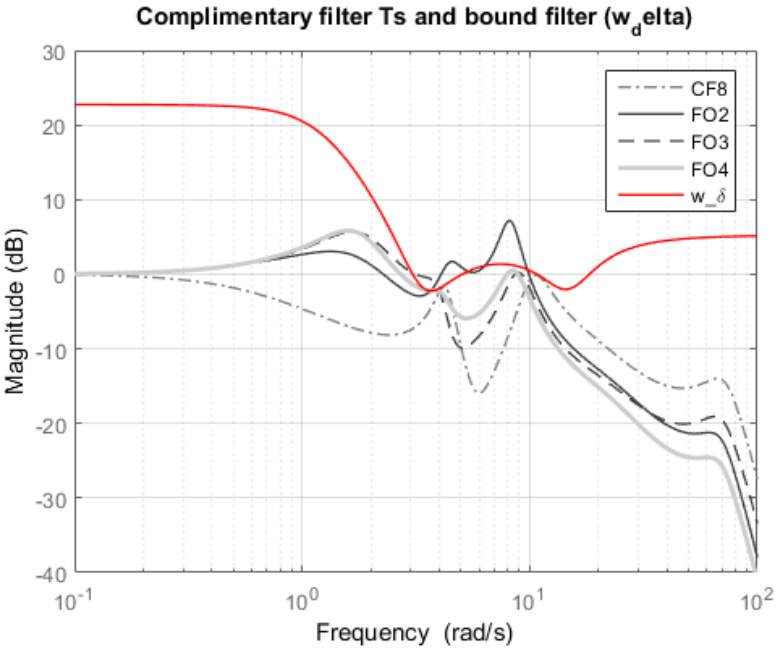

(b)

FIGURE 5.13: Closed loop complementary sensitivity bound for (a) Ziegler-Nichols optimised, CF3,CF6,CF7 (b) CF8,FO2,FO3,FO4

design proposal provides the best results compared to the other optimization based approaches presented here. The chapter has also presented a trend of outcomes that stem from the different optimization problems (again a point of particular interest to the practising control engineer).

Chapter 6

Robust loop shaping based tilt control design

We choose to present two loop-shaping based controller designs for the tilt control problem, maintaining the SISO control set-up as before. The first approach, and a major contribution in the topic studied in the thesis, is PID with fractional order shaping of the compensated loop (targeting so called partial cancellation of the NMP zero characteristics). This also illustrates additional benefits via fractional order methods. The chapter then completes by enhancing the robust (integer) H_∞ mixed sensitivity design (originally presented in (Zolotas, 2002)) by introducing optimization of the weighting functions. As in the previous chapter, nominal performance analysis first occurs and then both proposed approaches are assessed for robust performance. Note that the fractional order based approach will naturally result to rational approximation controllers of higher order than a simple PID, hence the comparison with a conventional H-infinity model-based approach which also offers controllers of comparable size.

6.1 Fractional order control with NMP zero shaping

We have introduced fractional order control in the previous chapter, in particular the FOPID case in section 5.3. Here we present an alternative fractional order control based approach comprising an integer-based PID controller and a fractional order NMP zero cancellation filter.

More particularly, motivated by maintaining a PID-type controller structure and explore shaping of the NMP characteristics of the tilt design plant TF (based on seminal work of Merrikh-Bayat in (Merrikh-Bayat, 2013) on using fractional order filters to partially cancel unstable TF zeros), the design of an integer-order PID is presented on the shaped tilt design TF (shaped by use of NMP zero partial cancellation fractional order filter). Only partial cancellation is considered, due to full cancellation of unstable zeros being undesirable (e.g. note system uncertainty always exists in practice). The process is rather straightforward, (i) shape the plant TF by using of the cancellation fractional order filter Q_n^{-1}; (ii) design the rational-order PID controller on the shaped plant, i.e. on $G_{yu} \times Q_n^{-1}$; (iii) get the final controller as $Q_n^{-1} \times K_{pid}^i$ and implement on original plant (practically the implementation will utilise the rational order approximation of the Q-filter (e.g. after Oustaloup's method) i.e. denoted as $\tilde{Q}_n^{-1}$). This design set-up is used in Figure 6.1. A simplified setup used with no feed-forward of disturbances. The rationale is twofold: (i) accurate estimation of railtrack disturbance inputs is possible (Zolotas and Goodall, 2000) but challenging, while adding complexity to the solution, (ii) the impact of fractional order methods on simple tilt control design is emphasized.

A cancellation example (Merrikh-Bayat, 2013) for a single unstable zero is shown in (6.1) (n is integer; z_u the unstable zero freq.)

$$1 - s/z_u = 1 - (s/z_u)^{n/n} = \left[1 - \left(\frac{s}{z_u}\right)^{1/n}\right] \sum_{k=1}^{n} \left(\frac{s}{z_u}\right)^{(k-1)/n} \tag{6.1}$$

Essentially the partial cancellation of the NMP characteristics of the plant ultimately enables refined shaping of the plant by a series of lead-lag networks in the frequency domain, hence the potential for improved performance margins. A note on the cancellation nature in the shaped plant TF, e.g. $n = 2$ results to 1/2 portion of the NMP zeros characteristic is cancelled, $n = 3$ to 2/3, $n = 4$ to 3/4 etc. This clearly shows the impact of fractional order methods from the loop-shaping viewpoint.

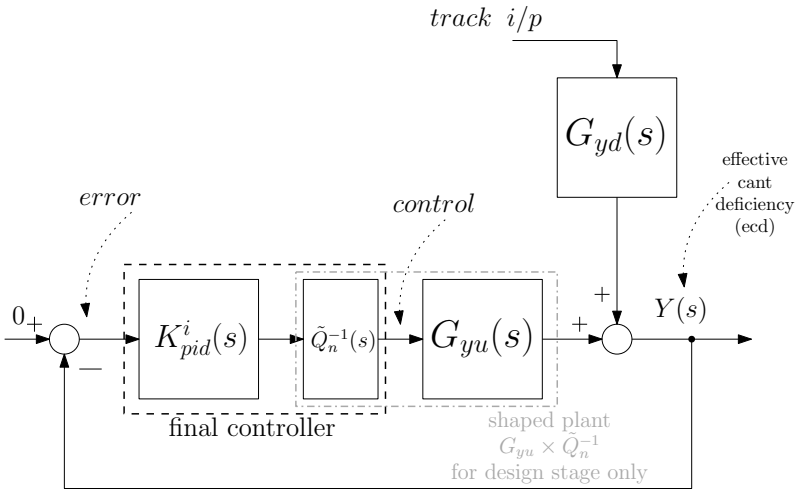

FIGURE 6.1: The feedback structure for the fractional order shaping controller design

The design of the PID controller here is also following the optimization problem given by,

$$\begin{aligned} \underset{K_{pid}}{\text{minimize}} \quad & f(x) = P_{CT}\ standing \\ \text{subject to} \quad & rqd \leq 7.5\% \\ & \|S(j\omega)\|_\infty \leq 2 \\ & \|W_\delta(j\omega)T(j\omega)\|_\infty \leq 1, \end{aligned} \tag{6.2}$$

However the optimization runs over all integer order PID controllers using the shaped by Q_n^{-1} plant TF. The consideration for initial conditions (given the global optimization) are similar to the case of the conventional PID (still have only three gains to tune) but the initial gains given by Z-N rules are obtained from the shaped

plant TF). For completeness, the multi-start approach here perturbs initial conditions with a random initial value generation in the interval $[0.01\vec{x}_0, 2\vec{x}_0]$, where $\vec{x}_0$ is a row vector of initial gains given by Z-N rules are obtained from the shaped, per Q filter, plant TF.

The fractional order shaping filters Q_n^{-1} for the increasing level of NMPZ part cancellation from $n = 2$ up to $n = 7$ are:

$$Q_{\{n=2\}} = 0.0752s + 0.592s^{0.5} + 1 \tag{6.3}$$

$$Q_{\{n=3\}} = 0.0318s^{1.33} + 0.156s + 0.586s^{0.67} + 0.874s^{0.33} + 1 \tag{6.4}$$

$$\begin{aligned} Q_{\{n=4\}} = {} & 0.0206s^{1.5} + 0.0803s^{1.25} + 0.2376s + 0.632s^{0.75} + 0.867s^{0.5} \ldots \\ & + 1.068s^{0.25} + 1 \end{aligned} \tag{6.5}$$

$$\begin{aligned} Q_{\{n=5\}} = {} & 0.0159s^{1.6} + 0.0541s^{1.4} + 0.14s^{1.2} + 0.32s + 0.696s^{0.8} \ldots \\ & + 0.901s^{0.6} + 1.1s^{0.4} + 1.21s^{0.2} + 1 \end{aligned} \tag{6.6}$$

$$\begin{aligned} Q_{\{n=6\}} = {} & 0.0135s^{1.6667} + 0.048s^{1.5} + 0.098s^{1.3333} + 0.21s^{1.1667} + 0.41s \ldots \\ & + 0.77s^{0.8333} + 0.96s^{0.6667} + 1.15s^{0.5} + 1.3s^{0.3333} + 1.31s^{0.1667} + 1 \end{aligned} \tag{6.7}$$

$$\begin{aligned} Q_{\{n=7\}} = {} & 0.012s^{1.7143} + 0.035s^{1.5714} + 0.076s^{1.4286} + 0.15s^{1.2857} \ldots \\ & + 0.28s^{1.1429} + 0.49s + 0.85s^{0.8571} + 1.02s^{0.7143} + 1.2s^{0.5714} \ldots \\ & + 1.37s^{0.4286} + 1.46s^{0.286} + 1.4s^{0.1429} + 1 \end{aligned} \tag{6.8}$$

The obtained controller gains for the integer-order PID portion, from the optimization process on the shaped plant using the above filters, are given (time constant in seconds):

$$\begin{aligned} &\text{on case } n{=}0: \quad k_p = 0.045 \quad \tau_i = 0.056 \quad \tau_d = 0.533 \\ &\text{on case } n{=}2: \quad k_p = 0.1057 \quad \tau_i = 0.0568 \quad \tau_d = 0.6743 \\ &\text{on case } n{=}3: \quad k_p = 0.2821 \quad \tau_i = 0.0810 \quad \tau_d = 0.5315 \\ &\text{on case } n{=}4: \quad k_p = 0.4782 \quad \tau_i = 0.0839 \quad \tau_d = 0.5401 \\ &\text{on case } n{=}5: \quad k_p = 0.7691 \quad \tau_i = 0.0917 \quad \tau_d = 0.5165 \\ &\text{on case } n{=}6: \quad k_p = 1.000 \quad \tau_i = 0.083 \quad \tau_d = 0.574 \\ &\text{on case } n{=}7: \quad k_p = 1.398 \quad \tau_i = 0.088 \quad \tau_d = 0.555 \end{aligned}$$

The implementation of the fractional order filter Q_n^{-1} within the final controller $\tilde{Q}_n^{-1} \times K_{pid}^i$ also utilises a 5th order Oustaloup continuous-time (CT) realization (Vinagre et al., 2000). Below few details on the overall controller integer-order approximation is presented., while the full order transfer function of $\tilde{Q}_n^{-1}$ filter is available in Appendix C.1. Note that the overall controller order comprises the order of the PID (being 2nd order) portion and the order of $\tilde{Q}_n^{-1}$ after minimal realization (per n case). Hence (note that the filter integer-order is after minimal realization),

for n=2: filter integer-order= 6 (final contr. integer-order= 8)
for n=3: filter integer-order= 11 (final contr. integer-order= 13)
for n=4: filter integer-order= 16 (final contr. integer-order= 18)
for n=5: filter integer-order= 21 (final contr. integer-order= 23)
for n=6: filter integer-order= 26 (final contr. integer-order= 28)
for n=7: filter integer-order= 31 (final contr. integer-order= 33)

Note that: (a) for n=0 the results are the ones obtained for the optimized integer-order PID as there is no NMP zero portion cancellation; (b) a 5th order CT approximation of the fractional power has been found to be sufficient; (c) we consider up to $n = 7$ NMPZ cancellation as after that value performance differences become less significant. Figure 6.2 presents the compensated open loop magnitude frequency plot for this loop shaping design case, i.e. $G_{yu} \times (\tilde{Q}_n^{-1} K_{pid}^i)$ per case n.

TABLE 6.1: Performance assessment (P_{CT} / Ride qual.) under different FO partial cancellation degree (incl. PID)

Deterministic(as per given units)		Full Order **1/2** cancel.	Full Order **2/3** cancel.	Full Order **3/4** cancel.	Full Order **4/5** cancel.	Full Order **5/6** cancel.	Full Order **6/7** cancel.
Lateral accel.	RMS Deviation ($\%g$)	3.394	3.006	2.842	2.771	2.684	2.664
	Peak value ($\%g$)	15.335	13.893	12.995	12.468	12.069	11.887
Roll gyro.	RMS deviation(rad/s)	0.030	0.030	0.030	0.030	0.030	0.030
	Peak value (rad/s)	0.103	0.113	0.119	0.122	0.125	0.126
P_{CT} related	Peak jerk level($\%g/s$)	8.239	7.790	7.579	7.398	7.334	7.231
	Standing (% of passenger)	59.245	56.887	55.481	54.543	54.173	53.874
	Seated (% of passenger)	17.581	16.246	15.459	14.941	14.641	14.436
Stochastic (acceleration %g) @58m/s **							
**Ride quality for non-tilting train if running at the higher speed = 2.848%g							
Ride quality	Tilting train	2.930	2.955	2.981	3.002	3.011	3.024
	Degradation (%)	2.867	3.757	4.656	5.396	5.724	6.168

TABLE 6.2: Stability margins for PID+Q_n^{-1} controller

Final Controller	**GM(dB)**	**PM(deg)**	**B/W(rad/s)**	$\|S\|_\infty$
PID only (0 canc.)	6.01	89.9	0.7	1.99
PID with 1/2 canc.	6.171	70.939	0.83	1.99
PID with 2/3 canc.	6.305	61.547	0.88	1.99
PID with 3/4 canc.	6.479	55.278	0.91	1.99
PID with 4/5 canc.	6.567	51.883	0.93	1.99
PID with 5/6 canc.	6.582	47.931	0.96	1.99
PID with 6/7 canc.	6.63	46.34	0.96	1.99

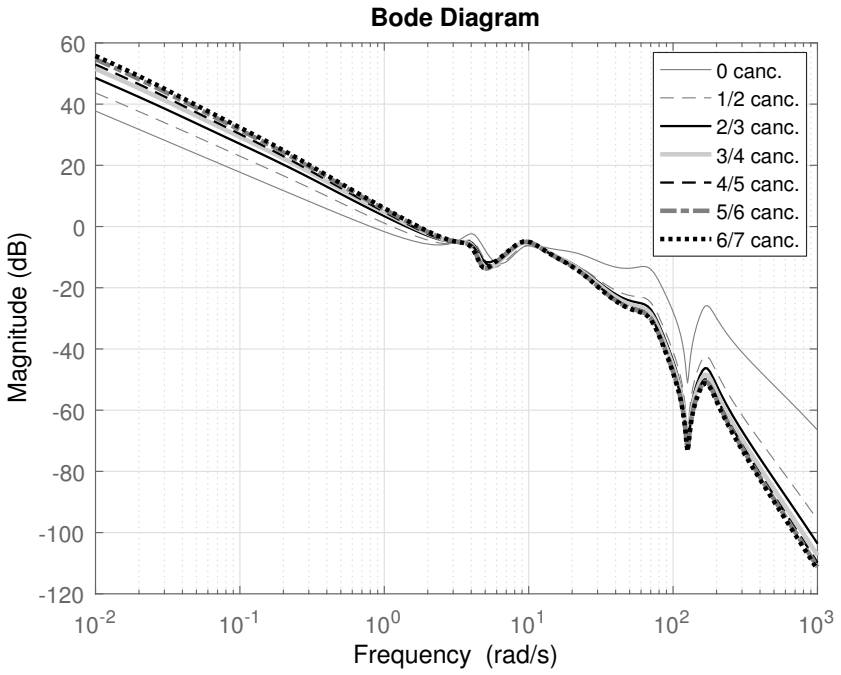

FIGURE 6.2: Designed open loop magnitude plot for the fractional order loop shaping case

6.1.1 Reduced order considerations of the loop-shaping fractional order controller

We have discussed about rational order representation of fractional order controllers in section 5.3. However, here one has a slightly different case where the high order contribution of the controller comes from the so called cancellation filter (when this is combined with the PID part in the implementation stage). Hence, the overall rational order controller (as shown in the previous section) will be high to very high

order. Still, the question posed here is whether it is still practical to implement the approximated rational order controller. In this context, controller reduction (Obinata and Anderson, 2012) aims to preserve the properties of the closed loop in which the controller would operate. Designers seek as much closeness as possible in the behaviour of the closed-loop of the plant with the high-order controller and the closed-loop of the plant with the low-order controller. The controller reduction problem is posed as a frequency-weighted one, emphasizing approximation in critical frequency ranges for the closed-loop system. The process is as follows, a low-order

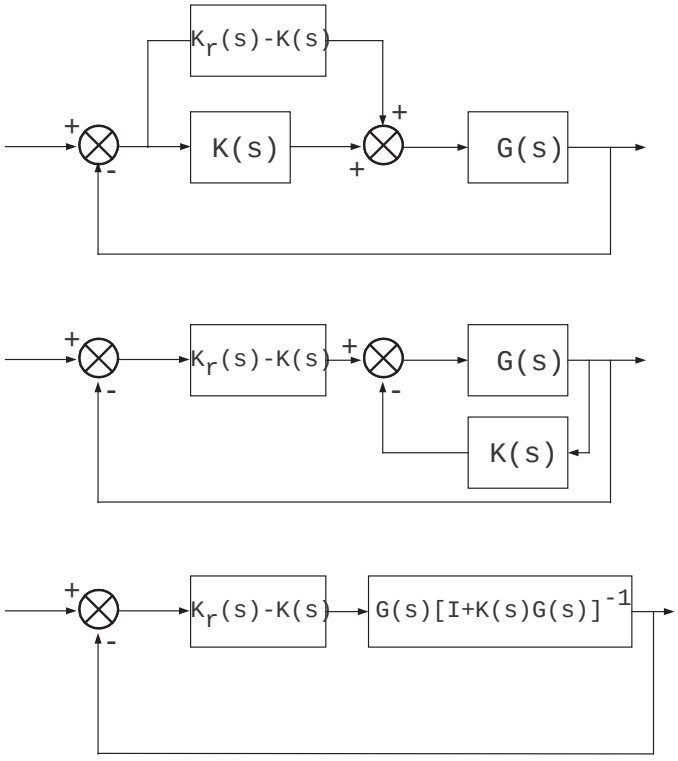

FIGURE 6.3: Reduced-order controller feedback formulation for stability criteria

controller $K_r(s)$ is required to replace the high-order IOR approximation, of the FO controller, $K(s)$ in the closed-loop. This is shown in the top feedback structure of Figure 6.3 (introduced in an additive sense), while the middle and bottom modified feedback structures in the same figure have the same stability properties, leading to the (most usual) frequency weighted formulation of the controller design. In particular, the reduction problem is to find (a stabilising) low-order controller $K_r(s)$

such that the quantity (note that here all elements are rational order TFs)

$$||(K(j\omega) - K_r(j\omega))F(j\omega)||_\infty \tag{6.9}$$

is minimized, with $F(j\omega) = G(j\omega)(I+K(j\omega)G(j\omega))^{-1}$ (the reduction algorithm can be found in (Obinata and Anderson, 2012) and thus we omit its theoretical details). In the expressions $K(j\omega)$ and $G(j\omega)$ refer to the rational order approximation of the fractional order controllers and $G_{yu}(j\omega)$ resp. Note that there are also alternative frequency weighted formulations with more details also available in (Obinata and Anderson, 2012). The frequency weight $F(j\omega)$ essentially introduces the importance of the true plant and controller information in the design procedure via the closed loop consideration. The low-order controller $K_r(s)$ will then be implemented on the original plant to control.

Although controller reduction could be incorporated as part of an extended global optimization problem, it is normal for control designers to investigate controller reduction after the actual design of the original (full-order) controller (Obinata and Anderson, 2012). In addition, although there are other ways of controller reduction (such as frequency domain identification of lower order equivalents), the one used here is of particular interest to the control community in terms of maintaining closed-loop properties.

Here, frequency weighted model reduction using balanced truncation is employed on the full order controller. This is rather popular method for model reduction problem due to it provides an error bound while still maintain the stability of the high order model. This thesis will not go into detail of the theory of this method rather use it as a tools for controller reduction (Besselink et al., 2013).

The controller reduction results are presented for the full order rational approximation (after Oustaloup's method is applied and the minimal realization) of the loop shaping case of the PID plus shaping filter $\tilde{Q}_{n=7}^{-1}$ (the reduction process rationale is rather similar also for $n = 2, \ldots, 6$ hence we omit these cases). Figure 6.4 presents (only the stable closed-loop cases) controller reduction level and the related P_{CT} factor and ride quality performance trade-off.

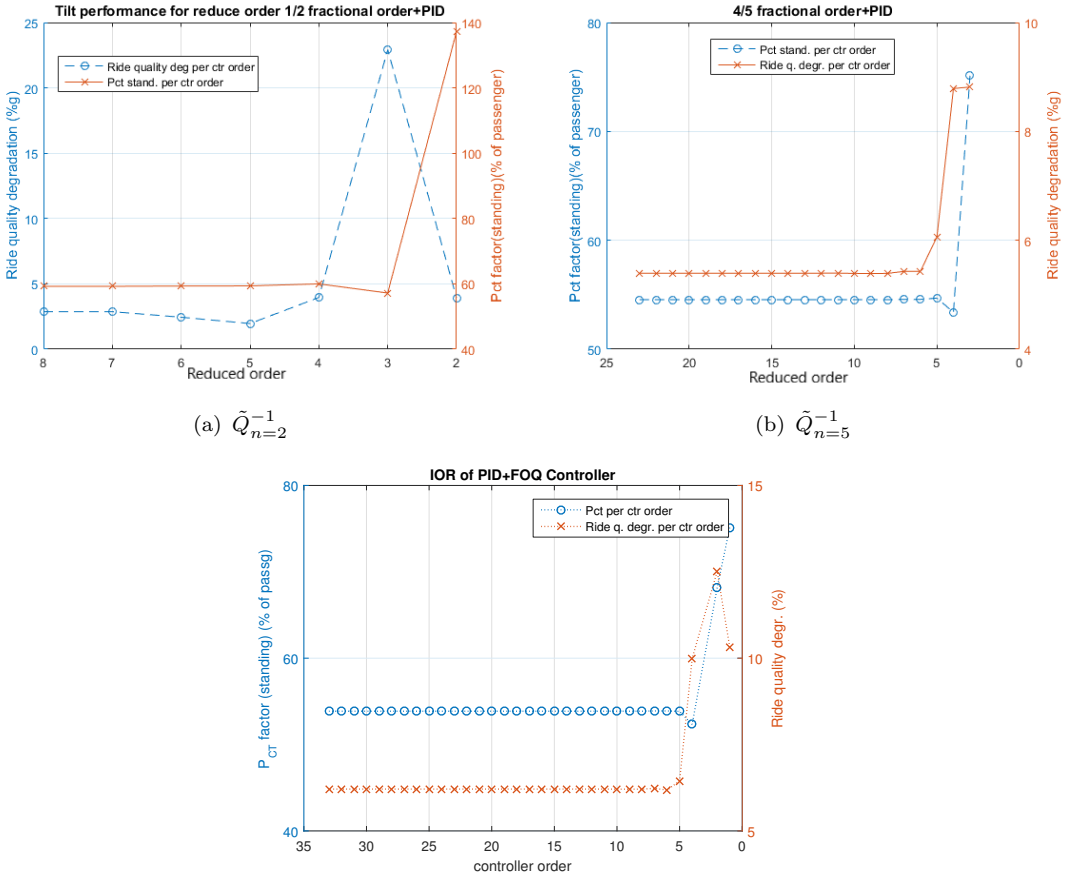

(a) $\tilde{Q}^{-1}_{n=2}$ (b) $\tilde{Q}^{-1}_{n=5}$

(c) $\tilde{Q}^{-1}_{n=7}$

FIGURE 6.4: Controller reduction and performance trade-off (of the rational-order approximated fractional-order based controllers(Approximation of PID + $\tilde{Q}^{-1}_{n=2}$,$\tilde{Q}^{-1}_{n=5}$ and $\tilde{Q}^{-1}_{n=7}$)

To also maintain the typical robustness properties (i.e. robust stability and sensitivity peak) 7th order loop shaping controller employed for robust analysis in the next section. This also illustrates the usefulness the controller reduction approach combined with the integer-order approximation of the FO controllers (up to 85% reduction for the loop-shaping controller $\tilde{Q}^{-1}_{n=7}$ case). It is worth noting that controller order has immense impact on hardware resources required for practical implementation of the controller algorithm, i.e. low-order controllers are always favourable, (an example on FPGAs for LQG controllers can be seen in (Deliparaschos et al., 2016)).

6.1.2 Nominal Performance (nominal plant and controller)

Few nominal system performance results have been presented in previous sections, while here a set of time-domain simulation figures is included to complement the design outcome. The Optimized integer-order PID controllers is already 2nd order, while the reduced order rational-order controllers are utilised for all loop-shaping controllers (for the latter case we refer to case $\tilde{Q}_n^{-1}$).

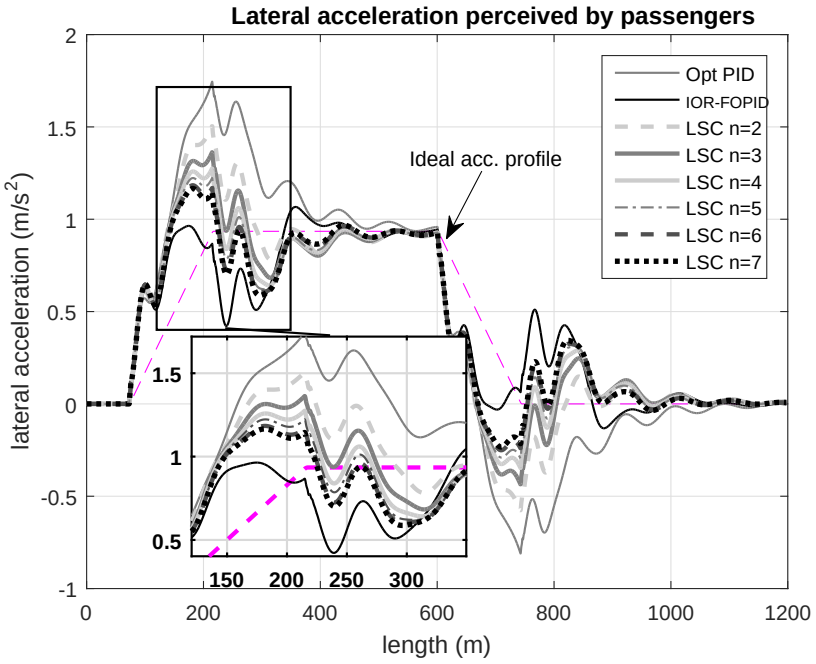

FIGURE 6.5: Passenger acceler. (determ.) (a) Conventional PID; (b) Optim. PID and Fractional order based control(Optim. PID, IOR-FOPID, PID+$\tilde{Q}_n^{-1}$ (LSC) for $n = 2, \ldots, 7$ (no reduction yet(full order)))

Figure 6.5 illustrates the immense benefit of fractional order based control on improvement of deterministic response (track curve following). This is proven via the passenger acceleration plot in Figure 6.5 where $\tilde{Q}_7^{-1}$ case provides much less oscillation compare to PID(via optimization) case which means much faster controller is achieved. In Figure 6.5 no reduction for the fractional order based controllers applied yet. Figure 6.6 further illustrates the benefit that arises from fractional order based control used in non-precedent tilt, i.e. its close proximity to the industrial-norm curving response of tilt with precedence (recall that tilt precedence schemes are more complex in their set-up as described earlier in the paper). In Figure 6.6 reduced order controllers are utilized.

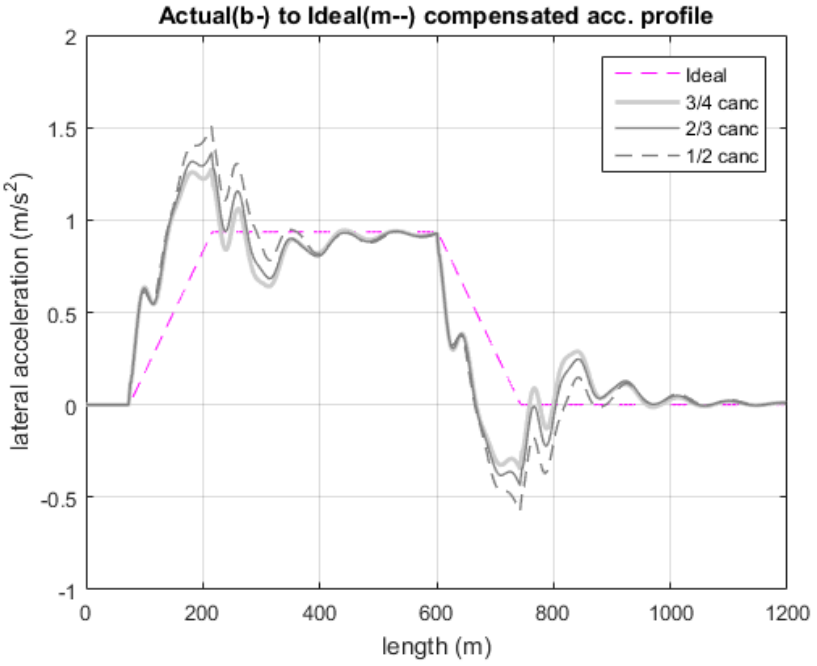

(a) 7th order reduced controller for 1/2, 2/3 and 3/4 canc. case

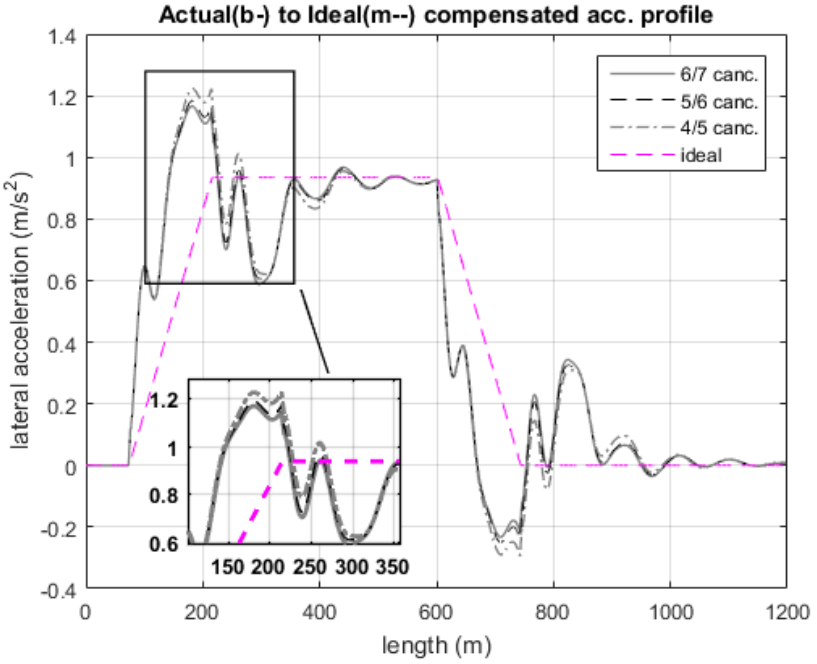

(b) 7th order reduced controller for 4/5, 5/6 and 6/7 canc. case

FIGURE 6.6: Passenger acceleration (determ.) (the precedence scheme uses tilt angle preview information to provide the 60% tilt compensation and integer-order PID for tracking

6.1.3 Robust performance (plant uncertainty)

For robust performance analysis, 7th order reduced controller will be used here for each PID + $\tilde{Q}_n^{-1}$ cases. Nominal performance on 7th order controller reduction shows no difference in term of P_{CT} and ride quality performance. It is worth noting that the reduced order controllers maintain the required robust stability result, this being clearly seen on Figure 6.7. This is further supported in Table 6.3 and Table 6.4 illustrating P_{CT} and ride quality degradation for the different plants (noting that the controllers where designed on the nominal plant i.e. $P0$).

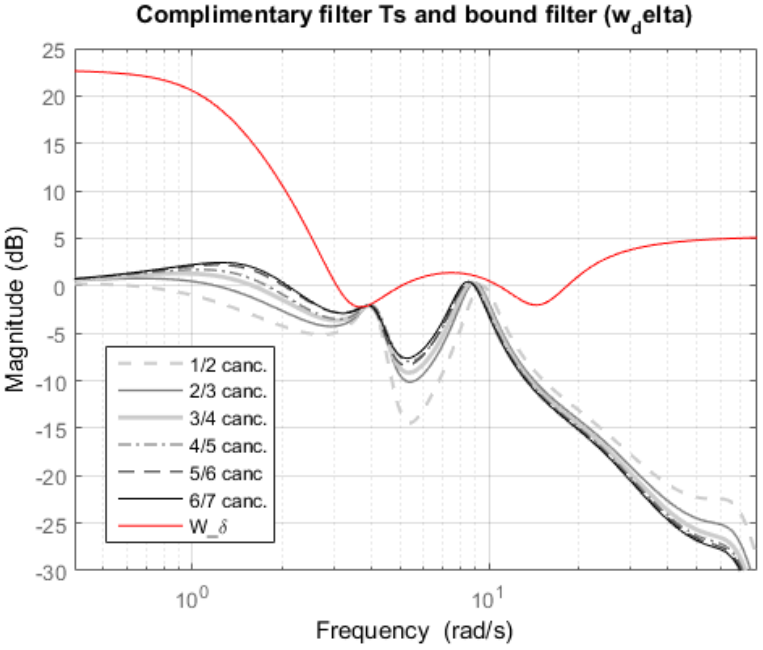

FIGURE 6.7: Reduced-order controller complementary sensitivity(T) with W_δ bound.

TABLE 6.3: Robust performance for P_{CT} standing (7th order controller)

Case	**P0 nominal**	**P1**	**P2**	**P3**	P4
1/2 cancel.	59.244	61.996	61.816	64.185	65.161
2/3 cancel.	56.888	59.080	61.395	65.775	61.667
3/4 cancel.	55.482	57.632	59.603	64.755	59.746
4/5 cancel.	54.575	56.728	58.335	64.071	58.670
5/6 cancel.	54.207	55.843	57.406	62.995	57.382
6/7 cancel.	53.907	55.542	56.709	62.466	56.878

TABLE 6.4: Robust performance for ride quality (7th order controller)

Case	**P0 nominal**	**P1**	**P2**	**P3**	P4
1/2 cancel.	2.871	14.975	-4.933	-4.755	46.382
2/3 cancel.	3.748	16.932	-5.021	-6.825	54.566
3/4 cancel.	4.680	18.417	-3.943	-5.621	60.385
4/5 cancel.	5.429	19.187	-2.837	-4.198	61.920
5/6 cancel.	5.745	20.248	-2.530	-3.730	68.821
6/7 cancel.	6.181	20.534	-1.795	-2.751	68.165

Robust stability is clearly seen on P_{CT} (as it directly treats deterministic problems), however the design naturally does not directly cater for robust ride quality performance (i.e. the stochastic criterion, which is not in the scope of this paper). In few cases the stochastic ride quality result is outside the ride quality bounds which is expected. Plant case $P4$ is a rather extreme case of vehicle parameter uncertainty (e.g. under such vehicle conditions, the vehicle would be transferred to the depot for maintenance/replacement of the suspensions). This plant case is used here to illustrate the extend of robust stability the designed controllers achieve.

6.2 $H\infty$ mixed sensitivity loop shaping

6.2.1 Mixed sensitivity

This second method listed here, stems from initial work presented in (Zolotas, 2002). We extend the initial SISO advanced (integer-order) robust approach by using optimization in tuning the related weighting functions for the mixed sensitivity design. In such way, we illustrate how a more advanced integer-order approach will be compared to the previous fractional order based loop shaping design as well. Mixed-sensitivity refers to closed loop transfer function shaping problems where the sensitivity S is shaped together with other closed loop transfer functions like KS (control sensitivity) and/or T (complementary sensitivity) (Skogestad and Postlethwaite, 2007).

The SISO control problem feedback set-up for this control structure is shown in Figure 6.8. W_1 is the frequency weight for $S(jw)$, W_2 is the frequency weight for $KS(jw)$ and W_3 for $T(j\omega)$. The overall minimisation problem can be summarised as (note that here we present all three sensitivity functions),

$$\min_{K\in\mathbb{S}} \left\| \begin{matrix} W_1 S \\ W_2 KS \\ W_3 T \end{matrix} \right\|_\infty$$
$$\min_{K\in\mathbb{S}} \left\| \begin{matrix} W_1(I+GK)^{-1} \\ W_2 K(I+GK)^{-1} \\ W_3 GK(I+GK)^{-1} \end{matrix} \right\|_\infty \tag{6.10}$$

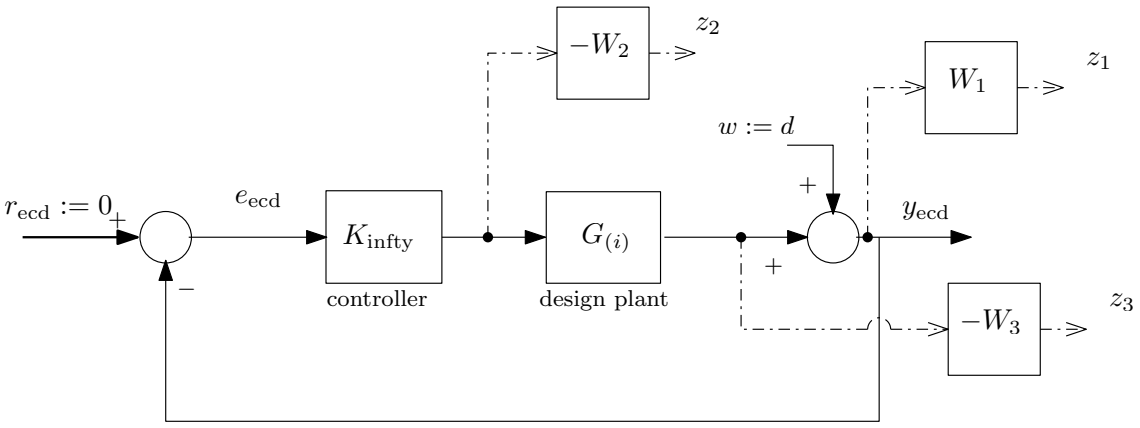

FIGURE 6.8: Feedback set-up for the tilt related robust H_∞ mixed sensitivity-regulation problem

Hence, the design problem is to get a model-based controller K(s), based upon the presented framework, to meet several requirements such as closed loop stability, good tracking or disturbance rejection performance and robust stability in the presence of modelling uncertainties in the model. A rather different approach followed here, compared to what was addressed in (Zolotas, 2002), is to apply mixed sensitivity on both the NMP plant transfer function (G_p) and the MP factorized transfer function (G_{mp}). Note that in the latter case one already obtains a given multiplicative uncertainty bound for the complementary sensitivity (discussed in

section 3.4.1). The non-linear optimization via different weighted choices presented in Table 6.5. For P_{2_xNMP} and P_{2_xMP}, where W1 is achieved via optimization, W3 is W_δ for NMP(nominal plant G_p) model case and $W_{\delta MP}$ for MP(factorized plant (G_{mp})) model (this model is presented in Chapter 3). The second order transfer function formula for sensitivity frequency weight W_1 presented in (6.11) introduced by (Skogestad and Postlethwaite, 2007) where W_B* is maximum frequency bandwidth, M is maximum peak of sensitivity ($S(j\omega)$) and A is maximum steady state tracking error. The initial value for W_1 parameters obtain from PID design in previous chapter. Also note for optimisation purpose we choose W_1 parameters value for NMP and MP model a decade above and lower as upper and lower bound.

$$W_1 = \frac{(s/(M^(1/2)) + W_B*)^2}{(s + W_B * (A)(1/2))^2} \tag{6.11}$$

For either level of initial values for W_2 in all cases or for fixed level of W_2 in all cases, we follow a simple PID design (not presented here) to give us an indication of the expected range of W_2 (and values around the obtained one is investigated, i.e. around 0.5).

Here we also present 4 cases of fixed W_2 and W_3 for P_{x2NMP} case where W_3 is W_δ and W_2 are 0.75, 0.5, 0.1 and high pass filter respectively. Note that W_2 as high pass filter presented here as completeness following the work by (Zolotas, 2002).

The optimization process, which targets tuning of the weighting functions, follows similar process as in previous optimization based control design and implemented via using $f$mincon() in MATLAB. The minimization problem for mixed H_∞ sensitivity cost is given by

$$\begin{aligned} \underset{W1\,W2}{\text{minimize}} \quad & f(x) = P_{CT}\, standing \\ \text{subject to} \quad & < \mathbf{constraint} = \mathbf{rqd} \leq \mathbf{7.5}\% > \end{aligned} \tag{6.12}$$

TABLE 6.5: Minimization approach identifiers and weight sensitivity parameters(transfer function) for H_∞ Mixed Sensitivity optimization (Note: rqd denotes ride quality degradation)

Minimization ID	W_1	W_2	W_3
P_{1NMP}	$\frac{s^2+1.317s+0.4337}{1.255s^2+0.06102s+0.0007416}$	0.9355	not used
P_{2NMP}	$\frac{s^2+3.06s+2.341}{2s^2+0.1374s+0.00236}$	0.7047	W_δ
P_{1MP}	$\frac{s^2+0.8792s+0.1932}{1.311s^2+0.03184s+0.0001933}$	0.5338	not used
P_{2MP}	$\frac{s^2+1.063s+0.2823}{2s^2+0.06721s+0.0005646}$	0.309	$W_{\delta MP}$

We also refer to design cases with fixing W_2 weights for the NMP and MP plant respectively. Table 6.6 presents the cases, note that for the NMP plant the identifier is P_{x2NMP}, for the MP case the identifier is P_{x2MP}.

TABLE 6.6: Minimization approach identifiers and weight sensitivity parameters(transfer function) for H_∞ Mixed Sensitivity optimization for P_{x2NMP} and P_{x2MP} with fixed W_2 and W_3 (Note: rqd denotes ride quality degradation)

$W2_{NMP}$	$W1_{NMP}$	$W2_{MP}$	$W1_{MP}$
W2=0.75	$\frac{s^2+3.033s+2.3}{2s^2+0.1356s+0.0023}$	W2=0.5	$\frac{s^2+0.972s+0.2362}{1.2s^2+0.03367s+0.0002362}$
W2=0.5	$\frac{s^2+2.579s+1.663}{1.972s^2+0.1145s+0.001663}$	W2=0.1	$\frac{s^2+1.4s+0.4899}{1.813s^2+0.08429s+0.0009799}$
W2=0.1	$\frac{s^2+0.818s+0.1673}{2s^2+0.0413s+0.000213}$	W2=0.05	$\frac{s^2+1.407s+0.4949}{1.851s^2+0.08562s+0.0009898}$
$W2_{hpf}$	$\frac{s^2+2.219s+1.231}{1.212s^2+0.09887s+0.002016}$		

Essentially we proceed with a nonlinear constrained minimization problem for W_1 (and in some cases W_2) based on the internal H_∞ process that will aim to guarantee the given mixed-sensitivity design.

6.2.2 Nominal performance analysis

The nominal tilt performance for P_{1NMP} , P_{2NMP}, P_{1MP} and P_{2MP} with full order controller is presented in Table 6.7. Note that the relevant controller TF can be seen in Appendix D.1. The table clearly shows the design progress, whereby the conservativeness introduced by the consideration of the MP plant with the associated uncertainty impacts the design. The results for the NMP plant are very satisfactory and in fact are highly improved compared to the initial ones presented in (Zolotas, 2002). Time domain responses can be seen in Figure 6.13.

TABLE 6.7: H_∞ Mixed sensitivity controller performance assessment with the different time-domain optimisation approaches

Deterministic(as per given units)		P_{1NMP}	P_{2NMP}	P_{1MP}	P_{2MP}
Lateral accel.	RMS Deviation ($\%g$)	2.194	2.064	2.921	3.474
	Peak value ($\%g$)	11.434	10.137	12.476	14.388
Roll gyro.	RMS deviation(rad/s)	0.024	0.024	0.031	0.033
	Peak value (rad/s)	0.118	0.124	0.127	0.114
P_{CT} related	Peak jerk level($\%g/s$)	6.495	6.279	8.025	7.933
	Standing (% of passenger)	48.703	46.41	57.359	58.672
	Seated (% of passenger)	13.029	11.912	15.737	16.832
Stochastic (acceleration %g) @58m/s **					
**Ride quality for non-tilting train if running at the higher speed = 2.848%g					
Ride quality	Tilting train	3.059	3.052	3.063	2.914
	Degradation (%)	7.413	7.166	7.55	2.331
Performance Margins					
Freq. resp.	Gain margin(dB)	8.306	6.243	8.475	10.607
	Phase margin (deg)	52.682	44.513	41.083	57.123
	Bandwidth (rad/s)	1.25	1.23	0.809	0.723
	$\|S(j\omega)\|_\infty$	1.625	1.952	1.993	1.535
	Gamma γ	1.3139	1.3221	0.8409	0.6412

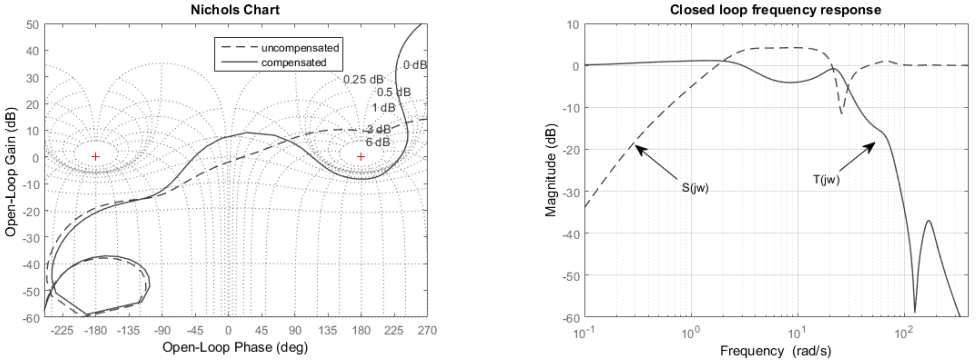

(a) (b)

FIGURE 6.9: Loop (a) and closed-loop (b) (complementary sensitivity($T(j\omega)$) and sensitivity($S(j\omega)$) plots for P_{1NMP} case

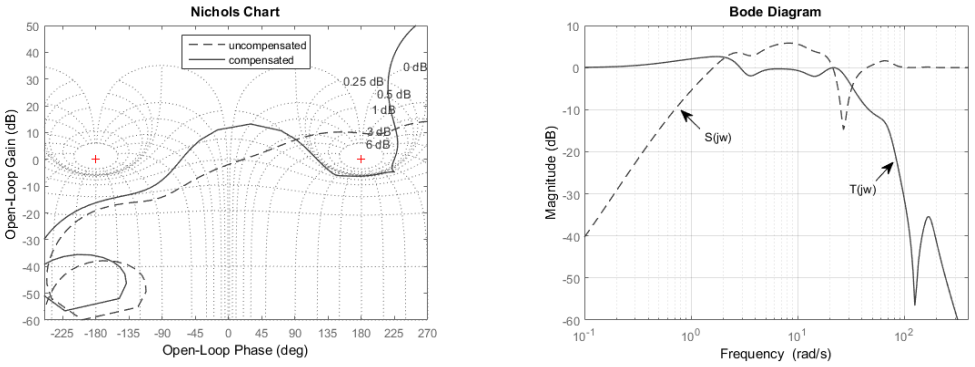

(a) (b)

FIGURE 6.10: Loop (a) and closed-loop (b) (complementary sensitivity($T(j\omega)$) and sensitivity($S(j\omega)$) plots for P_{2NMP} case

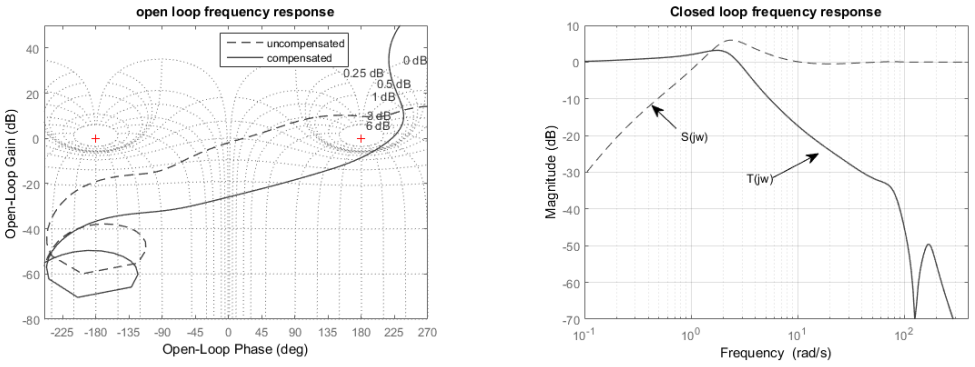

(a) (b)

FIGURE 6.11: Loop (a) and closed-loop (b) (complementary sensitivity($T(j\omega)$) and sensitivity($S(j\omega)$) plots for P_{1MP} case

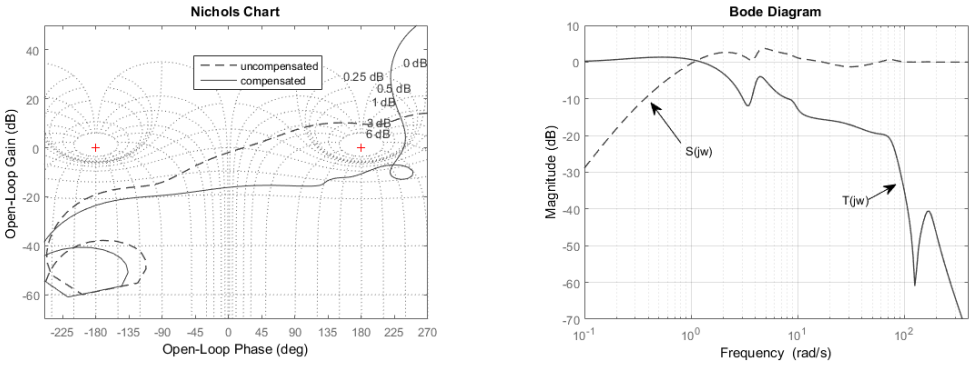

(a) (b)

FIGURE 6.12: Loop (a) and closed-loop (b) (complementary sensitivity($T(j\omega)$) and sensitivity($S(j\omega)$) plots for P_{2MP} case

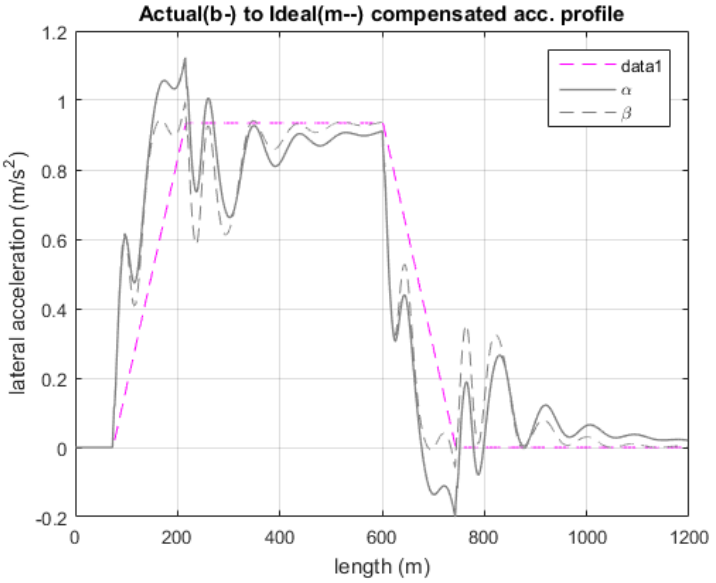

(a)

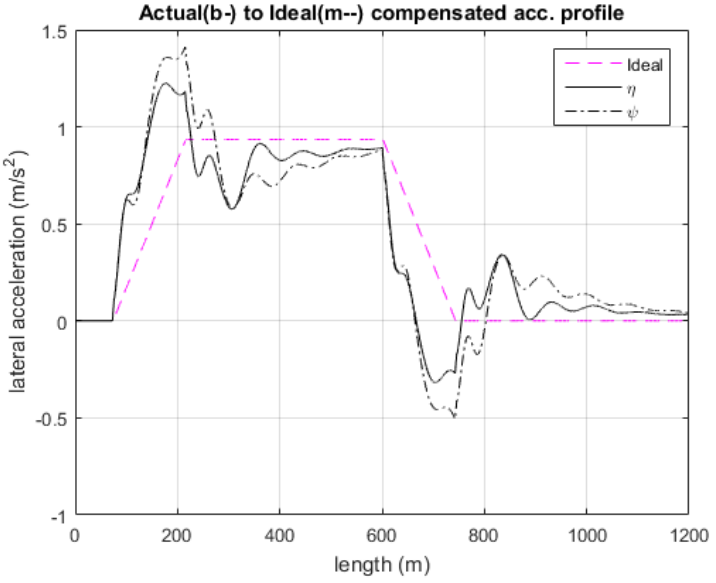

(b)

FIGURE 6.13: Lateral acceleration plot for P_{1NMP} and P_{2NMP} case (a), P_{1MP} and P_{2MP}

For case of P_{x2NMP} P_{x2MP}, nominal performance are given in Table 6.8 for NMP case and Table 6.9 for MP case. For NMP case, P_{CT} and ride quality trade-off can be achieved with W2 value of 0.75 and 0.5. Controller design with MP model(for all cases) show extra conservativeness of the design resulting much higher P_{CT} performance. This can be seen in sensitivity plot Figure 6.14 for P_{x2NMP} $W_2 = 0.5$ and P_{x2MP} $W_2 = 0.1$ case. P_{x2MP} $W_2 = 0.1$ show a very narrow gap between $S(jw)$ and γ/W_1 in Figure 6.14 prove the conservativeness of the design.

The trend of the robust designs is also presented for the remainder system identifiers P_{x2NMP}, P_{x2MP} The choice of fixed W_2 and the impact on the design is also provided. The best result is shown for the NMP case, but note the consistency for the MP case. Table 6.8 and Table 6.9 list the results.

TABLE 6.8: H_∞ Mixed sensitivity controller performance assessment with the different W2 values for P_{x2NMP} case.

Deterministic (as per given units)		**W2** 0.75	**W2** 0.5	**W2** 0.1	**W2** HPF
P_{CT} related	Peak jerk level($\%g/s$)	6.29	6.674	9.004	7.140
	Standing (% of passenger)	46.341	48.706	66.045	52.106
	Seated (% of passenger)	11.902	12.786	20.138	14.124
Stochastic (acceleration %g) @58m/s **					
**Ride quality for non-tilting train if running at the higher speed = 2.848%g					
Ride quality	Tilting train	3.056	3.032	3.062	2.957
	Degradation (%)	7.306	6.462	7.52	3.840
Performance Margins					
Freq. resp.	Gain margin(dB)	6.142	7.484	15.858	8.540
	Phase margin (deg)	44.19	48.263	65.457	52.718
	$\|S(j\omega)\|_\infty$	1.974	1.736	1.195	1.596
	Gamma γ	1.294	1.112	0.623	1.446

A general note that from a strict theoretical point of view, values of γ larger than 1 indicate the the desired specifications in the stacked requirements are not exactly achieved. This is not a vital issue here as we mainly refer to the control assessment for the tilt control design (presented earlier) rather than just the obtained value of γ. However, one could relax the control specifications to obtain values of γ less than 1. For completeness we present sensitivity plots with respect to γ/W_1 (see Figure 6.14).

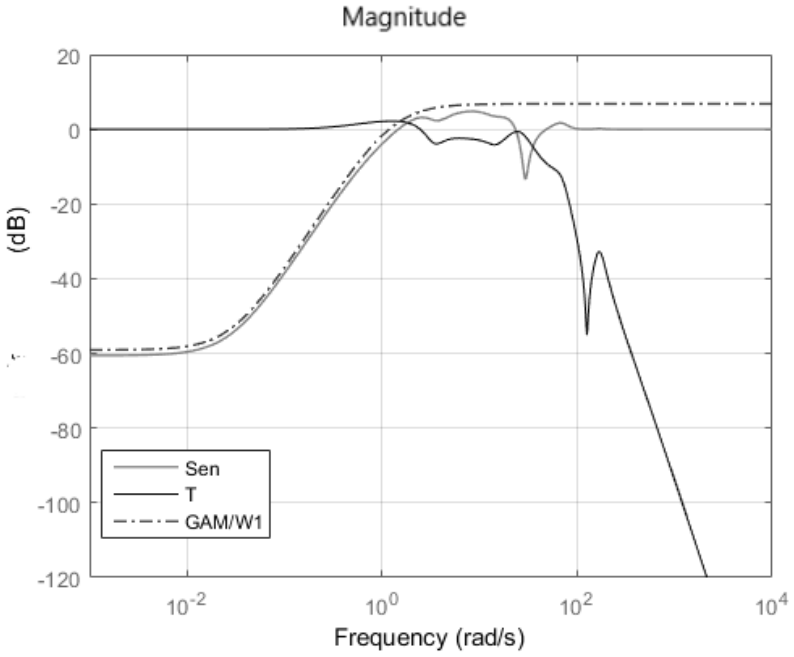

(a)

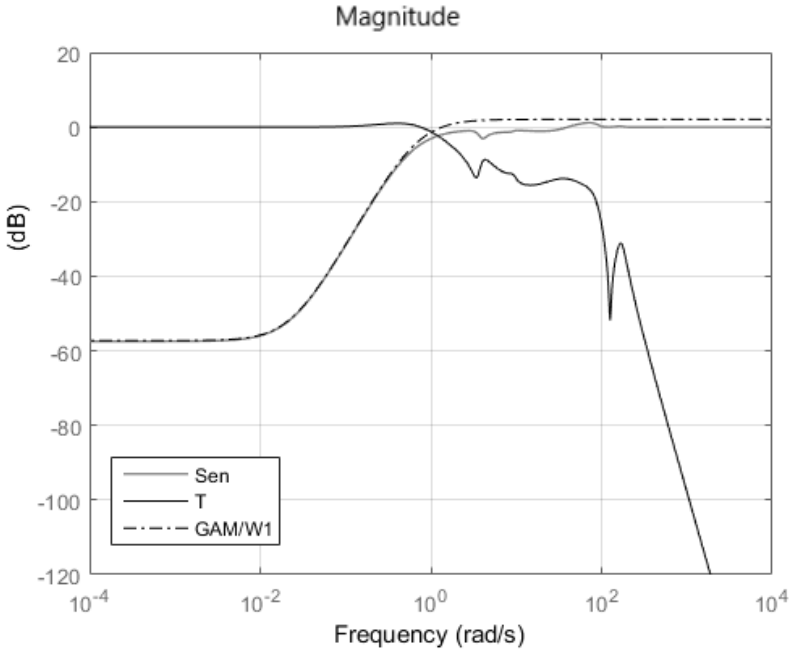

(b)

FIGURE 6.14: Sensivity(S), complementary sensitivity(T) and γ/W_1 plot for (a)$P_{x2NMP}\,W_2 = 0.5$ (b)$P_{x2MP}\,W_2 = 0.1$

TABLE 6.9: H_∞ Mixed sensitivity controller performance assessment with the different W_2 values for P_{x2MP} case.

Deterministic (as per given units)		**W2 0.5**	**W2 0.1**	**W2 0.05**
P_{CT} related	Peak jerk level($\%g/s$)	7.647	7.638	7.671
	Standing (% of passenger)	56.884	56.451	56.595
	Seated (% of passenger)	15.964	15.897	15.973
Stochastic (acceleration %g) @58m/s **				
**Ride quality for non-tilting train running at the higher speed = 2.848%g				
Ride quality	Tilting train	3.062	2.961	3.022
	Degradation (%)	7.497	3.971	6.120
Performance Margins				
Freq. resp.	Gain margin(dB)	8.689	10.299	10.508
	Phase margin (deg)	55.339	55.307	55.538
	$\|S(j\omega)\|_\infty$	1.827	1.585	1.559
	Gamma γ	0.9130	0.6869	0.6752

6.2.3 Controller reduction and robust performance investigation

The order of H_∞ controllers tend to be large (compared to the nature of the model studied), as these are model based controllers with the addition of the closed-loop shaping weights. Here we briefly present controller reductions results, we follow the same controller reduction approach as previously in Section 6.1.1. Referring to Figure 6.15, for all cases, P_{CT} and ride quality performance trade-off are still maintained up to 7th order reduction. Note that the original controller order number differs for each case.

Based on the reduced controllers obtained, we present a brief encounter on robust performance. The perturbed plants are presented in Table 3.3 in Section 3.4.2. The controller used is that of 8th order reduced size. For P_{x2NMP}/P_{x2MP} case, we present the "best" case. The robustness performance of P_{CT} and ride quality degradation of all chosen cases is presented in Table 6.10 and Table 6.11. P_{CT} factor is pretty much sustained for all plant uncertainty cases. With the extra conservativeness of the MP model, the ride quality degradation is maintained below 15% worst for P_{2MP} and

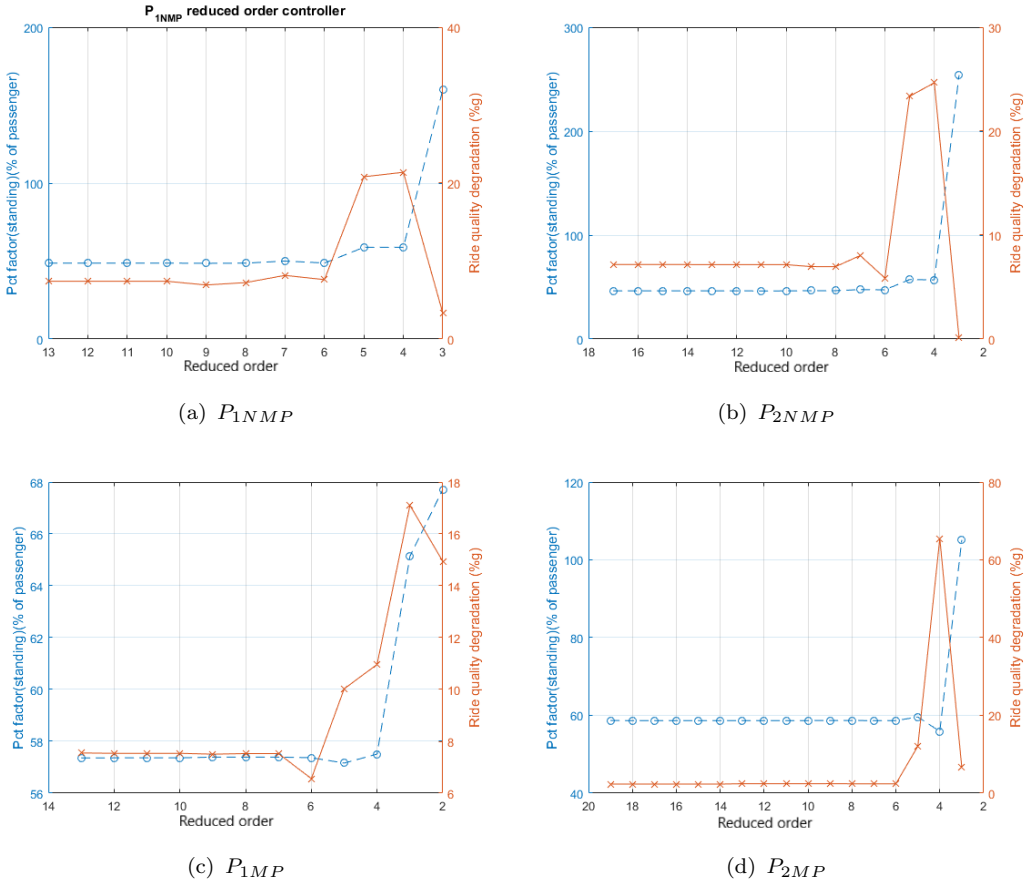

(a) P_{1NMP} (b) P_{2NMP}

(c) P_{1MP} (d) P_{2MP}

FIGURE 6.15: Controller reduction and performance trade-off for H_∞ mixed sensitivity cases

$P_{x2MPW_2=0.1}$ for the worst plant uncertainty case, $P4$. The case for the NMP model shows unstable ride quality degradation in the $P4$ case.

More conservative controller designs tend to provide better robust performance but can be far from the desired aim of improved nulling-type tilt control performance (which should be as close as possible to the performance provided by a tilt with precedence equivalent).

TABLE 6.10: Robust performance for P_{CT} standing for 8th order H_∞ controller

Case	**P0 nominal**	**P1**	**P2**	**P3**	P4
P_{1NMP}	48.674	49.965	50.264	50.606	51.688
P_{2NMP}	46.535	46.196	48.957	57.200	47.904
$P_{2xNMP0.5}$	48.816	49.583	49.910	50.230	50.662
P_{1MP}	57.392	59.567	55.362	55.571	63.388
P_{2MP}	58.682	62.161	59.943	60.860	65.678
$P_{2xMP0.1}$	56.667	59.831	58.944	59.765	63.196

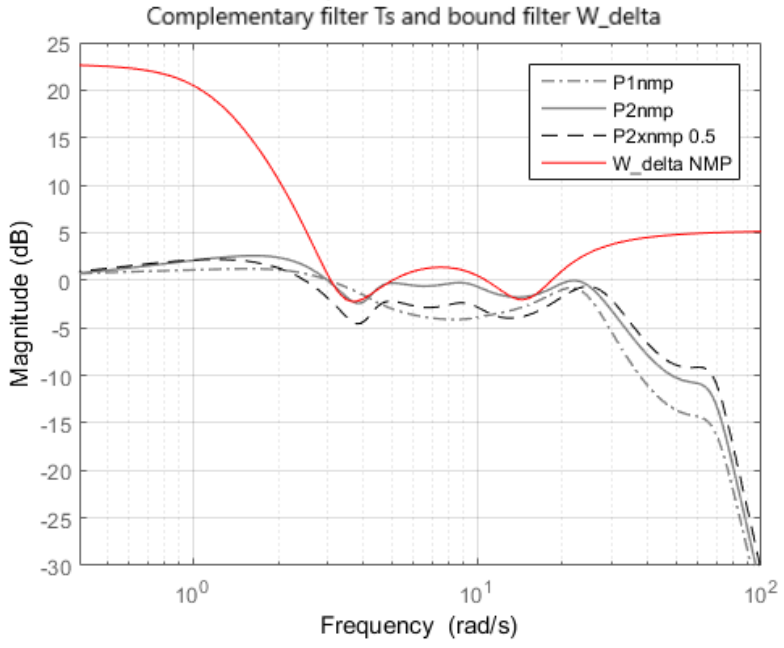

(a)

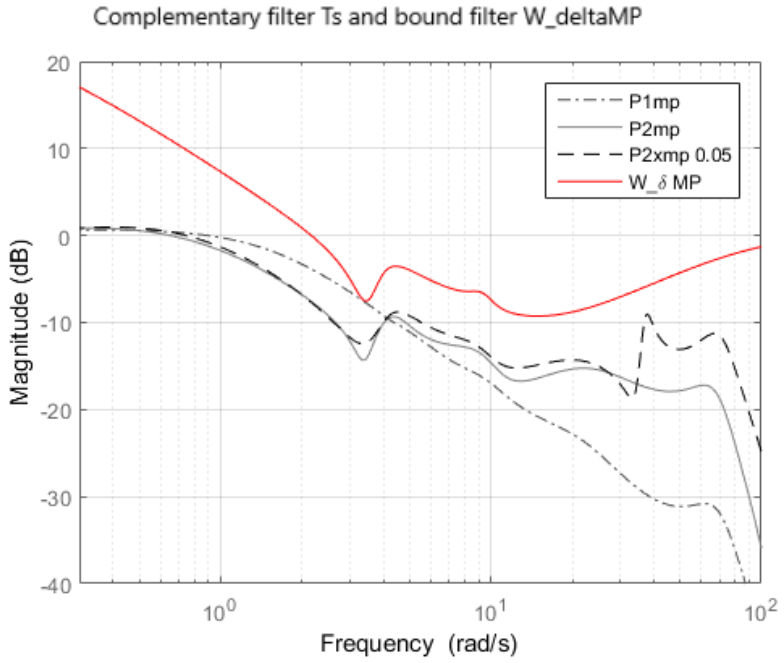

(b)

FIGURE 6.16: Complementary sensitivity ($T(s)$) for the reduced order controller (a) NMP model (b) MP model with multiplicative bound W_δ,$W_{\delta mp}$

TABLE 6.11: Robust performance for ride quality for 8th order H_∞ controller

Case	**P0 nominal**	**P1**	**P2**	**P3**	P4
P_{1NMP}	7.241	29.453	14.539	36.730	unstable
P_{2NMP}	6.966	24.418	22.475	92.808	unstable
$P_{2xNMP0.5}$	6.210	15.509	17.379	35.497	69.424
P_{1MP}	7.527	14.288	4.581	4.168	29.282
P_{2MP}	2.403	5.866	-0.481	-1.253	10.002
$P_{2xMP0.1}$	4.372	7.692	2.698	2.137	13.244

6.3 Summary

This chapter has presented two alternative ways of tilt control via loop shaping design. The first refers to non-conventional fractional order based, the second to a conventional robust H_∞ based design. The discussion provided an insight to how conservative the design can be and its impact to overall performance for the tilt control problem and also on related robustness issues.

Chapter 7

Comparing proposed SISO nulling-type tilt control to precedence

This chapter looks into an overall comparison of the proposed SISO nulling-type control strategies to the equivalent precedence controller. The precedence control setup follows the suggestion from (Zolotas, 2002), however ride quality assessment is now taking into account the weighting/shaping filter Wertungszahl(W_z) lateral sperling index for lateral human comfort.

7.1 A note on the precedence controller used

The precedence controller benchmark utilised here is the one presented by (Zolotas, 2002). It involves a PI+Low pass filter controller for the tilting vehicle (that is the trailing vehicle) and this is performed under ideal operating conditions (no extra signal delays, assuming ideal signal processing and conditioning, and no uncertainty). The tilt command is assumed to be obtained from the leading non-tilting vehicle's bogie and the preview exactly matches the filter delay (for tilt command smoothing). The controller is shown below,

$$K_{PI+LPF} = \frac{300s + 600}{s(0.5s^2 + 14.14s + 200)} \tag{7.1}$$

The difference from the precedence controller results in (Zolotas, 2002) is that here we now employ the Wertungszahl(W_z) index for the weighting of ride quality) in the assessment. In addition, as in the case of the nulling-type controllers, no measurement noise is included in the simulations (we emphasize tilt response, while can notice basic noise attenuation properties from the relevant complementary sensitivity transfer functions if required). The results of tilt performance for the precedence scheme are presented in Table 7.1. The time domain characteristic on curved track are also shown in Figure 7.1. It is clear that precedence provides an ideal tilt response case.

TABLE 7.1: Precedence tilt performance

Deterministic(as per given units)		**Precedence** K_{PI+LPF}
Lateral accel.	RMS Deviation (%g)	1.462
	Peak value (%g)	11.634
Roll gyro.	RMS deviation(rad/s)	0.017
	Peak value (rad/s)	0.103
	Peak jerk level(%g/s)	5.989
P_{CT} related	Standing (% of passengers)	44.329
	Seated (% of passengers)	12.188
Stochastic (acceleration %g) @58m/s **		
**Ride quality of non-tilt. train if running @ high speed = 2.798%g		
Ride quality	Tilting train	2.718
	Degradation (%)	-2.861

7.2 Appraisal of tilt performance

Here, we discuss the comparison of tilt performance of the "best" selected proposed SISO nulling-type schemes with the benchmark precedence one. Note that no robustness consideration will be discussed here rather we refer to it looks nominal tilt performance for illustration purposes.

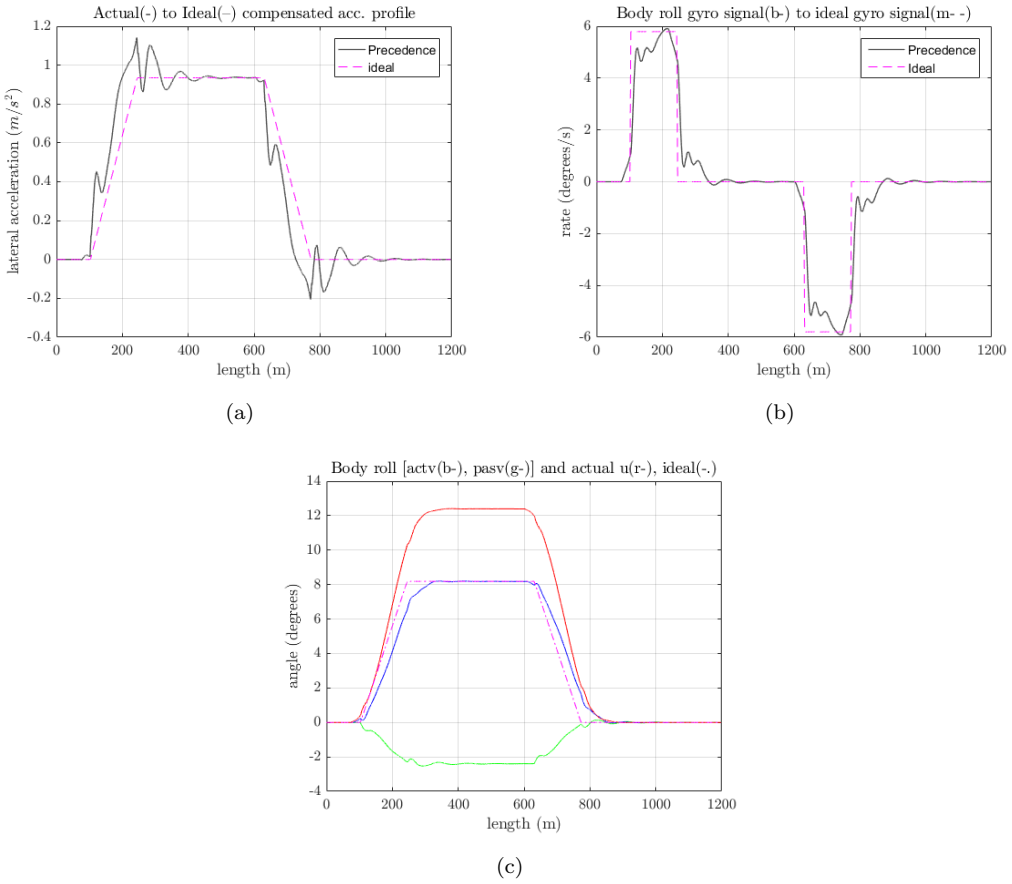

FIGURE 7.1: Precedence approach on curved track for (a) Passenger acceleration (b) Tilt angles (c) Body roll rate

The three proposed SISO nulling-type controller designs, (i) FOPID controller(FO4) (ii)PID with loop shaping fractional order filter($\tilde{Q}_{n=7}^{-1}$) and (iii)one of the H_∞ mixed sensitivity based, i.e. i.d P_{2NMP}. Note that the reduced controller sizes are implemented here for cases (ii) and (iii) i.e. the 7th and 8th order reduced controllers in employed respectively. The SISO nulling tilt cases and Precedence tilt case comparison (tilt assessment results) is presented in Table 7.2. It can be seen that nulling-type case (iii) performance is quite close to that of Precedence tilt. This can be further supported by the time domain plots on curved track shown on Figures 7.4, 7.3 and 7.2. To avoid confusion regarding ride quality, although the precedence approach seems to provide the best ride quality, note that the criterion is to obtain ride quality degradation less than 7.5% worst compared to the non-tilting train at high speed. In such case the nulling type controllers achieve the criterion satisfactorily.

Hence, once again it is illustrated that it is possible to obtain improved tilt responses using advanced control within the remit of nulling-type control schemes. In addition, it is worth mentioning that the preview signals in the precedence scheme should be filtered rather precisely to avoid problems of correlation between track misalignment components and the tilt command, which may impact ride quality in a negative way (this is not of particular concern in the case of nulling-type approaches).

TABLE 7.2: Nominal Performance assessment (P_{CT} / Ride quality (R.Q.))

		Precedence tilt PI+LPF	**P_{2NMP}**	**Local partial nulling tilt PID + $\tilde{Q}_{n=7}^{-1}$**	**FO4**
Deterministic					
Lat acc	RMS dev. (%g)	1.462	2.062	2.662	2.609
Lat acc	peak value (%g.)	11.634	10.150	11.886	10.884
Roll gyro	RMS dev. (rad/s)	0.017	0.024	0.030	0.031
Roll gyro	peak value (rad/s)	0.103	0.125	0.127	0.140
P_{CT}	peak jerk level (rad/s)	5.989	6.276	7.234	6.652
P_{CT}	Stand. (% psg.)	44.329	46.535	53.907	51.454
P_{CT}	Seated (% psg.)	12.188	11.932	14.442	12.621
Stochastic (acceleration %g) @58m/s **					
rq	Non tilt(%g)	2.798	2.848	2.848	2.848
rq	Tilting(%g)	2.718	3.046	3.024	3.063
rq	Degrad.(%)	-2.861	6.966	6.181	7.543

% psg. = % of passengers

7.3 Summary

This chapter presents a concise comparison between the proposed nulling-type tilt controllers in this thesis to a benchmark Precedence tilt controller. The aim of the thesis is further supported, i.e. not only it is possible to achieve appropriate tilt responses via nulling-type tilt but it is possible to achieve this by maintaining a SISO tilt control approach and still satisfy the challenging tilt performance trade-off.

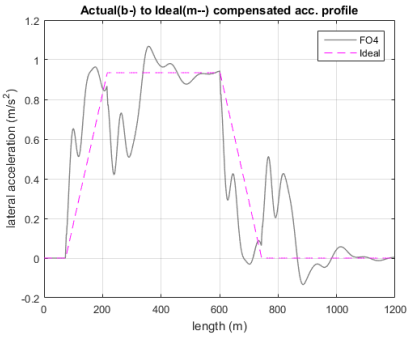

(a) FO4

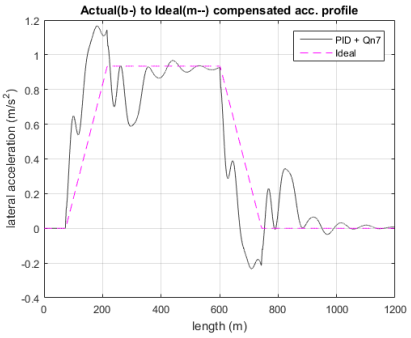

(b) PID + $\tilde{Q}_{n=7}^{-1}$

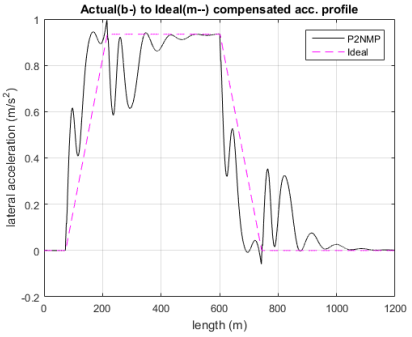

(c) P_{2NMP}

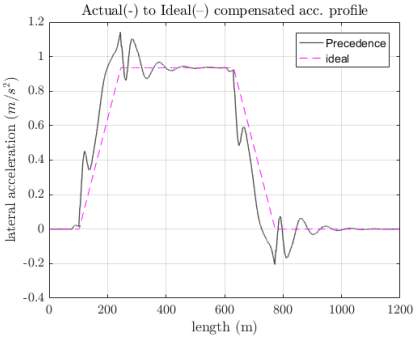

(d) Precedence PI+LPF

FIGURE 7.2: Lateral acceleration responses

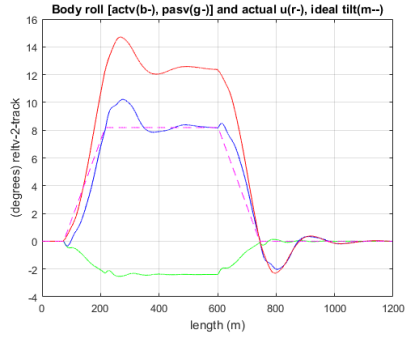

(a) FO4

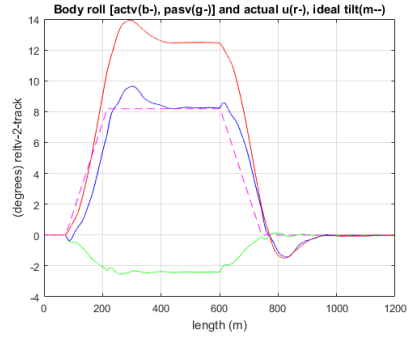

(b) PID + $\tilde{Q}_{n=7}^{-1}$

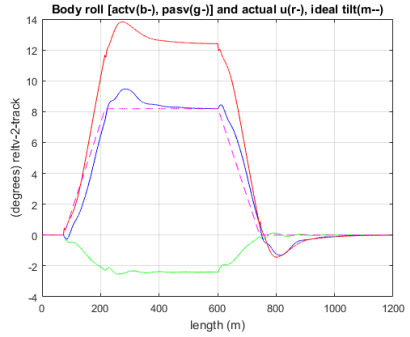

(c) P_{2NMP}

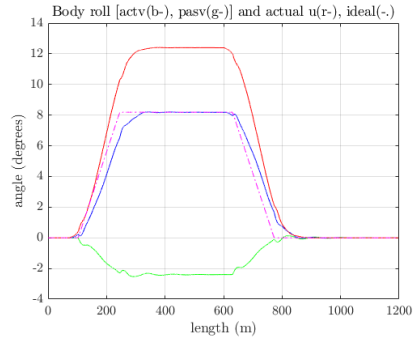

(d) Precedence PI+LPF

FIGURE 7.3: Body roll responses

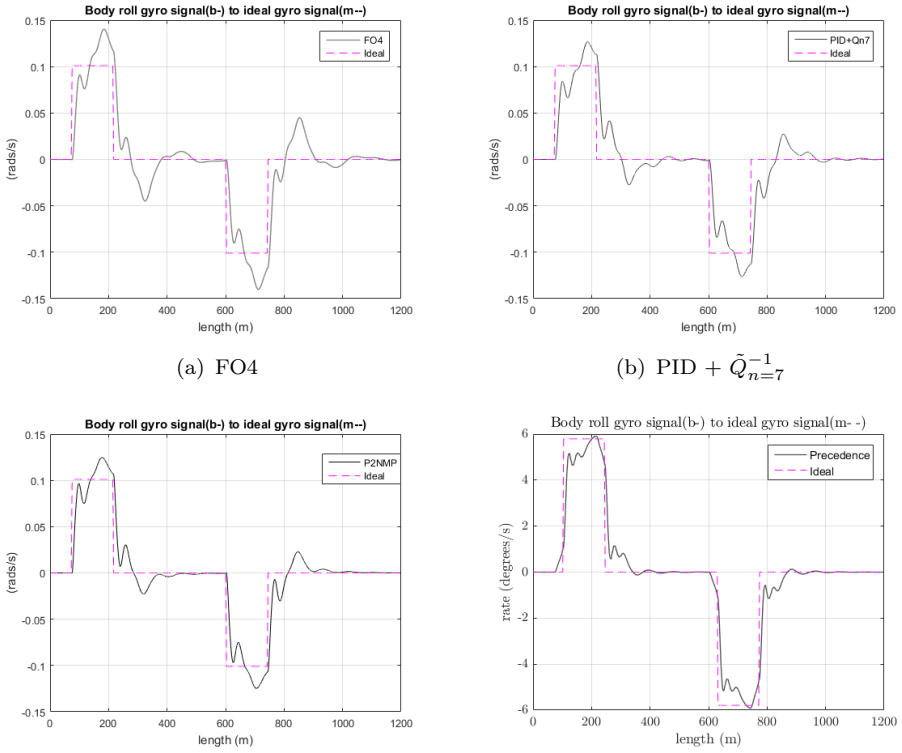

(a) FO4

(b) PID + $\tilde{Q}_{n=7}^{-1}$

(c) P_{2NMP}

(d) Precedence PI+LPF

FIGURE 7.4: Body gyro responses

Chapter 8

Conclusions and future work

8.1 Conclusions

The area of active suspensions for railway vehicles has been under considerable investigation for more than 3 decades now Goodall (1997), however in terms of their applications in service operation few cases exist Bruni et al. (2007). The story around tilting trains though is quite different, and a rather successful one given that the clear benefit of tilting trains from a commercial viewpoint is substantial reduction in journey times still using the conventional railway infrastructure. One can say that tilting train technology is now an established technology with a number of countries utilising tilting trains as means of high speed railway transportation.

Most core tilting train related literature tends to relate to the current industrial norm of precedence tilt, which uses preview tilt information to achieve fast tilt response and maintain good passenger comfort. These schemes tend to suffer from an increased level of complexity, mainly due to the advanced signal processing required for the used signals and the inter-vehicle signal connections. In addition, advanced signal processing is required to cater for appropriate fault detection. However, early tilt control designs (prior to using precedence) employed simple classical methods based on local per vehicle measurements, so called nulling-type tilt. At that time these simple tilt schemes suffered in terms of acceptable tilt performance (which

essentially led to use of preview signals). Still, the potential of returning to the use of nulling-type tilt approach is an important research question especially due to the simplicity these offer both in terms of control solution and fault detection. This has been highlighted from recent more analytical study on advanced tilt control in Zolotas (2002) (and a couple of more research works discussed extensions to intelligent and MIMO possibility).

This thesis rigorously investigates an aspect that has not been answered yet, i.e. although the use of nulling-type tilt control using advanced methods has been highlighted, whether it is possible to achieve comparable performance to precedence tilt by *strictly* maintaining a SISO nulling-type tilt control setup. Obtained results highly support this idea and the thesis has contributed to the following (the first two points are the major contributions of this thesis):

- The novel idea of employing fractional order control for the nulling-type tilt control problem (this being twofold: (i) fractional order based PID solution, (ii) fractional order based loop-shaping solution).
- Rigorous investigation of optimisation in PID tilt control design and appraisal of its impact to the challenging tilt trade-off.
- Investigation of the non-minimum phase model characteristics of the SISO tilt system and their mapping to multiplicative uncertainty (i.e. modelling for control).
- Enhanced H_∞ mixed sensitivity design via weight optimization and thorough investigation of the tilt models within this framework (original non minimum phase(NMP) system and the factorised equivalent with uncertainty).
- Investigation of robust performance and robust stability in the framework of SISO tilt control design.

As in most tilt control related studies, this thesis has also referred to partial-nulling tilt, i.e. compensating only for portion of the passenger acceleration on steady

curves. This is done in order to comply with common practice of tilting train operators.

The author in the first three chapters concentrated on providing a concise introduction to the topic of this research and background research work that links to the topic and presenting important aspects of vehicle modelling and tilt assessment. A particular point relates to modelling whereby ways of dealing with modelling for control" capability for the tilt control problem. In this context, discussion around useful model factorisation and uncertainty representation was presented.

After presenting details on conventional PID (classical) design for the tilt control model, Chapters 5 and 6 comprised of major contributions this thesis makes to the area of tilt control design for high speed railway vehicles. In particular, alongside optimised classical PID control design for improved nulling-type tilt introduced fractional order based equivalent controllers (a non-conventional classical type of control design). Benefits of designing tilt controller based on fractional order methods were twofold (i) in the form of fractional order PID, (ii) in the form of loop-shaping control design. The latter catering with shaping of the non-minimum phase characteristics of the design TF. The path from fractional order tuning to integer-order approximation and controller reduction while maintaining robust stability.

Moreover, in the context of loop shaping an optimised H_∞ mixed sensitivity based approach was presented. This complemented the more classical (but non-conventional) fractional order based loop shaping design, being a post-modern control method. The H_∞ mixed sensitivity approach made considerable use of the modelling for control considerations this thesis presented. The usefulness of incorporating a simple optimization problem (to cater for the ride quality constraint) was illustrated and the different levels of performance achievement exhibited. As in all design cases, a brief discussion on robustness was included.

It is worth noting that the SISO nulling-type control approaches were mostly non-estimator based (different to many of the designs presented to date in the topic literature). However, it is noted that the H_∞ mixed sensitivity design is model based (still avoiding use of H_∞/H_2). The benefit of model-based design is also

shown in the comparison with the precedence controller where the best nulling-type result was provided by the H_∞ mixed sensitivity approach closely followed by the FOPID based approach.

In the author's opinion, the fractional-order based approach and the H_∞ based approach seem highly beneficial to be further exploited (from an implementation point of view) in SISO nulling-type control for tilting trains.

8.2 Future work recommendation

The results obtained in this thesis work are very promising and strongly support the idea of re-employing nulling type tilt control strategies in tilting train with the substantial contribution in performance improvement stemming from use of advanced control design and analysis tools. Below, the author recommends possible next steps in this topic.

- Incorporating fractional order controller design has shown superb benefits in tilt performance and robustness properties for nulling-type control. An interesting next step would be investigation of such an approach in a MIMO framework.

- SISO nulling-type control with comparable performance to precedence is possible for the tilt application, but most of the controllers based on advanced control methodologies i.e. fractional-order (this especially when implemented as approximate rational-order), robust H_∞, result to high order of controller size. The recommendation for future work here is twofold, (i) close investigation of direct to processor fractional order implementation (no intermediate rational order approximation), (ii) close investigation of controller reduction and implementation on processor for the H-infinity case. FPGAs are increasingly becoming popular and the above can be targeted for such an embedded framework.

- Chapter 7 presented a comparison of the proposed SISO nulling-tilt control solutions with a typical preview tilt scheme. The work can be extended to address a rigorous robustness analysis between the two schemes, especially to investigate the effect of preview under system uncertainty and possibly facilitate a hybrid tilt solution.

- Stemming from all previous points, a very important aspect to look into further is co-simulation (with the controller framework on H/W and a dedicated vehicle dynamics software for the railway vehicle model).

In fact, it is worth noting that part of the work presented in this thesis has motivated a new collaborative venture with two core railway related centers (Italy and UK) to look further into this point. The author is very glad to see that the presented work had such an impact that enables continuous research scholarship in the subject.

Appendix A

Vehicle model information

A.1 Vehicle Model Equations

Actuator (tilt command-to applied tilt relationship) position servo-dynamics

$$\ddot{\delta}_{(t)}(t) = -a^{-1}\dot{\delta}_{(t)}(t) + a^{-1}K_m k_a(\delta_{(ti)}(t) - \delta_{(t)}(t))$$

Note that (t) has been dropped for simplicity.

A.1.1 Vehicle body (lateral and roll)

$$m_{\mathrm{v}}\ddot{y}_{\mathrm{v}} = -2k_{sy}(y_{\mathrm{v}} - h_1\theta_{\mathrm{v}} - y_b - h_2\theta_b) - 2c_{sy}(\dot{y}_{\mathrm{v}} - h_1\dot{\theta}_{\mathrm{v}} - \dot{y}_b - h_2\dot{\theta}_b) - \frac{m_{\mathrm{v}}v^2}{R}$$
$$\ldots + m_{\mathrm{v}}g\theta_0 - h_{g1}m_{\mathrm{v}}\ddot{\theta}_0 \quad \text{(A.1)}$$

$$i_{\mathrm{vr}}\ddot{\theta}_{\mathrm{v}} = -k_{\mathrm{vr}}(\theta_{\mathrm{v}} - \theta_b - \delta_t) + 2h_1[K - sy(y_{\mathrm{v}} - h_1\theta_{\mathrm{v}} - y_b - h_2\theta_b) + c_{sy}(\dot{y}_{\mathrm{v}} - h_1\dot{\theta}_{\mathrm{v}})]$$
$$\ldots + m_{\mathrm{v}}g(y_{\mathrm{v}} - y_b) + 2d_1[-k_{az}(d_1\theta_{\mathrm{v}} - d_1\theta_b) - k_{sz}(d_1\theta_{\mathrm{v}} - d_1\theta_r)] - i_{\mathrm{vr}}\ddot{\theta}_0 \quad \text{(A.2)}$$

A.1.2 Vehicle bogie (lateral and roll)

$$m_b\ddot{y}_b = 2k_{sy}(y_\mathrm{v} - h_1\theta_\mathrm{v} - y_b - h_2\theta_b) - 2c_{sy}(\dot{y}_\mathrm{v} - h_1\dot{\theta}_\mathrm{v} - \dot{y}_b - h_2\dot{\theta}_b)$$
$$\ldots - 2k_{py}(y_b - h_3\theta_b - y_w) - 2_{cpy}(\dot{y}_b - h_3\dot{\theta}_b - \dot{y}_w) - \frac{m_b v^2}{R} + m_b g\theta_0 - h_{g2}m_b\ddot{\theta}_0 \tag{A.3}$$

$$i_{br}\ddot{\theta}_b = k_{\mathrm{vr}}(\theta_\mathrm{v} - \theta_b - \delta_a) + 2h_2[k_{sy}(y_\mathrm{v} - h_1\theta_\mathrm{v} - y_b - h_2\theta_b) + c_{sy}(\dot{y}_\mathrm{v} - h_1\dot{\theta}_\mathrm{v} - \dot{y}_b - h_2\dot{\theta}_b)]$$
$$\ldots - 2d_1[-k_{az}(d_1\theta_\mathrm{v} - d_1\theta_b) - k_{sz}(d_1\theta_\mathrm{v} - d_1\theta_r)] + 2d_2(-d_2k_{pz}\theta_b - d_2c_{pz}\dot{\theta}_b)$$
$$\ldots + 2h_3[k_{py}(y_b - h_3\theta_b - y_w) + c_{py}(\dot{y}_b - h_3\dot{\theta}_b - \dot{y}_w)] - i_{br}\ddot{\theta}_0 \tag{A.4}$$

A.1.3 Simplified: Airspring, Tilt actuation, Bogie kinematics

$$\theta_r = -\frac{k_{sz} + k_{rz}}{c_{rz}}\theta_r + \frac{k_{sz}}{c_{rz}}\theta_\mathrm{v} + \frac{k_{rz}}{c_{rz}}\theta_b + \dot{\theta}_b \tag{A.5}$$

$$\ddot{\delta}_a = -22\dot{\delta}_a - 483.6\delta_a + 483.6\delta_{a_i} \tag{A.6}$$

$$\ddot{y}_w = -12.57\dot{y}_w - 987y_w + 987y_0 \tag{A.7}$$

A.2 Variables and Parameters list

y_{v}, y_b, y_0	Lateral displacement of body,bogie and railtrack (m)
$\dot{y_{\mathrm{v}}}, \dot{y_b}, \dot{y_0}$	Roll rate of body,bogie and railtrack (m/s)
$\theta_{\mathrm{v}}, \theta_b$	Roll displacement of body,bogie and actuator (rad)
$\delta_{\mathrm{t}}, \dot{\delta}_{\mathrm{t}}$	Applied tilt (rad) and tilt rate(rad/s)
$\mathrm{R}^{-1}, \dot{\mathrm{R}^{-1}}$	Curve radius rate and acceleration
θ_0	Rail track cant, curve radius (rad)
θ_r	Airspring reservoir roll deflection (rad)
v	Vehicle forward speed (tilting: 58 m/s)
m_{v}	Half body mass, 19000(kg)
i_{vr}	Half body inertia, 25000(kgm)
m_b	Bogie mass, 2500(kg)
i_{br}	Bogie roll inertia, 1500(kgm^2)
k_{az}	Airspring area stiffness, $210e^3$ N/m
k_{sz}	Airspring series stiffness, $620e^3$ N/m
k_{rz}	Airspring reservoir stiffness, $244e^3$ N/m
c_{rz}	Airspring reservoir damping, $33e^3$ Ns/m
k_{sy}	Secondary lateral stiffness, $260e^3$ N/m
c_{sy}	Secondary lateral damping,$33e^3$ Ns/m
$y_w, \dot{y_w}$	Bogie kinematics position(m),rate(m/s)

A.3 State space matrices

A.3.1 17th states space matrices for SISO modelling

$$
A = \begin{bmatrix}
0 & 0 & 0 & 0 & 1 & 0 \\
0 & 0 & 0 & 0 & 0 & 1 \\
0 & 0 & 0 & 0 & 0 & 0 \\
0 & 0 & 0 & 0 & 0 & 0 \\
\frac{2k_{sy}}{m_v} & \frac{2h_1k_{sy}}{m_v} & \frac{2k_{sy}}{m_v} & \frac{2h_2k_{sy}}{m_v} & \frac{-(2c_{sy})}{m_v} & \frac{2c_{sy}h_1}{m_v} \\
\frac{2h_1k_{sy}+gm_v}{i_{vr}} & \frac{-(k_{vr}+2d_1^2(k_{az}+k_{sz})+2_h1^2*k_{sy})}{i_{vr}} & \frac{-(2h_1k_{sy}+gm_v)}{i_{vr}} & \frac{(2k_{az}d_1^2+k_{vr}-2h_1h_2k_{sy})}{i_{vr}} & \frac{2c_{sy}h_1}{i_{vr}} & \frac{-(2c_{sy}h_1^2)}{i_{vr}} \\
\frac{2k_{sy}}{m_b} & \frac{-(2h_1k_{sy})}{m_b} & \frac{-(2k_{py}+2k_{sy}}{m_b} & \frac{2h_3k_{py}-2h_2k_{sy}}{m_b} & \frac{2c_{sy}}{m_b} & \frac{-(2c_{sy}h_1)}{m_b} \\
\frac{2h_2k_{sy}}{i_{br}} & \frac{k_{vr}+2d_1^2(k_{az}+k_{sz})-2h_1h_2k_{sy}}{i_{br}} & \frac{2h_3k_{py}-2h_2k_{sy}}{i_{br}} & \frac{-(2k_{az}d_1^2+2k_{pz}d_2^2+2k_{sy}h_2^2+2k_{py}h_3^2+k_{vr})}{i_{br}} & \frac{(2c_{sy}h_2)}{i_{br}} & \frac{-(2c_{sy}h_1h_2)}{i_{br}} \\
0 & \frac{k_{sz}}{c_{rz}} & 0 & \frac{k_{rz}}{c_{rz}} & 0 & 0 \\
0 & 0 & 0 & 0 & 0 & 0 \\
0 & 0 & 0 & 0 & 0 & 0 \\
0 & 0 & 0 & 0 & 0 & 0 \\
0 & 0 & 0 & 0 & 0 & 0 \\
0 & 0 & 0 & 0 & 0 & 0 \\
0 & 0 & 0 & 0 & 0 & 0 \\
0 & 0 & 0 & 0 & 0 & 0
\end{bmatrix} \cdots
$$

$$
\cdots \begin{bmatrix}
0 & 0 & 0 & 0 & 0 & 0 & 0 & 0 & 0 & 0 & 0 \\
0 & 0 & 0 & 0 & 0 & 0 & 0 & 0 & 0 & 0 & 0 \\
1 & 0 & 0 & 0 & 0 & 0 & 0 & 0 & 0 & 0 & 0 \\
0 & 1 & 0 & 0 & 0 & 0 & 0 & 0 & 0 & 0 & 0 \\
\frac{2c_{sy}}{m_v} & \frac{2c_{sy}h_2}{m_v} & 0 & 0 & 0 & 0 & 0 & g & 0 & -v^2 & 0 \\
\frac{-(2c_{sy}h_1)}{i_{vr}} & \frac{-(2c_{sy}h_1h_2)}{i_{vr}} & \frac{(2d_1^2 * k_{sz})}{i_{vr}} & \frac{k_{vr}}{i_{vr}} & 0 & 0 & 0 & 0 & 0 & 0 & 0 \\
\frac{-(2c_{py}+2c_{sy}}{m_b} & \frac{2c_{py}h_3-2c_{sy}h_2}{m_b} & 0 & 0 & 0 & \frac{2k_{py}}{m_b} & \frac{2c_{py}}{m_b} & g & 0 & -v^2 & 0 \\
\frac{2c_{py}h_3-2c_{sy}h_2}{i_{br}} & \frac{-(2c_{pz}d_2^2+2c_{sy}h_2^2+2c_{py}h_3^2)}{i_{br}} & \frac{-(2d_1^2 * k_{sz})}{i_{br}} & \frac{-k_{vr}}{i_{br}} & 0 & \frac{-(2h_3k_{py})}{i_{br}} & \frac{-(2c_{py}h_3)}{i_{br}} & 0 & 0 & 0 & 0 \\
0 & 1 & \frac{-(k_{rz}+k_{sz})}{c_{rz}} & 0 & 0 & 0 & 0 & 0 & 0 & 0 & 0 \\
0 & 0 & 0 & 0 & 1 & 0 & 0 & 0 & 0 & 0 & 0 \\
0 & 0 & 0 & -w_{cm1}^2 & -2w_{cm1}z_{etam1} & 0 & 0 & 0 & 0 & 0 & 0 \\
0 & 0 & 0 & 0 & 0 & 0 & 1 & 0 & 0 & 0 & 0 \\
0 & 0 & 0 & 0 & 0 & -w_{cm0}^2 & -2w_{cm0}z_{etam0} & 0 & 0 & 0 & w_{cm0}^2 \\
0 & 0 & 0 & 0 & 0 & 0 & 0 & 0 & 1 & 0 & 0 \\
0 & 0 & 0 & 0 & 0 & 0 & 0 & 0 & 0 & 0 & 0 \\
0 & 0 & 0 & 0 & 0 & 0 & 0 & 0 & 0 & 0 & 0 \\
0 & 0 & 0 & 0 & 0 & 0 & 0 & 0 & 0 & 0 & 0
\end{bmatrix} \tag{A.8}
$$

$$B = \begin{bmatrix} 0 & 0 & 0 & 0 \\ 0 & 0 & 0 & 0 \\ 0 & 0 & 0 & 0 \\ 0 & 0 & 0 & 0 \\ 0 & 0 & -h_{g1} & 0 \\ 0 & 0 & -1 & 0 \\ 0 & 0 & -h_{g2} & 0 \\ 0 & 0 & -1 & 0 \\ 0 & 0 & 0 & 0 \\ 0 & 0 & 0 & 0 \\ w_{cm1}^2 & 0 & 0 & 0 \\ 0 & 0 & 0 & 0 \\ 0 & 0 & 0 & 0 \\ 0 & 0 & 0 & 0 \\ 0 & 0 & 1 & 0 \\ 0 & 1 & 0 & 0 \\ 0 & 0 & 0 & 1 \end{bmatrix} \tag{A.9}$$

A.4 Track regularities representation

Lateral track measured spatial spectra approximation is;

$$S_S(f_s) = \frac{\Omega_l}{f_s^3} \quad m^2(cycle/m)^{-1} \tag{A.10}$$

Spatial frequency f_s in the expression above can be converted in temporal frequency (f_t) by

$$f_s(cycles/m) = \frac{f_t(cycles/s)}{v(m/s)} \tag{A.11}$$

Subtitute the above expression into A.10;

$$S_s(f_t) = \frac{\Omega_l v^3}{f_t^3} \quad m^2(cycle/m)^1 \tag{A.12}$$

Converting intro spectrum with temporal base;

$$S_T(f_t) \quad m^2(cycle/s)^{-1} = \frac{S_S(f_t) \quad m^2(cycle/m)^{-1}}{v \quad m/s} \tag{A.13}$$

Expressing $S_T(f_t)$ in terms of radians;

$$S_T(f_t) = \frac{\Omega_l v^2}{2\pi f_t^3} \quad m^2(rad/s)^{-1} \tag{A.14}$$

Therefore,

$$\dot{S_T}(\omega_t) = \frac{2\pi\Omega_l v^2}{f_t} \quad (m/s)^2(rad/s)^{-1} \tag{A.15}$$

In terms of cycles, spectrum expression is given by;

$$\dot{S_T}(f_t) = \frac{(2\pi)^2\Omega_l v^2}{f_t} \quad (m/s)^2(Hz)^{-1} \tag{A.16}$$

Appendix B

Tilt assessment PCT factor

$P_{CT} = (A\ddot{y} + B\dddot{y} - C)_{\geq 0} + D\dot{\theta}^E$; whereby the constants are:

Condition	A	B	C	D	E
Standing passengers	2.80	2.03	11.1	0.185	2.283
Seated passengers	0.88	0.95	5.9	0.120	1.626

with:

P_{CT} = passenger comfort index on curve transition, represents percentage of passengers feeling discomfort

$\ddot{y}$ = maximum vehicle body lateral acceleration, in the time interval: start of curve transition and 1.6sec after the end of transition (expressed in % of g), g denotes gravity

$\dddot{y}$ = maximum lateral jerk level, calculated as the maximum difference between two subsequent values of $\ddot{y}$ no closer than 1sec, in the time interval: 1sec before start of curve transition and end of transition (expressed in % of g/sec)

$\dot{\theta}$ = maximum absolute value of vehicle body roll speed, in the time interval between start of curve transition to the end of curve transition (expressed in deg/sec), 'dot' denotes $\frac{d()}{dt}$.

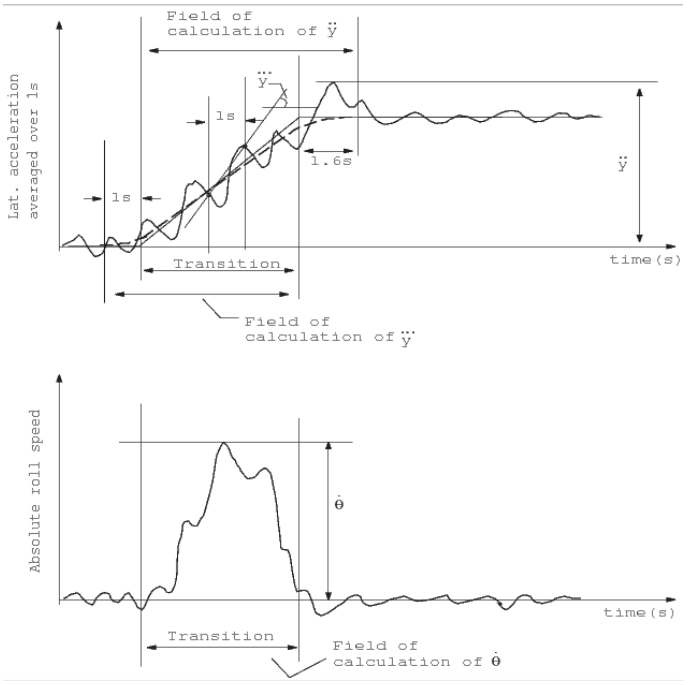

(a) P_{CT} calculation visualisation (acceleration and roll velocity

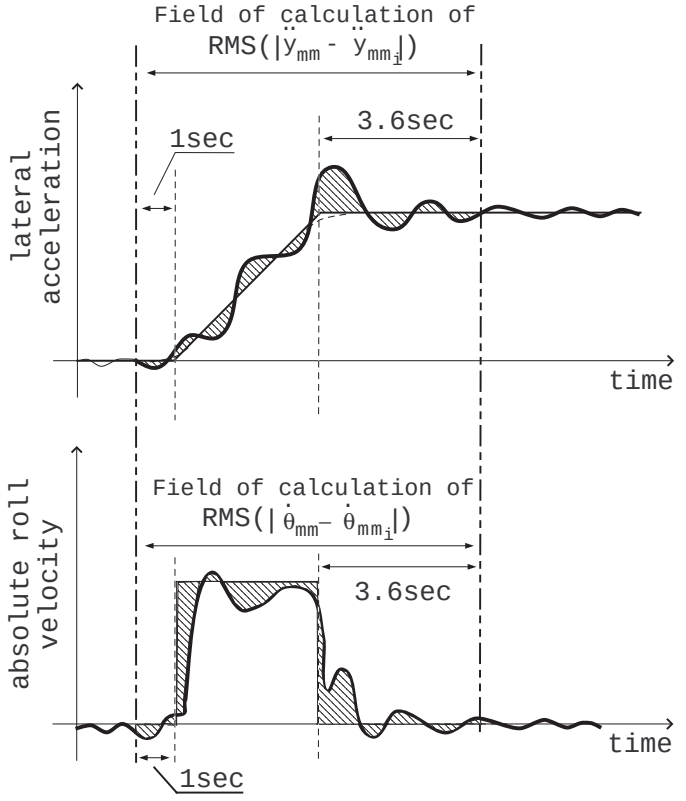

(b) Calculating deviations of actual vs ideal tilt response for both acceleration and roll velocity

FIGURE B.1: Deterministic time-domain assessment elements for P_{CT} and 'ideal tilt'

Appendix C

Fractional order controller

C.1 Full order fractional order controller IOR approximation

C.1.1 FOPID

FOPID controller transfer function after 5th order Oustalop approximation after minimize realization.

$FO1$ case

$$K_{FO1} = \frac{9.773 \times 10^4 s^{12} + 7.065 \times 10^7 s^{11} + 1.193 \times 10^{10} s^{10} + 4.884 \times 10^{11} s^9 + 7.337 \times 10^{12} s^8}{\begin{array}{r} s^13 + 2909 s^12 + 3.044 \times 10^6 s^11 + 1.372 \times 10^9 s^{10} + 2.479 \times 10^{11} s^9 \\ +6.118 \times 10^{13} s^7 + 2.919 \times 10^{14} s^6 + 1.17 \times 10^{15} s^5 + 1.7 \times 10^{15} s^4 + 7.359 \times 10^{14} s^3 \\ \hline +1.12 \times 10^{13} s^8 + 1.618 \times 10^{14} s^7 + 4.836 \times 10^{14} s^6 + 4.47 \times 10^{14} s^5 + 8.238 \times 10^{13} s^4 \\ +7.133 \times 10^{13} s^2 + 1.678 \times 10^{12} s + 3.095 \times 10^9 \\ \hline +4.464 \times 10^{12} s^3 + 3.026 \times 10^{10} s^2 \end{array}}$$

$FO2$ case

$$K_{FO2} = \frac{4249s^{11} + 2.674\times10^{6}s^{10} + 3.567\times10^{8}s^{9} + 1.479\times10^{10}s^{8} + 2.26\times10^{11}s^{7}}{s^{12} + 2321s^{11} + 1.785\times10^{6}s^{10} + 4.961\times10^{8}s^{9} + 3.287\times10^{10}s^{8}} \\ \frac{+1.219\times10^{12}s^{6} + 4.744\times10^{12}s^{5} + 1.021\times10^{13}s^{4} + 6.07\times10^{12}s^{3} + 9.703\times10^{11}s^{2}}{+6.753\times10^{11}s^{7} + 2.911\times10^{12}s^{6} + 3.792\times10^{12}s^{5} + 9.956\times10^{11}s^{4}} \\ \frac{+2.811\times10^{10}s + 5.613\times10^{7}}{+7.318\times10^{10}s^{3} + 4.858\times10^{8}s^{2}}$$

$FO3$ case

$$K_{FO3} = \frac{1.461\times10^{4}s^{12} + 1.006\times10^{7}s^{11} + 1.904\times10^{9}s^{1}0 + 9.266\times10^{10}s^{9} + 1.847\times10^{12}s^{8}}{s^{13} + 2723s^{12} + 2.589\times10^{6}s^{11} + 1.013\times10^{9}s^{10} + 1.532\times10^{11}s^{9}} \\ \frac{+1.687\times10^{13}s^{7} + 7.266\times10^{13}s^{6} + 3.037\times10^{14}s^{5} + 4.241\times10^{14}s^{4} + 1.896\times10^{14}s^{3}}{+5.568\times10^{12}s^{8} + 6.394\times10^{13}s^{7} + 1.52\times10^{14}s^{6} + 1.111\times10^{14}s^{5} + 1.629\times10^{13}s^{4}} \\ \frac{+1.73\times10^{13}s^{2} + 4.376\times10^{11}s + 9.834\times10^{8}}{+6.988\times10^{11}s^{3} + 3.823\times10^{9}s^{2}}$$

$FO4$ case

$$K_{FO4} = \frac{3747s^{11} + 2.056\times10^{6}s^{10} + 2.536\times10^{8}s^{9} + 1.063\times10^{10}s^{8} + 1.677\times10^{11}s^{7}}{s^{12} + 2368s^{11} + 1.83\times10^{6}s^{10} + 4.949\times10^{8}s^{9} + 3.321\times10^{10}s^{8}} \\ \frac{+9.333\times10^{11}s^{6} + 3.946\times10^{12}s^{5} + 9.985\times10^{12}s^{4} + 6.948\times10^{12}s^{3} + 1.288\times10^{12}s^{2}}{+6.57\times10^{11}s^{7} + 2.869\times10^{12}s^{6} + 3.591\times10^{12}s^{5} + 9.513\times10^{11}s^{4}} \\ \frac{+4.371\times10^{10}s + 1.026e08}{+6.551\times10^{10}s^{3} + 3.734\times10^{8}s^{2}}$$

C.1.2 Loop shaping fractional order controller(full order)

1/2 cancellation transfer function of NMP zeros after 5th order Oustalop approximation,

$$Q_{\{n=2\}} = \frac{13.294(s + 0.05623)(s + 0.5623)(s + 5.623)(s + 56.23)(s + 562.3)}{(s + 768.7)(s + 98.44)(s + 16.53)(s + 2.887)(s + 0.4266)(s + 0.0514)}$$

2/3 cancellation transfer function of NMP zeros after 5th order Oustalop approximation,

$$Q_{\{n=3\}} = \frac{2.113(s+0.04642)^2(s+0.06813)(s+0.4642)^2}{(s+749.6)(s+464.2)(s+328.3)(s+87.66)(s+46.42)(s+43.77)(s+13.51)} \frac{(s+0.6813)(s+4.642)^2(s+6.813)(s+46.42)^2(s+68.13)}{(s+5.419)(s+4.642)(s+2.263)(s+0.6154)(s+0.4642)(s+0.3246)} \frac{(s+464.2)^2(s+681.3)}{(s+0.06593)(s+0.04642)(s+0.03941)}$$

3/4 cancellation transfer function of NMP zeros after 5th order Oustalop approximation,

$$Q_{\{n=4\}} = \frac{0.74526(s+0.05623)^2(s+0.07499)}{(s+788)(s+562.3)(s+481.6)(s+421.7)(s+283.1)} \frac{(s+0.04217)^2(s+0.4217)^2(s+0.5623)^2}{(s+86.58)(s+56.23)(s+54.98)(s+42.17)(s+38.02)(s+12.38)} \frac{(s+0.7499)(s+4.217)^2(s+5.623)^2}{(s+6.467)(s+5.623)(s+4.517)(s+4.217)(s+2.022)(s+0.706)} \frac{(s+7.499)(s+42.17)^2(s+56.23)^2(s+74.99)}{(s+0.5623)(s+0.4966)(s+0.4217)(s+0.2856)(s+0.07362)} \frac{(s+421.7)^2(s+562.3)^2(s+749.9)}{(s+0.05623)(s+0.05303)(s+0.04217)(s+0.03445)}$$

4/5 cancellation transfer function of NMP zeros after 5th order Oustalop approximation,

$$Q_{\{n=5\}} = \frac{0.36545(s+0.0631)^2(s+0.07943)(s+0.05012)^2}{(s+820.3)(s+631)(s+570.3)(s+501.2)(s+427.8)(s+398.1)}$$
$$\frac{s+0.03981)^2(s+0.3981)^2(s+0.5012)^2}{(s+261.4)(s+87.26)(s+63.1)(s+62.71)(s+50.12)(s+47.27)}$$
$$\frac{(s+0.631)^2(s+0.7943)(s+3.981)^2}{(s+39.81)(s+35.51)(s+11.8)(s+7.135)(s+6.31)(s+5.409)}$$
$$\frac{(s+5.012)^2(s+6.31)^2(s+7.943)}{(s+5.012)(s+4.118)(s+3.981)(s+1.892)(s+0.7623)(s+0.631)}$$
$$\frac{(s+39.81)^2(s+50.12)^2(s+63.1)^2}{(s+0.5834)(s+0.5012)s+0.4419)(s+0.3981)(s+0.2652)}$$
$$\frac{(s+79.43)(s+398.1)^2(s+501.2)^2}{(s+0.07848)(s+0.0631)(s+0.06102)(s+0.05012)}$$
$$\frac{(s+631)^2(s+794.3)}{(s+0.04663)(s+0.03981)(s+0.03185)}$$

5/6 cancellation transfer function of NMP zeros after 5th order Oustalop approximation,

$$Q_{\{n=6\}} = \frac{0.21282(s+0.06813)^2(s+0.08254)(s+0.05623)^2}{(s+845.1)(s+681.3)(s+634.2)(s+562.3)(s+502.4)(s+464.2)}$$
$$\frac{(s+0.04642)^2(s+0.03831)^2(s+0.3831)^2}{(s+401)(s+383.1)(s+248.5)(s+88.28)(s+68.26)(s+68.13)}$$
$$\frac{(s+0.4642)^2(s+0.5623)^2(s+0.6813)^2}{(s+56.23)(s+54.27)(s+46.42)(s+43.33)(s+38.31)(s+34.1)}$$
$$\frac{(s+0.8254)(s+3.831)^2(s+4.642)^2}{(s+11.45)(s+7.596)(s+6.813)(s+6.057)(s+5.623)(s+4.857)}$$
$$\frac{(s+5.623)^2(s+6.813)^2(s+8.254)}{(s+4.857)(s+4.642)(s+3.896)(s+3.831)(s+1.809)(s+0.80)}$$
$$\frac{(s+38.31)^2(s+46.42)^2(s+56.23)^2}{(s+0.6813)(s+0.6443)(s+0.5623)(s+0.517)(s+0.4642)}$$
$$\frac{(s+68.13)^2(s+82.54)(s+383.1)^2}{(s+0.411)(s+0.3831)(s+0.2525)(s+0.08182)(s+0.06813)}$$
$$\frac{(s+464.2)^2(s+562.3)^2}{(s+0.06663)(s+0.05623)(s+0.05385)(s+0.04642)}$$
$$\frac{(s+681.3)^2(s+825.4)}{(s+0.04642)(s+0.04294)(s+0.03831)(s+0.03027)}$$

6/7 cancellation transfer function of NMP zeros after 5th order Oustalop approximation,

$$Q_{\{n=7\}} = \frac{0.13864(s+0.07197)^2(s+0.06105)^2(s+0.05179)^2}{(s+864.2)(s+719.7)(s+682.2)(s+610.5)(s+560.5)(s+517.9)}$$
$$\frac{(s+0.08483)(s+0.04394)^2(s+0.03728)^2}{(s+464)(s+439.4)(s+384.7)(s+372.8)(s+239.8)(s+89.25)}$$
$$\frac{(s+0.3728)^2(s+0.4394)^2(s+0.5179)^2}{(s+72.4)(s+71.97)(s+61.05)(s+59.71)(s+51.79)(s+49.45)}$$
$$\frac{(s+0.6105)^2(s+0.7197)^2(s+0.8483)}{(s+43.94)(s+40.93)(s+37.28)(s+33.2)(s+11.22)(s+7.934)}$$
$$\frac{(s+3.728)^2(s+4.394)^2(s+5.179)^2}{(s+7.197)(s+6.551)(s+6.105)(s+5.438)(s+5.179)}$$
$$\frac{(s+6.105)^2(s+7.197)^2(s+8.483)}{(s+4.52)(s+4.394)(s+3.757)(s+3.728)(s+1.754)}$$
$$\frac{(s+37.28)^2(s+43.94)^2(s+51.79)^2}{(s+0.8287)(s+0.7197)(s+0.6899)(s+0.6105)(s+0.574)}$$
$$\frac{(s+61.05)^2(s+71.97)^2(s+84.83)}{(s+0.5179)(s+0.476)(s+0.4394)(s+0.3921)(s+0.3728)}$$
$$\frac{(s+372.8)^2(s+439.4)^2(s+517.9)^2}{(s+0.244)(s+0.08428)(s+0.07197)(s+0.07083)}$$
$$\frac{(s+610.5)^2(s+719.7)^2}{(s+0.06105)(s+0.05928)(s+0.05179)(s+0.04933)}$$
$$\frac{(s+848.3)}{(s+0.04394)(s+0.04059)(s+0.03728)(s+0.02922)}$$

C.1.3 7th order controller reduction loop shaping FOC

1/2 cancellation (PID+$Qn = 2$). Reduced order controller (7th order) transfer function for PID+$Qn = 2$(after approximation).

$$k_{n2-7thorder} = \frac{991s^6 + 6.692\times10^4 s^5 + 5.003\times10^5 s^4 + 2.483\times10^6 s^3}{s^7 + 1491s^6 + 1.778\times10^5 s^5 + 3.063\times10^6 s^4 + 8.62\times10^6 s^3}$$
$$\frac{+1.013\times10^7 s^2 + 5.508\times10^6 s + 2.798\times10^5}{+3.517\times10^6 s^2 + 1.593\times10^5 s + 1.592}$$

2/3 cancellation (PID+$Qn = 3$). Reduced order controller (7th order) transfer function for PID+$Qn = 3$(after approximation).

$$k_{n3-7thorder} = \frac{295.9s^6 + 1.622 \times 10^4 s^5 + 1.233 \times 10^5 s^4 + 5.746 \times 10^5 s^3}{s^7 + 860.4s^6 + 5.516 \times 10^4 s^5 + 6.705 \times 10^5 s^4 + 1.453 \times 10^6 s^3} \\ \frac{+2.099 \times 10^6 s^2 + 1.081 \times 106s + 5.131 \times 10^4}{+4.763 \times 10^5 s^2 + 1.795 \times 10^4 s + 0.1787}$$

3/4 cancellation (PID+$Qn = 4$). Reduced order controller (7th order) transfer function for PID+$Qn = 4$(after approximation).

$$k_{n4-7thorder} = \frac{164.1s^6 + 1305s^5 + 6090s^4 + 2.321 \times 10^4 s^3}{s^7 + 559.4s^6 + 7164s^5 + 1.441 \times 10^4 s^4 + 5051s^3} \\ \frac{+1.325 \times 10^4 s^2 + 1344s + 34.33}{+414.1s^2 + 8.712s + 8.696 \times 10^{-5}}$$

4/5 cancellation (PID+$Qn = 5$). Reduced order controller (7th order) transfer function for PID+$Qn = 5$(after approximation).

$$k_{n5-7thorder} = \frac{112.1s^6 + 827s^5 + 3961s^4 + 1.375 \times 10^4 s^3}{s^7 + 412.9s^6 + 4377s^5 + 7967s^4 + 3137s^3} \\ \frac{+8483s^2 + 1414s + 52.81}{+403.3s^2 + 10.91s + 0.0001087}$$

5/6 cancellation (PID+$Qn = 6$). Reduced order controller (7th order) transfer function for PID+$Qn = 6$(after approximation).

$$k_{n6-7thorder} = \frac{88.55s^6 + 650.7s^5 + 3321s^4 + 1.171 \times 10^4 s^3}{s^7 + 338.7s^6 + 3349s^5 + 7312s^4 + 5440s^3} \\ \frac{+1.264 \times 10^4 s^2 + 4374s + 190.1}{+1137s^2 + 32.67s + 0.0003247}$$

6/7 cancellation (PID+$Qn = 7$). Reduced order controller (7th order) transfer function for PID+$Qn = 7$(after approximation).

$$k_{n7-7thorder} = \frac{74.92s^6 + 602.5s^5 + 3292s^4 + 1.167 \times 10^4 s^3}{s^7 + 296.1s^6 + 2938s^5 + 8419s^4 + 8817s^3} \\ \frac{+1.926 \times 10^4 s^2 + 8223s + 365.5}{+2005s^2 + 56.43s + 0.0005599}$$

Appendix D

$H\infty$ Mixed sensitivity

D.1 Full order controller for $H\infty$ Mixed sensitivity

Controller transfer function for P_{1NMP} case,

$$k_{P1NMP} = \frac{\begin{array}{r}2.956\times10^{4}s^{12} + 3.631\times10^{6}s^{11} + 1.172\times10^{9}s^{10} + 8.722\times10^{10}s^{9}\\ +7.193\times10^{12}s^{8} + 2.809\times10^{14}s^{7} + 6.727\times10^{15}s^{6} + 1.036\times10^{17}s^{5} + 8.808\times10^{17}s^{4}\end{array}}{\begin{array}{r}s^{13} + 2.661\times10^{4}s^{12} + 3.636\times10^{6}s^{11} + 1.097\times10^{9}s^{10} + 9.093\times10^{10}s^{9}\\ +7.489\times10^{12}s^{8} + 3.195\times10^{14}s^{7} + 8.827\times10^{15}s^{6} + 1.933\times10^{17}s^{5} + 2.614\times10^{18}s^{4}\\ +6.684\times10^{18}s^{3} + 1.812\times10^{19}s^{2} + 7.496\times10^{19}s + 1.772\times10^{19}\end{array}}{+1.424\times10^{19}s^{3} + 3.081\times10^{19}s^{2} + 1.473\times10^{18}s + 1.78\times10^{16}}$$

Controller transfer function for P_{2NMP} case

$$k_{P2NMP} = \frac{\begin{array}{r}347.7s^{16} + 4.611\times10^{4}s^{15} + 1.429\times10^{7}s^{14} + 1.172\times10^{9}s^{13}\\ +9.804\times10^{10}s^{12} + 4.39\times10^{12}s^{11} + 1.327\times10^{14}s^{10} + 2.846\times10^{15}s^{9} + 4.353\times10^{16}s^{8}\\ +5.273\times10^{17}s^{7} + 4.359\times10^{18}s^{6} + 3.086\times10^{19}s^{5} + 1.305\times10^{20}s^{4} + 5.459\times10^{20}s^{3}\\ +1.138\times10^{21}s^{2} + 2.605\times10^{21}s + 1.16\times10^{21}\end{array}}{\begin{array}{r}s^{17} + 350.6s^{16} + 7.371\times10^{4}s^{15} + 1.285\times10^{7}s^{14} + 1.161\times10^{9}s^{13}\\ +8.705\times10^{10}s^{12} + 4.069\times10^{12}s^{11} + 1.352\times10^{14}s^{10} + 3.539\times10^{15}s^{9} + 6.752\times10^{16}s^{8}\\ +9.117\times10^{17}s^{7} + 9.152\times10^{18}s^{6} + 5.598\times10^{19}s^{5} + 2.237\times10^{20}s^{4} + 5.637\times10^{20}s^{3}\\ +8.875\times10^{20}s^{2} + 5.901\times10^{19}s + 1.002\times10^{18}\end{array}}$$

Controller transfer function for P_{1MP} case

$$k_{P1MP} = \frac{71.94s^{12} + 8833s^{11} + 2.851\times10^{6}s^{10} + 2.121\times10^{8}s^{9}}{s^{13} + 378s^{12} + 8.283\times10^{4}s^{11} + 1.477\times10^{7}s^{10} + 1.456\times10^{9}s^{9}}$$
$$\frac{+1.749\times10^{10}s^{8} + 6.827\times10^{11}s^{7} + 1.634\times10^{13}s^{6} + 2.513\times10^{14}s^{5} + 2.13\times10^{15}s^{4}}{+1.116\times10^{11}s^{8} + 5.327\times10^{12}s^{7} + 1.465\times10^{14}s^{6} + 2.179\times10^{15}s^{5} + 1.605\times10^{15}s^{4}}$$
$$\frac{+1.616\times10^{16}s^{3} + 4.324e16s^{2} + 1.803\times10^{17}s + 3.378\times10^{16}}{+6.068\times10^{16}s^{3} + 9.049\times10^{16}s^{2} + 2.171\times10^{15}s + 1.313\times10^{13}}$$

Controller transfer function for P_{2MP} case

$$k_{P2MP} = \frac{151.5s^{18} + 2.297e04s^{17} + 6.6e06s^{16} + 6.279\times10^{8}s^{15}}{s^{19} + 324.8s^{18} + 7.804\times10^{4}s^{17} + 1.311\times10^{7}s^{16} + 1.432\times10^{9}s^{15}}$$
$$\frac{+5.218\times10^{10}s^{14} + 2.7\times10^{12}s^{13} + 9.221\times10^{13}s^{12} + 2.232\times10^{15}s^{11} + 3.933\times10^{16}s^{10}}{+1.17\times10^{11}s^{14} + 6.84\times10^{12}s^{13} + 2.82\times10^{14}s^{12} + 8.221\times10^{15}s^{11} + 1.695\times10^{17}s^{10}}$$
$$\frac{+5.302\times10^{17}s^{9} + 5.618\times10^{18}s^{8} + 4.713\times10^{19}s^{7} + 3.097\times10^{20}s^{6} + 1.645\times10^{21}s^{5}}{+2.487\times10^{18}s^{9} + 2.682\times10^{19}s^{8} + 2.226\times10^{20}s^{7} + 1.367\times10^{21}s^{6} + 6.106\times10^{21}s^{5}}$$
$$\frac{+6.274\times10^{21}s^{4} + 2.162\times10^{22}s^{3} + 4.102\times10^{22}s^{2} + 8.778\times10^{22}s + 1.901\times10^{22}}{+1.985\times10^{22}s^{4} + 4.532\times10^{22}s^{3} + 6.058\times10^{22}s^{2} + 1.998\times10^{21}s + 1.668\times10^{19}}$$

Controller TF for P_{x2NMP} case for $W_2 = 0.75$

$$k_{PX2NMPW_2=0.75} = \frac{409.1s^{1}6 + 5.425\times10^{4}s^{1}5 + 1.681\times10^{7}s^{1}4 + 1.378\times10^{9}s^{1}3}{s^{1}7 + 395.3s^{1}6 + 8.019\times10^{4}s^{1}5 + 1.476\times10^{7}s^{1}4 + 1.333\times10^{9}s^{1}3}$$
$$\frac{+1.153\times10^{11}s^{1}2 + 5.164\times10^{12}s^{1}1 + 1.561\times10^{14}s^{1}0 + 3.347\times10^{15}s^{9} + 5.118\times10^{16}s^{8}}{+1.016\times10^{11}s^{1}2 + 4.768\times10^{12}s^{1}1 + 1.584\times10^{14}s^{1}0 + 4.143\times10^{15}s^{9} + 7.883\times10^{15}s^{8}}$$
$$\frac{+6.198\times10^{17}s^{7} + 5.121\times10^{18}s^{6} + 3.625\times10^{19}s^{5} + 1.531\times10^{20}s^{4} + 6.404e20s^{3}}{+1.063\times10^{18}s^{7} + 1.064\times10^{19}s^{6} + 6.5\times10^{19}s^{5} + 2.587\times10^{20}s^{4} + 6.52\times10^{20}s^{3}}$$
$$\frac{+1.331\times10^{21}s^{2} + 3.051\times10^{21}s + 1.33\times10^{21}}{+1.019\times10^{21}s^{2} + 6.689\times10^{19}s + 1.122\times10^{18}}$$

Controller TF for P_{x2NMP} case for $W_2 = 0.5$

$$k_{PX2NMP\,W_2=0.5} = \frac{766.2s^{16} + 1.016\times10^{5}s^{15} + 3.148\times10^{7}s^{14} + 2.581\times10^{9}s^{13}}{s^{17} + 543.3s^{16} + 1.049\times10^{5}s^{15} + 2.159\times10^{7}s^{14} + 2.036\times10^{9}s^{13}}$$
$$\frac{+2.159\times10^{11}s^{12} + 9.666\times10^{12}s^{11} + 2.92\times10^{14}s^{10} + 6.259\times10^{15}s^{9} + 9.567\times10^{16}s^{8}}{+1.625\times10^{11}s^{1}2 + 8.048\times10^{12}s^{1}1 + 2.838\times10^{14}s^{1}0 + 7.892\times10^{15}s^{9} + 1.573\times10^{17}s^{8}}$$
$$\frac{+1.158\times10^{18}s^{7} + 9.56\times10^{18}s^{6} + 6.763\times10^{19}s^{5} + 2.85\times10^{20}s^{4} + 1.192\times10^{21}s^{3}}{+2.185\times10^{18}s^{7} + 2.245\times10^{19}s^{6} + 1.391\times10^{20}s^{5} + 5.654\times10^{20}s^{4} + 1.427\times10^{21}s^{3}}$$
$$\frac{+2.462e21s^{2} + 5.66\times10^{21}s + 2.357\times10^{21}}{+2.282\times10^{21}s^{2} + 1.29\times10^{20}s + 1.856\times10^{18}}$$

Controller TF for P_{x2NMP} case for $W_2 = 0.1$

$$k_{PX2NMP\,W_2=0.1} = \frac{274.4s^16 + 3.63\times10^4s^15 + 1.126\times10^7s^14 + 9.208\times10^8s^13}{s^17 + 282.4s^16 + 6.945\times10^4s^15 + 1.085\times10^7s^14 + 1.135\times10^9s^13}$$
$$\frac{+7.706\times10^{10}s^12 + 3.438\times10^{12}s^11 + 1.035\times10^{14}s^10 + 2.21\times10^{15}s^9 + 3.36\times10^{16}s^8}{+8.982\times10^{10}s^12 + 4.798\times10^{12}s^11 + 1.9\times10^{14}s^10 + 5.89\times10^{15}s^9 + 1.263\times10^{17}s^8}$$
$$\frac{+4.047\times10^{17}s^7 + 3.302\times10^{18}s^6 + 2.324\times10^{19}s^5 + 9.516\times10^{19}s^4 + 3.993\times10^{20}s^3}{+1.832\times10^{18}s^7 + 1.948\times10^{19}s^6 + 1.222\times10^{20}s^5 + 5.047\times10^{20}s^4 + 1.26\times10^{21}s^3}$$
$$\frac{+7.653\times10^{20}s^2 + 1.816\times10^{21}s + 3.313\times10^{20}}{+2.047\times10^{21}s^2 + 4.188\times10^{19}s + 2.153\times10^{17}}$$

Controller TF for P_{x2NMP} case for $W_2 = HPF$

$$k_{PX2NMP\,W_2=HPF} = \frac{100.8s^{17} + 1.639\times10^4s^{16} + 4.541\times10^6s^{15} + 4.636\times10^8s^{14}}{s^{18} + 407.2s^{17} + 8.279\times10^4s^{16} + 1.54\times10^7s^{15} + 1.427\times10^9s^{14}}$$
$$\frac{+3.858\times10^{10}s^{13} + 2.123\times10^{12}s^{12} + 7.654\times10^{13}s^{11} + 1.975\times10^{15}s^{10} + 3.727\times10^{16}s^9}{+1.096\times10^{11}s^{13} + 5.429\times10^{12}s^{12} + 1.88\times10^{14}s^{11} + 4.89\times10^{15}s^{10} + 9.786\times10^{16}s^9}$$
$$\frac{+5.297\times10^{16}s^8 + 5.825\times10^{18}s^7 + 4.659\times10^{19}s^6 + 3.041\times10^{20}s^5 + 1.28\times10^{21}s^4}{+1.499\times10^{18}s^8 + 1.713\times10^{19}s^7 + 1.467\times10^{20}s^6 + 8.123\times10^{20}s^5 + 3.078\times10^{21}s^4}$$
$$\frac{+5.021\times10^{21}s^3 + 1.043\times10^{22}s^2 + 2.259\times10^{22}s + 9.192\times10^{21}}{+7.346\times10^{21}s^3 + 1.159\times10^{22}s^2 + 9.092\times10^{20}s + 1.83\times10^{19}}$$

Controller TF for P_{2xMP} case for $W_2 = 0.1$

$$k_{PX2MP\,W_2=0.5} = \frac{191s^{18} + 2.897\times10^4s^{17} + 8.323\times10^6s^{16} + 7.918\times10^8s^{15}}{s^{19} + 458.3s^{18} + 1.043\times10^5s^{17} + 1.998\times10^7s^{16} + 2.246\times10^7s^{15}}$$
$$\frac{+6.58\times10^{10}s^{14} + 3.404\times10^{12}s^{13} + 1.162\times10^{14}s^{12} + 2.813\times10^{15}s^{11} + 4.956\times10^{16}s^{10}}{+1.904\times10^{11}s^{14} + 1.125\times10^{13}s^{13} + 4.517\times10^{14}s^{12} + 1.252\times10^{16}s^{11} + 2.442\times10^{17}s^{10}}$$
$$\frac{+6.68\times10^{17}s^9 + 7.077\times10^{18}s^8 + 5.934\times10^{19}s^7 + 3.898\times10^{20}s^6 + 2.069\times10^{21}s^5}{+3.424\times10^{18}s^9 + 3.559\times10^{19}s^8 + 2.843\times10^{20}s^7 + 1.683\times10^{21}s^6 + 7.272\times10^{21}s^5}$$
$$\frac{+7.885\times10^{21}s^4 + 2.717\times10^{22}s^3 + 5.137\times10^{22}s^2 + 1.101\times10^{23}s + 2.258\times10^{22}}{+2.298\times10^{22}s^4 + 5.186\times10^{22}s^3 + 6.793\times10^{22}s^2 + 1.875\times10^{21}s + 1.309\times10^{19}}$$

Controller TF for P_{x2MP} case for $W_2 = 0.1$

$$k_{PX2MP\,W_2=0.5} == \frac{461.5s^18 + 7.004\times10^4s^17 + 2.012\times10^7s^16 + 1.915\times10^9s^15}{s^19 + 367.3s^18 + 9.351\times10^4s^17 + 1.682\times10^7s^16 + 2.052\times10^9s^15}$$
$$\frac{+1.592\times10^{11}s^14 + 8.242\times10^{12}s^13 + 2.818\times10^{14}s^12 + 6.827\times10^{15}s^11 + 1.205\times10^{17}s^10}{+1.863\times10^{11}s^14 + 1.21\times10^{13}s^13 + 5.493\times10^{14}s^12 + 1.744\times10^{16}s^11 + 3.857\times10^{17}s^10}$$
$$\frac{+1.627\times10^{18}s^9 + 1.727\times10^{19}s^8 + 1.452\times10^{20}s^7 + 9.569\times10^{20}s^6 + 5.098\times10^{21}s^5}{+5.942\times10^{18}s^9 + 6.618\times10^{19}s^8 + 5.658\times10^{20}s^7 + 3.568\times10^{21}s^6 + 1.628\times10^{22}s^5}$$
$$\frac{+1.957\times10^{22}s^4 + 6.758\times10^{22}s^3 + 1.308\times10^{23}s^2 + 2.779\times10^{23}s + 8.057\times10^{22}}{+5.408\times10^{22}s^4 + 1.26\times10^{23}s^3 + 1.758\times10^{23}s^2 + 7.934\times10^{21}s + 9.096\times10^{19}}$$

Controller TF for P_{x2MP} case for $W_2 = 0.05$

$$k_{PX2MP\,w=0.05} = \frac{1948s^{18} + 2.956\times10^5s^{17} + 8.491\times10^7s^{16} + 8.084e09s^{15}}{s^{19} + 536.5s^{18} + 1.471e05s^{17} + 3.049e07s^{16} + 4.202e09s^{15}}$$
$$\frac{+6.719\times10^{11}s^{14} + 3.479\times10^{13}s^{13} + 1.189\times10^{15}s^{12} + 2.881\times10^{13}s^{13} + 5.086\times10^{17}s10}{+1.593\times10^{15}s^{12} + 5.554\times10^{16}s^{11} + 1.328\times10^{18}s^{10}}$$
$$\frac{+6.867\times10^{18}s^9 + 7.29\times10^{19}s^8 + 6.13\times10^{20}s^7 + 4.04\times10^{21}s^6 + 2.152\times10^{22}s^5}{+2.157\times10^{19}s^9 + 2.48\times10^{20}s^8 + 2.184\times10^{21}s^7 + 1.411\times10^{22}s^6 + 6.559\times10^{22}s^5}$$
$$\frac{+8.264\times10^{22}s^4 + 2.854\times10^{23}s^3 + 5.525\times10^{23}s^2 + 1.174\times10^{24}s + 3.42\times10^{23}}{+2.214\times10^{23}s^4 + 5.232\times10^{23}s^3 + 7.445\times10^{23}s^2 + 3.361\times10^{23}s + 3.854\times10^{20}}$$

D.2 8th order controller reduction for $H\infty$ Mixed sensitivity

8th order reduced controller TF for P_{1NMP} case

$$k_{P1NMP} = \frac{1411s^7 + 3.949\times10^4s^6 + 1.016\times10^6s^5 + 8.103\times10^6s^4}{s^8 + 1391s^7 + 4.405\times10^4s^6 + 1.305\times10^6s^5 + 2.725\times10^7s^4}$$
$$\frac{+8.376\times10^7s^3 + 2.03\times10^8s^2 + 1.05\times10^9s + 2.495\times10^8}{+1.814\times10^8s^3 + 4.317\times10^8s^2 + 2.084\times10^7s + 2.497\times10^5}$$

8th order reduced controller TF for P_{2NMP} case

$$k_{P2NMP} = \frac{340.7s^7 + 8895s^6 + 2.277\times10^5s^5 + 1.877\times10^6s^4 + 1.866\times10^7s^3}{s^8 + 269s^7 + 8021s^6 + 2.573\times10^5s^5 + 5.026\times10^6s^4}$$
$$\frac{+4.808\times10^7s^2 + 2.23\times10^8s + 1.102\times10^8}{+3.531\times10^7s^3 + 8.246\times10^7s^2 + 5.62\times10^6s + 9.464\times10^4}$$

8th order reduced controller TF for $P_{x2NMP\,W_2=0.5}$ case

$$k_{P2NMP\,W=0.5} = \frac{603.7s^7 + 1.81\times10^4 s^6 + 4.532\times10^5 s^5 + 3.923\times10^6 s^4}{\begin{array}{r} s^8 + 388.9s^7 + 1.551\times10^4 s^6 + 4.662\times10^5 s^5 + 1.215\times10^7 s^4 \\ +3.724\times10^7 s^3 + 9.58\times10^7 s^2 + 4.356\times10^8 s + 2.033\times10^8 \\ \hline +7.879\times10^7 s^3 + 1.916\times10^8 s^2 + 1.121\times10^7 s + 1.585\times10^5 \end{array}}$$

8th order reduced controller TF for P_{1MP} case

$$k_{P1MP} = \frac{52.03s^7 + 2113s^6 + 1.948\times10^6 s^5 + 2.123\times10^5 s^4 + 5.369\times10^5 s^3}{\begin{array}{r} s^8 + 179s^7 + 2.171\times10^4 s^6 + 1.91\times10^5 s^5 + 8.807\times10^5 s^4 \\ +2.779\times10^6 s^2 + 9.666\times10^5 s + 8.869\times10^4 \\ \hline +1.498\times10^6 s^3 + 2.677\times10^5 s^2 + 5930s + 34.32 \end{array}}$$

8th order reduced controller TF for P_{2MP} case

$$k_{P2MP} = \frac{134s^7 + 1205s^6 + 2.239\times10^4 s^5 + 7.987\times10^4 s^4 + 5.52\times10^7 s^3}{\begin{array}{r} s^8 + 150.4s^7 + 1.032\times10^4 s^6 + 9.684\times10^4 s^5 + 4.156\times10^5 s^4 \\ +8.757\times10^5 s^2 + 3.338\times10^6 s + 7.445\times10^5 \\ \hline +1.301\times10^6 s^3 + 2.376\times10^6 s^2 + 7.781\times10^4 s + 656.8 \end{array}}$$

8th order reduced controller TF for $P_{x2MP\,W_2=0.1}$ case

$$k_{P2MP\,W_2=0.1} = \frac{280s^7 + 5994s^6 + 3.346\times10^5 s^5 + 2.799\times10^6 s^4 + 3.465\times10^7 s^3}{\begin{array}{r} s^8 + 99.86s^7 + 2.135\times10^4 s^6 + 3.365\times10^5 s^5 + 2.211\times10^7 s^4 \\ +7.238\times10^7 s^2 + 3.493\times10^8 s + 1.111\times10^8 \\ \hline +1.043\times10^8 s^3 + 2.409\times10^8 s^2 + 1.081\times10^8 s + 1.266\times10^5 \end{array}}$$

Appendix E

Certificate of award

The International Conference for Students on Applied Engineering (ICSAE 2016)
Newcastle Upon Tyne, United Kingdom
20-21 October 2016

School of Mechanical and Systems Engineering Newcastle University UK | Malaysia | Singapore

IEEE Advancing Technology for Humanity

Northumbria On Campus Group

IET Communities The Institution of Engineering and Technology

IRAQI STUDENTS SOCIETY

AL KINDI SOCIETY FOR ENGINEERS

NewcastleGateshead

NATIONAL INSTRUMENTS

Newcastle University IEEE Student Branch

BEST PAPER AWARD CERTIFICATE

Fazilah Hassan, Argyrios Zolotas and Rebecca Margetts

This Best Paper Award is presented to you for your outstanding paper entitled:

Improved PID Control for Tilting Trains

Whcih was presented at the International Conference for Students on Applied Engineering 2016 (ICSAE 2016), October 20-21, 2016, Newcastle, UK.

21 10 16

Zeyad Yousif Abdoon Al-Shibaany
General Chair of ICSAE 2016
Newcastle University - UK

Atheer F. Hameed
General Co-Chair of ICSAE 2016
Newcastle University - UK

Bibliography

Roger Goodall. Tilting trains and beyond-the future for active railway suspensions. part 1: Improving passenger comfort. *Computing & Control Engineering Journal*, 10(4):153–160, 1999a.

Roger Goodall. Tilting trains and beyond-the future for active railway suspensions. part 2: Improving stability and guidance. *Computing & Control Engineering Journal*, 10(5):221–230, 1999b.

Argyrios C Zolotas. *Advanced control strategies for tilting trains*. PhD thesis, © Argyrios C. Zolotas, 2002.

YangQuan Chen, Ivo Petras, and Dingyu Xue. Fractional order control-a tutorial. In *American Control Conference, 2009. ACC'09.*, pages 1397–1411. IEEE, 2009.

Justin Parkinson. Apt tilting train: The laughing stock that changed the world. *BBC News Magazine*, 2015.

D Boocock and M Newman. The advanced passenger train. *Proceedings of the Institution of Mechanical Engineers*, 190(1):653–663, 1976.

Michael C Duffy. *Electric Railways: 1880-1990*. Number 31. Iet, 2003.

Emily O'Dowd. The twisting and turning tale of britain's tilting trains. *Smart Rail World*, 2017.

Simon Iwnicki. *Handbook of railway vehicle dynamics*. CRC press, 2006. ISBN 1-4200-0489-1.

Katia Moskvitch. The trouble with trying to make trains go faster. *BBC Future*, 2014.

Edoardo F Colombo, Egidio Di Gialleonardo, Alan Facchinetti, and Stefano Bruni. Active carbody roll control in railway vehicles using hydraulic actuation. *Control Engineering Practice*, 31:24–34, 2014a.

D Boocock and BL King. The development of the prototype advanced passenger train. *Proceedings of the Institution of Mechanical Engineers*, 196(1):35–46, 1982.

R. M. Goodall, A. C. Zolotas, and Jeremy Evans. Assessment of the performance of tilt system controllers. In *Proceedings of the Railway Technology Conference IMechE. C*, volume 580, pages 231–239. Citeseer, 2000.

Rickard Persson, Roger M. Goodall, and Kimiaki Sasaki. Carbody tiltingtechnologies and benefits. *Vehicle System Dynamics*, 47(8):949–981, 2009.

John T. Pearson, Roger M. Goodall, and I. Pratt. Control system studies of an active anti-roll bar tilt system for railway vehicles. *Proceedings of the Institution of Mechanical Engineers, Part F: Journal of Rail and Rapid Transit*, 212(1):43–60, 1998.

Hag-Lae Rho, Seong-Ho Han, and Gang-Seog Kim. Development of the korean tilting train and its simulated run-time comparison with non-tilting train on the central line. In *European Transport Conference 2011*, 2011.

A. C. Zolotas, G. D. Halikias, and R. M. Goodall. A Comparison of Tilt Control Approaches for High Speed Railway Vehicles. *Proceedings of 14th International Conference on Systems Engineering ICSE 2000, Coventry University*, (2000):632–636, 2000.

B. H. Huber. The bogie-based tilt option-simplicity and flexibility. *Proceedings of the Institution of Mechanical Engineers, Part F: Journal of Rail and Rapid Transit*, 212(1):19–32, 1998.

Stefano Bruni, Roger Goodall, TX Mei, and Hitoshi Tsunashima. Control and monitoring for railway vehicle dynamics. *Vehicle System Dynamics*, 45(7-8):743–779, 2007.

Ronghui Zhou. *Integrated tilt and active lateral secondary suspension control in high speed railway vehicles*. PhD thesis, Loughborough University, 2010.

Hairi Zamzuri. *Intelligent Model-Based Robust Control for Tilting Railway Vehicles*. PhD thesis, Loughborough University, 2008.

Roger Goodall. Active railway suspensions: Implementation status and technological trends. *Vehicle System Dynamics*, 28(2-3):87–117, 1997.

Roger Goodall. Tilting trains and beyond-the future for active railway suspensions. part 1: Improving passenger comfort. *Computing & Control Engineering Journal*, 10(4):153–160, 1999c.

RM Goodall and TX Mei. 11 active suspensions. *Handbook of railway vehicle dynamics*, page 327, 2006.

Ronghui Zhou, Argyrios Zolotas, and Roger M Goodall. Integrated tilt and active lateral secondary suspension control. *International Symposium on Speed-Up, Safety and Service Technology for Railway and Maglev System (STECH'09)*, 2009.

Anneli Orvnäs. Active lateral secondary suspension in a high-speed train to improve ride comfort. 2009.

Edoardo F Colombo, Egidio Di Gialleonardo, Alan Facchinetti, and Stefano Bruni. Active carbody roll control in railway vehicles using hydraulic actuation. *Control Engineering Practice*, 31:24–34, 2014b.

Alireza Qazizadeh, Rickard Persson, and Sebastian Stichel. On-track tests of active vertical suspension on a passenger train. *Vehicle System Dynamics*, 53(6):798–811, 2015.

Anton Stribersky, Siegbert Steidl, Herbert Müller, and Bernard Rath. On dynamic analyses of rail vehicles with electronically controlled suspensions. *Vehicle System Dynamics*, 25(S1):614–628, 1996.

Roger Vickerman. High-speed rail in Europe: experience and issues for future development. *The annals of regional science*, 31(1):21–38, 1997.

Oskar Fröidh. Perspectives for a future high-speed train in the Swedish domestic travel market. *Journal of Transport Geography*, 16(4):268–277, 2008.

Mamoru Enomoto, Shogo Kamoshita, Masako Kamiyama, Kimiaki Sasaki, Toshihiro Hamada, and Akihito Kazato. Development of tilt control system using electro-hydraulic actuators. *Quarterly Report of RTRI*, 46(4):219–224, 2005.

Y Maki, M Enomoto, K Sasaki, and S Tsujino. A system to detect the train position using gps and a track geometry database. *RTRI Report*, 17(4):11–16, 2003.

A. C. Zolotas and R. M. Goodall. Advanced control strategies for tilting railway vehicles. *UKACC International Conference on Control, University of Cambridge*, page 6, 2000. ISSN 0 85296 240 1.

Argyrios C Zolotas and Roger M Goodall. Improving the tilt control performance of high-speed railway vehicles: an lqg approach. *IFAC Proceedings Volumes*, 38 (1):25–30, 2005.

H. Zamzuri, A. C. Zolotas, and R. M. Goodall. Intelligent control approaches for tilting railway vehicles. *Vehicle System Dynamics*, 44(sup1):834–842, January 2006a. ISSN 0042-3114. doi: 10.1080/00423110600886861. URL `http://dx.doi.org/10.1080/00423110600886861`.

Hairi Zamzuri, Argyrios C. Zolotas, and Roger M. Goodall. Tilt control design for high-speed trains: a study on multi-objective tuning approaches. *Vehicle System Dynamics*, 46(sup1):535–547, September 2008. ISSN 0042-3114. doi: 10.1080/00423110801993151. URL `http://dx.doi.org/10.1080/00423110801993151`.

Hairi Zamzuri, Argyrios Zolotas, Roger Goodall, et al. Integral sliding mode control design for high speed tilting trains. *International Journal of Simulation Systems, Science & Technology*, 11(5):61–67, 2010.

Hairi Zamzuri, Argyrios Zolotas, Roger Goodall, Saiful Amri Mazlan, et al. Advances in tilt control design of high-speed railway vehicles: a study on fuzzy

control methods. *International Journal of Innovative Computing, Information and Control*, 8(9):6067–6080, 2012.

Ronghui Zhou, Argyrios Zolotas, and Roger Goodall. Integrated tilt with active lateral secondary suspension control for high speed railway vehicles. *Mechatronics*, 21(6):1108–1122, 2011.

Ronghui Zhou, Argyrios Zolotas, and Roger Goodall. Lqg control for the integrated tilt and active lateral secondary suspension in high speed railway vehicles. In *Control and Automation (ICCA), 2010 8th IEEE International Conference on*, pages 16–21. IEEE, 2010a.

Ronghui Zhou, Argyrios Zolotas, and Roger Goodall. H-infinity based control system and its digital implementation for the integrated tilt with active lateral secondary suspensions in high speed trains. In *32nd ChineseControl Conference (CCC)*, July, 2013.

Ronghui Zhou, Argyrios Zolotas, and Roger Goodall. 9 dof railway vehicle modeling and control for the integrated tilting bolster with active lateral secondary suspension. 2010b.

Ronghui Zhou, Argyrios Zolotas, and Roger Goodall. Robust system state estimation for active suspension control in high-speed tilting trains. *Vehicle System Dynamics*, 52(sup1):355–369, 2014.

Mirza Muhammad Sabir and Junaid Ali Khan. Optimal design of pid controller for the speed control of dc motor by using metaheuristic techniques. *Advances in Artificial Neural Systems*, 2014:10, 2014.

Ingemar Persson and SD Iwnick. Optimisation of railway wheel profiles using a genetic algorithm. *Vehicle System Dynamics*, 41:517–526, 2004.

P Tormos, A Lova, Federico Barber, L Ingolotti, Montserrat Abril, and Miguel A Salido. A genetic algorithm for railway scheduling problems. In *Metaheuristics for scheduling in industrial and manufacturing applications*, pages 255–276. Springer, 2008.

Chao Lin, Xingqi Fang, Xia Zhao, Qiongyan Zhang, and Xun Liu. Study on energy-saving optimization of train coasting control based on multi-population genetic algorithm. In *Control, Automation and Robotics (ICCAR), 2017 3rd International Conference on*, pages 627–632. IEEE, 2017.

Hairi Zamzuri, Argyrios Zolotas, and Roger Goodall. Optimised intelligent tilt controller scheme using genetic algorithms. In *International Control Conference (ICC 2006)*, 2006b.

Kemal Keskin and Abdurrahman Karamancioglu. Energy-efficient train operation using nature-inspired algorithms. *Journal of Advanced Transportation*, 2017, 2017.

Ting Xie, Shuyi Wang, Xia Zhao, and Qiongyan Zhang. Optimization of train energy-efficient operation using simulated annealing algorithm. In *International Conference on Intelligent Computing for Sustainable Energy and Environment*, pages 351–359. Springer, 2012.

John A Nelder and Roger Mead. A simplex method for function minimization. *The computer journal*, 7(4):308–313, 1965.

Won Y Yang, Wenwu Cao, Tae-Sang Chung, and John Morris. *Applied numerical methods using MATLAB*. John Wiley & Sons, 2005.

Yung Chang Cheng, Chin Te Hsu, Te Wen Tu, Chern Hwa Chen, and Meng Ju Tsai. Derailment analysis of tilting railway vehicles with wind loads. In *Advanced Materials Research*, volume 488, pages 1252–1256. Trans Tech Publ, 2012.

Dale Frederick Enns. Model reduction for control system design. 1985.

Goro Obinata and Brian Anderson. Model reduction for control system design. 2001.

Argyrios Zolotas, George Halikias, Roger Goodall, and Jun Wang. Model reduction studies in lqg optimal control design for high-speed tilting railway carriages. In *American Control Conference, 2006*, pages 6–pp. IEEE, 2006.

Argyrios C. Zolotas, Jun Wang, and Roger M. Goodall. Reduced-order robust tilt control design for high-speed railway vehicles. *Vehicle System Dynamics*, 46(S1): 995–1011, 2008.

MG Safonov and RY Chiang. Model reduction for robust control: A schur relative error method. *International journal of adaptive control and signal processing*, 2 (4):259–272, 1988.

Ian Pratt. *Active suspension applied to railway trains.* PhD thesis, © Ian Pratt, 1996.

Sigurd Skogestad and Ian Postlethwaite. *Multivariable feedback control: analysis and design*, volume 2. Wiley New York, 2007.

Paolo Rocco. Stability of PID control for industrial robot arms. *Robotics and Automation, IEEE Transactions on*, 12(4):606–614, 1996.

Joseba Quevedo and Teresa Escobet. *Digital control: Past, present and future of PID control*. Elsevier Science Inc., 2000. ISBN 0-08-043624-2.

Zhihuan Chen, Yanbin Yuan, Xiaohui Yuan, Yuehua Huang, Xianshan Li, and Wenwu Li. Application of multi-objective controller to optimal tuning of pid gains for a hydraulic turbine regulating system using adaptive grid particle swam optimization. *ISA transactions*, 56:173–187, 2015.

Fereydoon Diba, Ankur Arora, and Ebrahim Esmailzadeh. Optimized robust cruise control system for an electric vehicle. *Systems Science & Control Engineering: An Open Access Journal*, 2(1):175–182, 2014.

PV Gopi Krishna Rao, MV Subramanyam, and K Satyaprasad. Design of internal model control-proportional integral derivative controller with improved filter for disturbance rejection. *Systems Science & Control Engineering: An Open Access Journal*, 2(1):583–592, 2014.

Vladimir Popovic, Dimitrije Jankovic, and Branko Vasic. Design and simulation of active suspension system by using Matlab. In *Proceedings of FISITA World*

Automotive Congress, 2000. URL `http://210.101.116.115/fisita/pdf/G269.pdf`.

Johan Förstberg. Ride comfort and motion sickness in tilting trains, human responses to motion environments in train and simulator experiments, trita-fkt report, 2000:28, kth railway technology, 2000. URL `https://www.diva-portal.org/smash/get/diva2:8728/FULLTEXT01.pdf`.

Karl Johan Åström and Tore Hägglund. *Advanced PID Control*. ISA - The Instrumentation, Systems, and Automation Society; Research Triangle Park, NC 27709, 2006. ISBN 9781556179426. URL `http://lup.lub.lu.se/record/535630`.

Fazilah Hassan, Argyrios Zolotas, and Rebecca Margetts. Improved pid control for tilting trains. In *Students on Applied Engineering (ISCAE), International Conference for*, pages 269–274. IEEE, 2016.

Fazilah Hassan, AC Zolotas, and RM Margetts. Optimised pid control for tilting trains. *Systems Science & Control Engineering*, 5(1):25–41, 2017.

MathWorks. Optimization toolbox. *https://mathworks.com*, 2017.

Karl Johan Åström and Tore Hägglund. Revisiting the ziegler–nichols step response method for pid control. *Journal of process control*, 14(6):635–650, 2004.

M Hypiusová and S Kajan. Pid controller design by modified ziegler-nichols method. *Technical Computing Prague 2013*, page 113.

Juan J Gude and Evaristo Kahoraho. Modified ziegler-nichols method for fractional pi controllers. In *Emerging Technologies and Factory Automation (ETFA), 2010 IEEE Conference on*, pages 1–5. IEEE, 2010.

Hélène Panagopoulos, KJ Astrom, and T Hagglund. Design of pid controllers based on constrained optimisation. *IEE Proceedings-Control Theory and Applications*, 149(1):32–40, 2002.

W. K. Ho, K. W. Lim, and Wen Xu. Optimal Gain and Phase Margin Tuning for PID Controllers. *Automatica*, 34(8):1009–1014, August 1998. ISSN 0005-1098. doi: 10.1016/S0005-1098(98)00032-6.

Stepan Ozana and Tomas Docekal. Pid controller design based on global optimization technique with additional constraints. *Journal of Electrical Engineering*, 67 (3):160–168, 2016.

Vojtech Veselỳ. Easy tuning of pid controller. *Journal of Electrical Engineering*, 54 (5-6):136–139, 2003.

Igor Podlubny. Fractional differential equations: An introduction to fractional derivatives, fractional differential equations, to methods of their solution and some of their applications, vol. 198 of. *Mathematics in Science and Engineering*, 1999.

Concepción A Monje, Blas M Vinagre, Vicente Feliu, and YangQuan Chen. Tuning and auto-tuning of fractional order controllers for industry applications. *Control engineering practice*, 16(7):798–812, 2008.

Gary W Bohannan. Analog fractional order controller in temperature and motor control applications. *Journal of Vibration and Control*, 14(9-10):1487–1498, 2008.

Ivo Petráš and B Vinagre. Practical application of digital fractional-order controller to temperature control. *Acta Montanistica Slovaca*, 7(2):131–137, 2002.

Dingyu Xue and YangQuan Chen. A comparative introduction of four fractional order controllers. In *Intelligent Control and Automation, 2002. Proceedings of the 4th World Congress on*, volume 4, pages 3228–3235. IEEE, 2002.

A Oustaloup, P Melchior, P Lanusse, O Cois, and F Dancla. The crone toolbox for matlab. In *Computer-Aided Control System Design, 2000. CACSD 2000. IEEE International Symposium on*, pages 190–195. IEEE, 2000.

Concepcion A Monje, Antonio J Calderón, Blas M Vinagre, and Vicente Feliu. The fractional order lead compensator. In *Computational Cybernetics, 2004. ICCC 2004. Second IEEE International Conference on*, pages 347–352. IEEE, 2004.

Concepcion A Monje, Blas M Vinagre, Antonio J Calderon, Vicente Feliu, and YangQuan Chen. Auto-tuning of fractional lead-lag compensators. *IFAC Proceedings Volumes*, 38(1):319–324, 2005.

YangQuan Chen, Kevin L Moore, Blas M Vinagre, and Igor Podlubny. Robust pid controller autotuning with a phase shaper. In *First IFAC workshop on fractional differentiation and its applications*, pages 162–167. Citeseer, 2004.

Farshad Merrikh-Bayat. Fractional-order unstable pole-zero cancellation in linear feedback systems. *Journal of Process Control*, 23(6):817–825, 2013.

Patrick Lanusse, Jocelyn Sabatier, and Alain Oustaloup. Extension of pid to fractional orders controllers: a frequency-domain tutorial presentation. *IFAC Proceedings Volumes*, 47(3):7436–7442, 2014.

Ivo Petráš. Tuning and implementation methods for fractional-order controllers. *Fractional Calculus and Applied Analysis*, 15(2):282–303, 2012.

BM Vinagre, I Podlubny, A Hernandez, and V Feliu. Some approximations of fractional order operators used in control theory and applications. *Fractional calculus and applied analysis*, 3(3):231–248, 2000.

Dingyu Xue, Chunna Zhao, and YangQuan Chen. A modified approximation method of fractional order system. In *Mechatronics and Automation, Proceedings of the 2006 IEEE International Conference on*, pages 1043–1048. IEEE, 2006.

Isaac M Horowitz. *Quantitative feedback design*. QFT publications Boulder, CO, 1993.

Goro Obinata and Brian DO Anderson. *Model reduction for control system design*. Springer Science & Business Media, 2012.

Bart Besselink, U Tabak, A Lutowska, N Van De Wouw, H Nijmeijer, DJ Rixen, ME Hochstenbach, and WHA Schilders. A comparison of model reduction techniques from structural dynamics, numerical mathematics and systems and control. *Journal of Sound and Vibration*, 332(19):4403–4422, 2013.

Kyriakos M Deliparaschos, Konstantinos Michail, Argyrios C Zolotas, and Spyros G Tzafestas. Fpga–based efficient hardware/software co–design for industrial systems with consideration of output selection. *Journal of Electrical Engineering*, 67 (3):150–159, 2016.